

DEVELOPMENT OF A LOW COST UNMANNED  
AIRCRAFT SYSTEM FOR ATMOSPHERIC  
CARBON DIOXIDE LEAK DETECTION

By

TAYLOR AUSTIN MITCHELL

Bachelor of Science in Aerospace Engineering

Bachelor of Science in Mechanical Engineering

Oklahoma State University

Stillwater, OK

2012

Submitted to the Faculty of the  
Graduate College of the  
Oklahoma State University  
in partial fulfillment of  
the requirements for  
the Degree of  
MASTER OF SCIENCE  
May, 2015

DEVELOPMENT OF AN UMNANNED AIRCRAFT  
SYSTEM FOR ATMOSPHERIC CARBON  
DIOXIDE LEAK DETECTION

Thesis Approved:

Dr. Jamey Jacob

---

Thesis Adviser

Dr. Girish Chowdhary

---

Dr. James Kidd

---

## ACKNOWLEDGEMENTS

First and foremost, I would like to thank my family for the wonderful life they have provided me and for raising me with solid values and work ethic. Their support has brought me to where I am today and they are always there for me for whatever I need, no matter how large or mundane, especially my parents who are, simply, the best parents I could ever hope to be blessed with.

This work would not be possible without the help of my advisor Dr. Jamey Jacob. His tireless effort is tremendous and he has created innumerable opportunities for myself and others through his work at OSU. I would also like to thank the rest of the faculty in the Mechanical and Aerospace Engineering Department. In particular, Dr. Arena and the incredible hands-on experience he provides in our unmatched senior design program taught me so much of what I know about aircraft design and development. I would also like to thank Dr. Chowdhary and his lab for donation of the second X-8 aircraft and the beneficial collaboration with his students.

I would also like to thank Fred Keating for allowing me to operate my sensor system aboard his Firebird aircraft and for all the help he provided with testing and aircraft development. The many test flights performed with his system provided invaluable data. These flights would also not have been possible without our primary pilots Seabrook Whyte and Jacob Hunter. In addition, thanks to all of the other Aerospace Engineering graduate students at Oklahoma State whom I have worked with, many of whom provided incredibly helpful time and advice and are a great group of friends I am fortunate to have.

Finally, I would like to thank Oklahoma State University for providing me the solid education that made this work possible. All of the opportunities and activities I have been fortunate enough to participate in, the projects I worked on, and the friends I have made created a truly incredible experience.

Name: Taylor Mitchell

Date of Degree: May 2015

Title of Study: DEVELOPMENT OF A LOW COST UNMANNED AIRCRAFT  
SYSTEM FOR ATMOSPHERIC CARBON DIOXIDE LEAK  
DETECTION

Major Field: Mechanical and Aerospace Engineering

Carbon sequestration, the storage of carbon dioxide gas underground, has the potential to reduce global warming by removing a greenhouse gas from the atmosphere. These storage sites, however, must first be monitored to detect if carbon dioxide is leaking back out to the atmosphere. As an alternative to traditional large ground-based sensor networks to monitor CO<sub>2</sub> levels for leaks, unmanned aircraft offer the potential to perform in-situ atmospheric leak detection over large areas for a fraction of the cost. This project developed a proof-of-concept sensor system to map relative carbon dioxide levels to detect potential leaks. The sensor system included a Sensair K-30 FR CO<sub>2</sub> sensor, GPS, and altimeter connected an Arduino microcontroller which logged data to an onboard SD card. Ground tests were performed to verify and calibrate the system including wind tunnel tests to determine the optimal configuration of the system for the quickest response time (4-8 seconds based upon flowrate). Tests were then conducted over a controlled release of CO<sub>2</sub> in addition to over controlled rangeland fires which released carbon dioxide over a large area as would be expected from a carbon sequestration source. 3D maps of carbon dioxide were developed from the system telemetry that clearly illustrated increased CO<sub>2</sub> levels from the fires. These tests demonstrated the system's ability to detect increased carbon dioxide concentrations in the atmosphere.

## TABLE OF CONTENTS

Chapter	Page
TABLE OF CONTENTS.....	v
LIST OF TABLES.....	ix
LIST OF FIGURES .....	x
CHAPTER I: INTRODUCTION.....	1
I.    Motivation.....	1
II.   Project Background.....	2
CHAPTER II: BACKGROUND .....	7
I.    Background.....	7
A.   Atmospheric Carbon Dioxide Trends .....	7
B.   Carbon Sequestration .....	8
C.   Current Atmospheric CO <sub>2</sub> Measurement Methods .....	11
D.   Atmospheric Plume Modeling .....	16
II.   Literature Review.....	17
A.   Manned Aircraft Testing.....	17
B.   UAS Testing of Environmental Levels.....	18
C.   UAS Testing of Simulated Leak Source .....	20
D.   Surface Level Carbon Isotope Measurements .....	22

E. NDIR Sensor Comparison Study .....	23
CHAPTER III: EQUIPMENT DESIGN AND TEST SETUP .....	25
I. Sensor System.....	25
A. Arduino Microcontroller .....	27
B. CO <sub>2</sub> Sensor.....	30
C. SD Logging Shield & Real Time Clock .....	34
D. GPS Receiver .....	36
E. Altimeter .....	37
F. Flowmeter .....	38
II. CO <sub>2</sub> Flight Test Configuration .....	39
A. Aircraft.....	40
B. CO <sub>2</sub> Flow System.....	44
III. Controlled Burn Flight Test Configuration.....	46
A. Aircraft.....	46
B. CO <sub>2</sub> System Configuration.....	47
C. Controlled Burn Locations.....	48
IV. Ground test configuration .....	49
A. CO <sub>2</sub> Calibration System .....	49
B. Wind Tunnel Setup .....	50
1. Flowmeter Test Setup .....	51
2. CO <sub>2</sub> Response Test Setup .....	53

C. Field Test Setup .....	54
CHAPTER IV: TEST RESULTS .....	56
I. Ground Test Results.....	56
A. CO <sub>2</sub> Calibration Test Results .....	56
B. Wind Tunnel Test Results.....	57
1. Flowmeter Test Results.....	57
2. Flowmeter Noise Tests .....	60
3. CO <sub>2</sub> Response Test Results.....	61
II. Flight Test Results .....	63
A. Preliminary Flight Tests & Lessons Learned.....	63
B. 160 Acre Controlled Burn Test Results .....	64
C. 2 Mile <sup>2</sup> Controlled Burn Test Results .....	69
D. CO <sub>2</sub> Release Test Result .....	80
E. Small Plot Fire Test Results .....	83
CHAPTER V: CONCLUSIONS .....	87
I. Conclusions.....	87
II. Improvements and Future Work .....	89
REFERENCES .....	93
APPENDIX A – Additional Figures.....	97
I. Additional Sensor System Details.....	97
A. Temperature & Humidity Sensor .....	97

B. Pressure Sensor .....	98
A. Voltage Step-up Circuitry .....	98
A. Programming.....	101
II. Aircraft Configuration Details .....	104
A. Aircraft Configuration Version 1 .....	104
B. Aircraft Configuration Version 2.....	108
C. Airfield.....	112
III. Autopilot Wiring Improvements .....	112
APPENDIX B – Additional Figures .....	115
I. Wind Tunnel CO <sub>2</sub> Response Test Charts .....	115



LIST OF TABLES

Table	Page
Table 1 - CO2 Sensor Comparison .....	33
Table 2 - GPS comparison .....	36
Table 3 - Airframe selection .....	41
Table 4 - Switching regulator step-up circuit calculations.....	100

## LIST OF FIGURES

Figure	Page
Figure 1 - SWP Farnsworth Oil Unit in Anadarko Basin (Clark, et al. 2013) .....	2
Figure 2 - Cross section of underground formations in Anadarko Basin (Clark, et al. 2013) .....	3
Figure 3 - Exposed fractures near Farnsworth Unit .....	4
Figure 4 - Illustration of CO <sub>2</sub> sequestration and potential leakage .....	4
Figure 5 - Average global CO <sub>2</sub> mole fraction (a) and growth rate (b) (World Meteorological Organization 2014) .....	8
Figure 6 - DoE CO <sub>2</sub> geologic sequestration infographic (U.S. Department of Energy Office of Fossil Energy n.d.) .....	10
Figure 7 - Vehicle and aircraft based DIAL systems (National Physical Laboratory 2012) (Brake 2005) .....	12
Figure 8 - Example DIAL methane survey (Brake 2005) .....	13
Figure 9 - Example eddy covariance tower sensors (Burba and Anderson 2007) .....	14
Figure 10 - Diurnal cycle of Earth's atmosphere (Clark, et al. 2013) .....	15
Figure 11 - Illustration of basic components of plume model from a smokestack (Holzbecher 2012) .....	16
Figure 12 - Sample Gaussian plume model in XY plane below the release point (Holzbecher 2012) .....	17

Figure 13 - Early atmospheric CO <sub>2</sub> measurement UAS and sensor system schematic (Watai, et al. 2006) .....	19
Figure 14 - Helicopter UAS for carbon sequestration leak detection (Poppa, et al. 2013) .....	20
Figure 15 - CO <sub>2</sub> levels recorded by helicopter UAS (Poppa, et al. 2013) .....	22
Figure 16 - Raw measurements of <sup>12</sup> CO <sub>2</sub> at ZERT field site (Krevor, et al. 2010) .....	23
Figure 17 - CO <sub>2</sub> sensor system enclosures, flowmeter, and water filter .....	26
Figure 18 - Sensor system battery .....	27
Figure 19 - Arduino microcontroller .....	28
Figure 20 - Arduino board with example Bluetooth shield .....	29
Figure 21 - Arduino Leonardo .....	30
Figure 22 - Adafruit Data Logging shield .....	35
Figure 23 - Sparkfun MPL3115A2 Altimeter Board .....	38
Figure 24 - Honeywell AWM5101VN flowmeter .....	38
Figure 25 - Stock Skywalker X-8 internal area .....	43
Figure 26 - X-8 test aircraft: configuration 1 (a) and 2 (b) .....	44
Figure 27 - Nose mounted air sample intake, Pitot tube, and FPV camera .....	45
Figure 28 - Air sample flow system and configurations .....	46
Figure 29 - Firebird UAS being launched by its developer .....	47
Figure 30 - Firebird internal layout .....	48
Figure 31 - Portion of 160 acre controlled burn .....	49
Figure 32 - CO <sub>2</sub> calibration system .....	50
Figure 33 - Flowrate test LabVIEW program .....	52
Figure 34 - Equipment changed during first round of flowmeter tests .....	52
Figure 35 - CO <sub>2</sub> response time test wind tunnel setup .....	53
Figure 36 - CO <sub>2</sub> response time test LabVIEW program .....	54
Figure 37 - Data from early field test .....	55

Figure 38 - CO2 sensor calibration.....	57
Figure 39 - Tunnel airspeed pressure transducer calibration .....	58
Figure 40 - Flowrate as a result of airspeed and configuration.....	59
Figure 41 - Noise comparison using Arduino system at 25 m/s in wind tunnel .....	60
Figure 42 - Sample CO2 sensor response test at 0.435 LPM flow rate; 14.25 m/s airspeed .....	61
Figure 43 - CO2 detection time based on flow rate .....	62
Figure 44 - CO2 peak time based on flowrate .....	62
Figure 45 - Successful (a) and failed (b) X-8 hand launch .....	63
Figure 46 - Sample grid flight paths: simple (a) and interleaved (b) .....	64
Figure 47 - Flank fire as seen on approach from north.....	65
Figure 48 - Firebird flight 1 launch.....	66
Figure 49 - 3D plot of flight 1 path and normalized CO2 levels .....	67
Figure 50 - 2D plot of flight 1 path and CO2 levels at nominal 300 ft altitude .....	68
Figure 51 - 3D interpolation of CO2 levels from flight 1 .....	69
Figure 52 - Lake Carl Blackwell burn area.....	70
Figure 53 - Flight 1 altitude vs CO2 level .....	71
Figure 54 - Southwest fire during flight 2 as seen from launch point.....	72
Figure 55 - 3D plot of flight 2 path and normalized CO2 levels .....	72
Figure 56 - First 12 minutes of flight 2: altitude vs CO2 levels and smoke levels .....	73
Figure 57 - Smoke seen from aircraft while passing through plume .....	74
Figure 58 - Abbreviated flight 2 path with smoke levels plotted below path .....	75
Figure 59 - Weather radar imagery of fires.....	75
Figure 60 - Flight 3 fire progression as seen from launch point .....	76
Figure 61 - 3D plot of small grid flight 3 path and normalized CO <sub>2</sub> levels .....	77
Figure 62 - 2D plot of small grid at 100 ft (a), 200 ft (b), and 300 ft (c) .....	77
Figure 63 - 3D plot of large grid flight 3-4 path and normalized CO2 levels.....	79

Figure 64 - 2D plot of large grid at 100 ft (a), 200 ft (b), 300 ft (c), and 400 ft (d).....	80
Figure 65 - Airfield controlled CO2 release test setup .....	81
Figure 66 - 2D plot of CO2 tank release flight path .....	82
Figure 67 - Longitude vs CO2 levels during east-west (downwind-upwind) passes over CO2 release .....	83
Figure 68 - Small plot burn.....	84
Figure 69 - 3D plot of small plot flight path and normalized CO2 levels .....	85
Figure 70 - 2D plot of 150 ft small plot flight path and normalized CO2 levels .....	85
Figure 71 - 2D plot of 150 ft small plot flight path and normalized CO2 levels and sample plume model overlay .....	86
Figure 72 - Sparkfun HH6130 temperature/humidity board .....	98
Figure 73 - Honeywell ASDX absolute pressure sensor.....	98
Figure 74 - Step-up circuit diagram .....	99
Figure 75 - Voltage step-up circuit .....	101
Figure 76 - Example data log file .....	102
Figure 77 - X-8 Test Airframe 1 .....	104
Figure 78 - X-8 center of gravity location .....	105
Figure 79 - SunnySky motor and 12x6" prop propulsion calculations .....	106
Figure 80 - X-8 Aircraft 1 internal layout.....	107
Figure 81 - Nose mounted FPV camera, CO2 intake, and pitot tubes .....	108
Figure 82 - X-8 Test Airframe 2 .....	108
Figure 83 - Turnigy motor and 13x6.5" prop propulsion calculations.....	110
Figure 84 - X-8 Aircraft 2 internal layout.....	111
Figure 85 - Oklahoma State Unmanned Aircraft Flight Station .....	112
Figure 86 - Epoxy potted DF13 connectors .....	113
Figure 87 - Improved autopilot cable.....	113

Figure 88 - Pixhawk strain relief enclosure .....	114
Figure 89 - Pixhawk strain relief enclosure with wiring.....	114

## CHAPTER I

### INTRODUCTION

#### I. MOTIVATION

Carbon sequestration is the injection of CO<sub>2</sub> for storage in geologic formations deep underground. It has the potential to greatly reduce the levels of greenhouse gases in the atmosphere and decrease one of the major driving factors behind climate change. To know if it is effective, however, low cost atmospheric gas monitoring technologies are necessary to understand how much CO<sub>2</sub> is leaking back into the atmosphere.

The application of unmanned aircraft systems (UAS) could potentially develop such a system. UAS are small, relatively inexpensive aircraft which can be remotely piloted or operate autonomously. They excel at what are referred to as the dull, dirty, and dangerous types of flying – the types which are best to have pilots avoid if at all possible. UAS also cost much less to operate than manned aircraft, allowing for them to be used more often and in situations that would not be financially feasible to use a manned aircraft. In particular, UAS have the potential to be used to efficiently monitor large areas of land to detect increased emissions of greenhouse gases such as methane (CH<sub>4</sub>) and especially carbon dioxide which could be released from large scale carbon sequestration projects.

## II. PROJECT BACKGROUND

This project is part of a much larger effort by the United States Department of Energy (DoE) and National Energy Technology Laboratory (NETL) to further understand the process of carbon sequestration and develop technologies and methodologies to allow it to become a safe, common commercial process. Their goal is ensure that 99% of CO<sub>2</sub> injected underground is stored permanently. To achieve this, they developed seven regional partnerships across the United States which consist of local energy companies, research universities, utilities, and government entities working together to perform and study carbon sequestration projects.

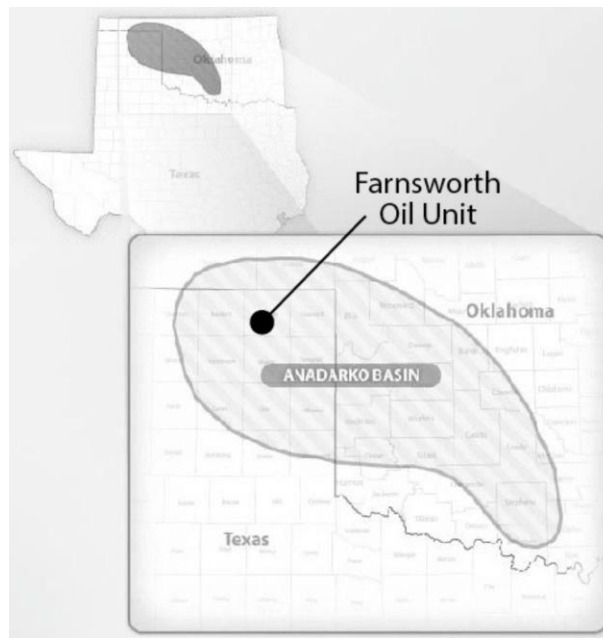


**Figure 1 - SWP Farnsworth Oil Unit in Anadarko Basin (Clark, et al. 2013)**

Oklahoma is part of the Southwest Regional Partnership (SWP) that also includes Kansas, Oklahoma, West Texas, New Mexico, Colorado, Arizona, Utah, and South Wyoming. One of SWP's major projects is the Farnsworth Unit located in the North Texas panhandle in the Anadarko Basin as shown in

Figure 1. It is a combined CO<sub>2</sub> enhanced oil recovery (EOR) and storage project in which carbon dioxide gas is pumped into oil and natural gas reservoirs to both store the CO<sub>2</sub> and help pump out



additional oil and natural gas. The goal of this project is to test CO<sub>2</sub>-EOR and storage on a commercial scale and apply the techniques to future planned commercial scale projects. The carbon dioxide is pumped into the Pennsylvanian upper Morrow sandstone play which is 20-40 ft thick and 8000 ft deep. The upper Morrow is capped by a Permian evaporate layer which acts as an upper seal as shown in Figure 2. The formation has an estimated storage capacity of 10 million tons of CO<sub>2</sub>. The plan for the Farnsworth unit is to inject 1 million tons over 5 years of the project starting in January 2011 and continuing through 2015. The carbon dioxide is primarily sourced from a fertilizer plant in Borger, TX and an ethanol plant in Liberal, KS. (US Department of Energy 2012)

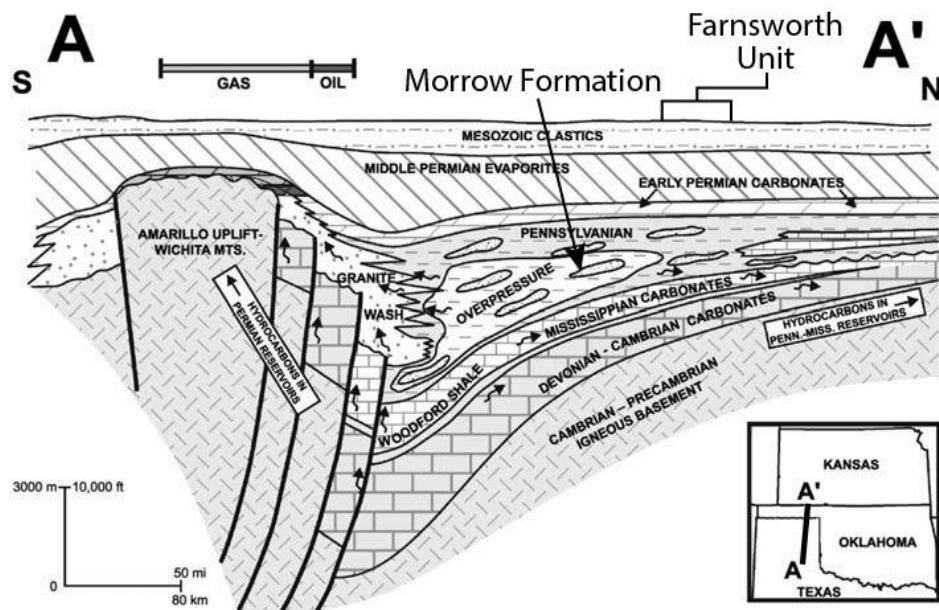


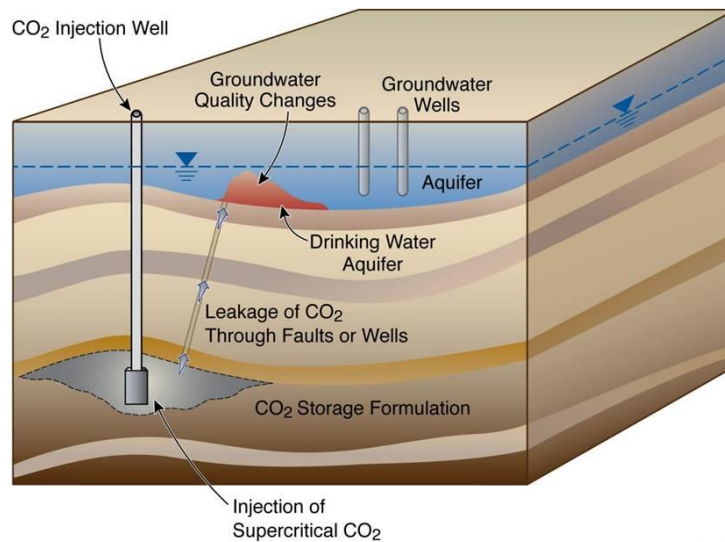
**Figure 2 - Cross section of underground formations in Anadarko Basin (Clark, et al. 2013)**

Oklahoma State University (OSU) has been funded through the DoE and NETL to help participate in the study of the Farnsworth Unit. In particular, OSU will study their area of interest which focuses on “Tools and technologies that clearly identify potential or actual CO<sub>2</sub> leakage pathways”. A concern is that fractures and faults in the Permian evaporate and other sealing layers such as those shown exposed to the surface in Figure 3 could allow carbon dioxide to

escape the underground reservoirs. In addition, flaws in the wellbore casing or cement could allow leaks in the drilled portions of the evaporate. In addition to leakage into the atmosphere, it is also a concern that CO<sub>2</sub> could leak into drinking water aquifers as illustrated in Figure 4.



**Figure 3 - Exposed fractures near Farnsworth Unit**



ESD08-002

**Figure 4 - Illustration of CO<sub>2</sub> sequestration and potential leakage**

To help study these potential issues, OSU has assembled a multi-departmental team to work on the various aspects of the project. The Geology Department will study the fractures and other potential subsurface leakage pathways. Their analysis will identify the locations of greatest

interest to monitor for possible leaks. Teams from the Chemical Engineering, Chemistry, and Civil Engineering Departments will then develop and deploy a ground sensor network to monitor for CO<sub>2</sub> and CH<sub>4</sub>. In addition to traditional monitoring techniques, they plan to deploy at least 160 sensors over a 640 acre site. This network consists of a series of low cost, wireless sensors that communicate with each other in addition to several larger, more expensive sensors that will serve as calibration nodes. The sensors will be placed immediately above the surface as well as drilled to a depth of 1m underground to measure both the atmospheric and subsurface flux of gases. To supplement this sensor network, the Mechanical and Aerospace Engineering Department will develop airborne sensor systems to be deployed aboard unmanned aircraft. The levels recorded from the aircraft can be verified against those from the ground network. Once proven as a reliable system, the aircraft can then be used to monitor levels over a large area while the sensors can be repositioned to study in more detail the areas of higher interest. Finally, data processing methods and algorithms will be developed by faculty from the Mechanical and Aerospace Engineering Department to find the most efficient methods to collect and analyze the data from the various systems (Clark, et al. 2013).

The goal of this thesis is to develop the first stage of the unmanned aircraft atmospheric carbon dioxide detection system. Accomplishing this will include development of a sensor system similar to those used on the ground sensor network and development of an unmanned aircraft to perform the CO<sub>2</sub> detection mission. This will culminate in the integration of the systems and flight testing to prove initial capabilities. The primary objective is to detect areas with increased levels of carbon dioxide in comparison to the ambient levels. This is opposed to quantifying the CO<sub>2</sub> emissions which would add complexity to the system and require detailed calibration and testing to determine the accuracy of system and the environmental factors that affect that accuracy. The secondary objective is to develop the system at a low cost in a range of several thousand dollars to create an economical alternative to ground based sensor networks. Ultimately,

the end result of this stage of the project is to demonstrate through ground and flight testing the feasibility of using a low-cost unmanned aircraft to detect locations with increased atmospheric carbon dioxide levels.

## CHAPTER II

### BACKGROUND

#### **I. BACKGROUND**

##### A. ATMOSPHERIC CARBON DIOXIDE TRENDS

The increased release of carbon dioxide into the atmosphere is a major concern of our industrial society's impact on the environment. It is a greenhouse gas which causes the Earth to retain more heat from the sun and contribute to global warming. In 2012 the United States alone released 5,358 million metric tons (MMT) of carbon dioxide which accounted for 82.2% of the 6,545 million metric tons (of CO<sub>2</sub> equivalent) of greenhouse gases (such as methane, nitrous oxide, and others) released by the US that year. 93.7% of that carbon dioxide came from the combustion of fossil fuels, our primary source of energy. That amount of CO<sub>2</sub> released, however, was only 16% of worldwide CO<sub>2</sub> emissions from fossil fuels in 2012, which totaled 32,310 MMT (U.S. Environmental Protection Agency 2015).

Earth can process and absorb carbon dioxide, but not in the increasingly high quantities produced as shown in Figure 5. The average CO<sub>2</sub> level in the atmosphere was  $396.0 \pm 0.1$  parts per million (ppm) in 2013. This is often compared to the level in 1750, the beginning of the industrial revolution and considered the starting point of manmade greenhouse release, which was 278 ppm – showing current values are a 142% increase. The atmospheric levels of CO<sub>2</sub> have increased

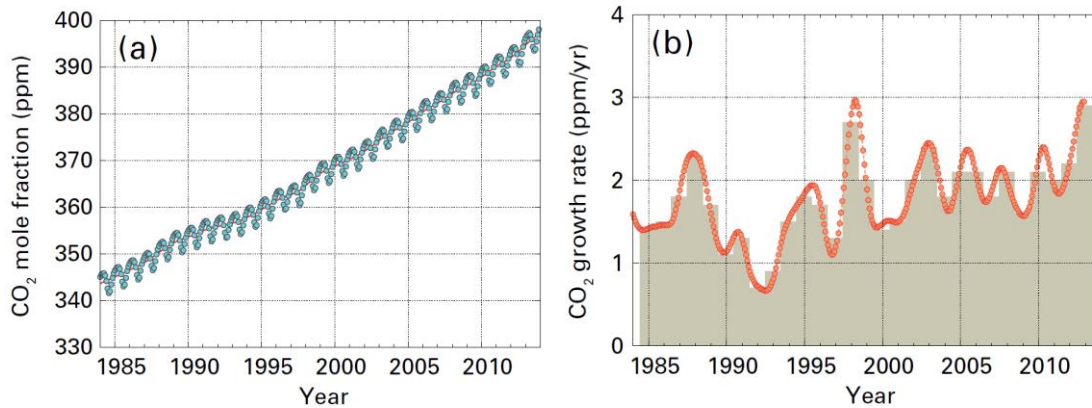


**Figure 5 - Average global CO<sub>2</sub> mole fraction (a) and growth rate (b) (World Meteorological Organization 2014)**

2.9 ppm between 2012 and 2013 alone, the highest yearly rise since 1984. Other gases contribute to climate change as well, but CO<sub>2</sub> is by and far the most abundant. In the last ten years it was responsible for 84% of the increase in radiative forcing – the cumulative increase in the amount of energy the Earth absorbs, essentially the increase in heat trapped by greenhouse gases. If the emissions of carbon dioxide continue unchecked at these rates it will continue to have negative impacts on our environment, with various disastrous consequences predicted. Because so much of the release of carbon dioxide comes from the combustion of fossil fuels, reducing their use is one of the solutions, but switching to alternate forms of energy will take decades and other means are needed to help curb and reduce carbon emissions. (World Meteorological Organization 2014)

## B. CARBON SEQUESTRATION

Geosequestration is “the storage of greenhouse gases in geological formations after capture from a source that would otherwise emit to the atmosphere” (Ethridge, et al. 2005). These gases are often captured from a fossil fuel or industrial gas waste stream. They are then pumped underground into geologic reservoirs for long-term storage. To be effective, the leak rates out of these storage sites must be low enough to make the process worthwhile, both financially and to counter the additional gas that could be produced in the transport and storage of the CO<sub>2</sub>. The gas will eventually return to the atmosphere: short term storage is considered 100-10,000 years while

long term storage is on the order of  $10^6$ - $10^8$  years. The goal is to store CO<sub>2</sub> underground long enough for the Earth's ecosystem to naturally process it after carbon use has been reduced (Ethridge, et al. 2005).

As previously mentioned, one of the biggest potential sources of carbon capture is fossil fuel power plants. A 1000 MW coal plant emits 6-8 megatons of CO<sub>2</sub> per year, oil fueled power plants produce roughly two-thirds of that amount, and natural gas produces half. Another major source is manufacturing processes. Natural gas refining produces large amounts of CO<sub>2</sub> that was originally trapped underground along with the methane and must be separated. Ammonia manufacturing, fermentation, and hydrogen production are all potential sources of carbon dioxide to be used in sequestration. For reference, in 2004 global emissions were 7 gigatons of carbon equivalent (GtC), a standardized unit of carbon-based gas emissions; 3.7 gigatons of CO<sub>2</sub> are equal to 1 GtC. Global capacity of carbon sequestration is estimated at 200-12,000 GtC in geosequestration and an additional 1000-10,000 GtC in the ocean – a separate process from that covered here (Herzog and Golomb 2004).

Underground CO<sub>2</sub> injection is a proven process that has actually been performed for decades. Carbon dioxide and other waste gases from drilling and refining are pumped into oil and gas reservoirs to pump out additional oil and natural gas in a process known as enhanced oil recovery (EOR). The focus now is to modify the process to also store the carbon underground permanently. As far back as 2000 there were 72 EOR projects in the United States (out of 84 worldwide) and combined they produced 200,772 barrels of oil per day (Herzog and Golomb 2004). One example is Mumford Hills, a carbon EOR well that is being studied by another partnership, the Midwest Geological Sequestration Consortium (MGSC), as a carbon storage case study. It went from a production rate of 0.5-1 barrels per day before carbon injection to 3-5 barrels per day after injection. Overall it produced an estimated 2100 barrels more than the expected 600 barrels and 99.5% of the 7000 tons of injected CO<sub>2</sub> stayed in the ground (US

Department of Energy 2012). Another major site being studied is Weyburn Field in Canada where, as of 2010, 18 million tons of CO<sub>2</sub> had been injected since the project started in 2000 and an additional 160 million barrels of oil were produced (Whittaker 2010).

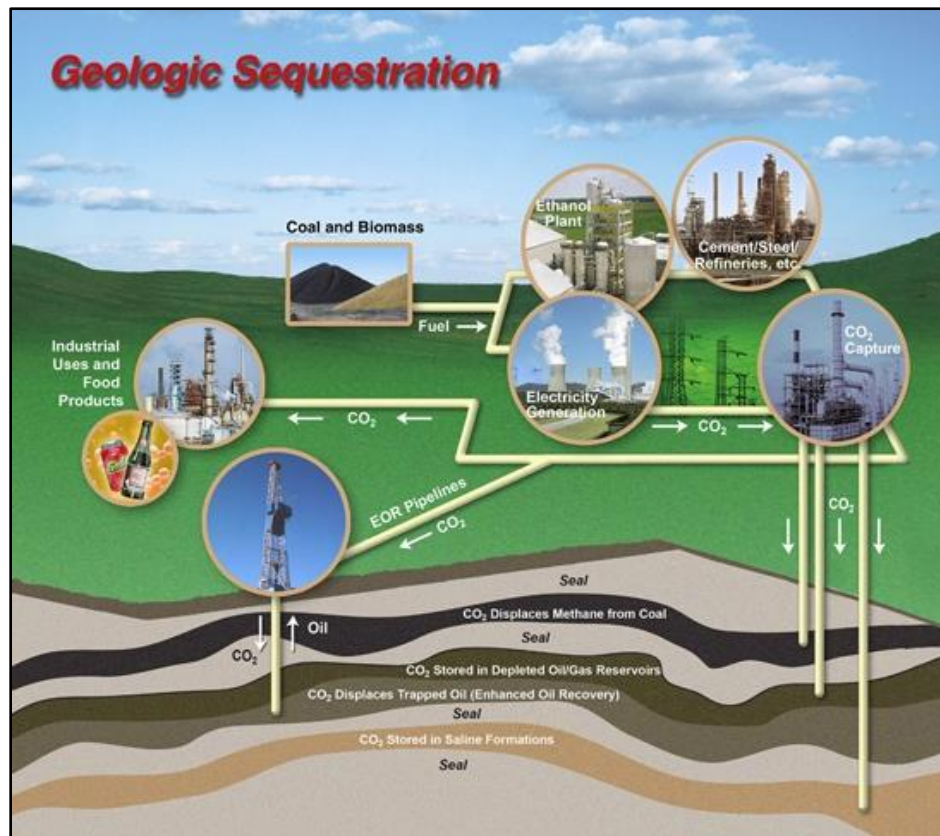


**Figure 6 - DoE CO<sub>2</sub> geologic sequestration infographic (U.S. Department of Energy Office of Fossil Energy n.d.)**

As illustrated in Figure 6, there are also several other ways to store carbon dioxide underground. It can be pumped into low-grade coal seams that aren't worth mining and the CO<sub>2</sub> is absorbed into the coal in a process similar to when using coal as a filter. In addition, this helps release coal bed methane, methane embedded in the coal formations. Another major method is storage in deep saline formations. The carbon dioxide is injected very deep, 800 m or more, when the gas is reaching a supercritical state and has a very high density. It is injected into very deep saline aquifers (which are far below drinking water aquifers and topped by cap rocks that seal them from the layers above). Because of solubility the CO<sub>2</sub> dissolves into the saline liquid or reacts



with minerals to become solid carbonites; though some recent research suggests that it does not react as effectively as thought and instead forms gas pockets (Cohen and Rothman 2014).

Otherwise, though, deep saline injection is considered the most permanent carbon sequestration method because it is no longer a gas and cannot leak out as in oil/gas reservoir EOR and storage and coal bed methane storage (Herzog and Golomb 2004).

### C. CURRENT ATMOSPHERIC CO<sub>2</sub> MEASUREMENT METHODS

There are already a variety of methods used to measure carbon dioxide levels in the atmosphere. These systems cover a range of technologies, but many of them are fundamentally based upon CO<sub>2</sub>'s absorption of certain wavelengths of light. Carbon dioxide absorbs several different wavelengths, such as 1.57  $\mu\text{m}$ , 2.05  $\mu\text{m}$ , and 4.26  $\mu\text{m}$ , among others (Fix, et al. 2011). Each wavelength offers different benefits such as ease of measurement, interference with other gases, range, etc. but they primarily all fall within the infrared spectrum. Point measurements of CO<sub>2</sub> can be performed with a large variety of instruments. Some low-cost personal detectors use electrochemical sensors, but the majority operate off of infrared absorption, or spectroscopy, technology. The most common form is non-dispersive infrared (NDIR) in which an infrared laser is shined through either a chamber or the open atmosphere and a detector measures how much of the light was absorbed by carbon dioxide. More advanced forms include Fourier Transform Infrared Spectroscopy (FT-IR) and Wavelength Scanned Cavity Ringdown Spectroscopy (WS-CRDS) which use much more advanced spectroscopy techniques that can detect multiple gases and isotopes, but still work on the same basic principle. These sensors can vary in size and shape from the small sensors that will be used in this project to large bench or rack mounted systems. Although they only take point measurements of whatever gas is introduced to their sensor, they are very accurate systems and comprise the majority of sensors used in scientific carbon dioxide measurement (US Department of Energy 2012).

Similar, but longer range, types of sensors are differential absorption LIDAR (laser-based radar), known as DIAL systems. Instead of directly measuring the infrared laser of a known strength across a known path, DIAL systems measure the amount of light that is reflected back when the laser is aimed at objects very long distances away. This is done by using two separate lasers, one that is tuned to the wavelength of the gas being measured (in this case CO<sub>2</sub>) and another at a wavelength which will not be absorbed and is used as a reference. This is considered a remote sensing system because it can measure gases from between hundreds to thousands of meters away. This makes them excel at measuring gases over large areas, but they are very complex, large, and expensive. They have been mounted to aircraft and vehicles with some success (Quatrevalet, et al. 2010) as shown in Figure 7 although it can be seen the large space required for such systems. These systems do, however provide a great way to identify high concentrations of leakage over large areas as shown in Figure 8.



**Figure 7 - Vehicle and aircraft based DIAL systems (National Physical Laboratory 2012) (Brake 2005)**

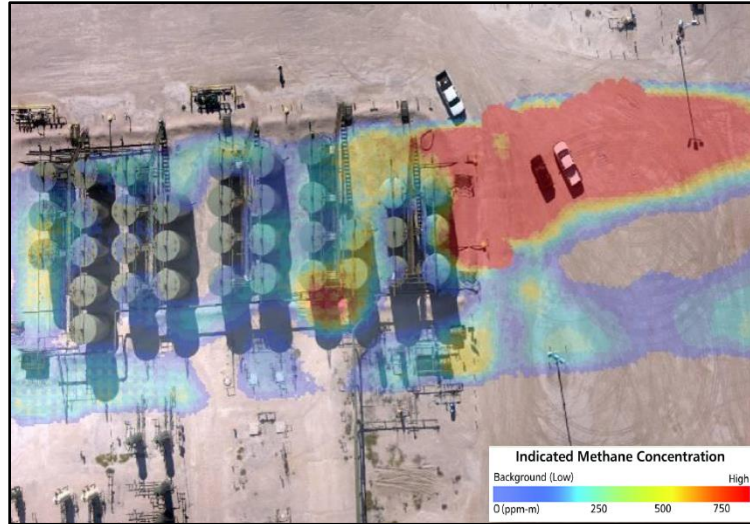


**Figure 8 - Example DIAL methane survey (Brake 2005)**

This technique also forms the basis for several satellites measuring greenhouse gases including NASA's recently launched Orbital Carbon Observatory satellite, although it uses the sun as its source of light in place of an onboard laser (Frankenberg, et al. 2015). Work is also currently being done to develop smaller DIAL systems for use at carbon sequestration sites, although these systems still take several racks of components and could not fit aboard an unmanned aircraft (Johnson, Repasky and Carlsten 2013).

One of the most common systems used to measure atmospheric CO<sub>2</sub> levels and flux over large areas are eddy covariance systems such as those manufactured by Li-Cor Biosciences. Although NDIR sensors are used to measure the CO<sub>2</sub> levels in these systems, the suite of sensors and measurement method make eddy covariance a unique type of system. They essentially compare how wind vectors in all three directions vary with CO<sub>2</sub> levels to determine the amount of CO<sub>2</sub> flux occurring over an area. Usually mounted on tower of varying height, eddy covariance systems include, as shown in Figure 9, an omni-directional sonic anemometer to measure the 3D direction of air flow, both open and closed (flow-through) path H<sub>2</sub>O/CO<sub>2</sub> NDIR sensors, and a fine wire thermocouple to serve as a hot-wire to measure turbulence.

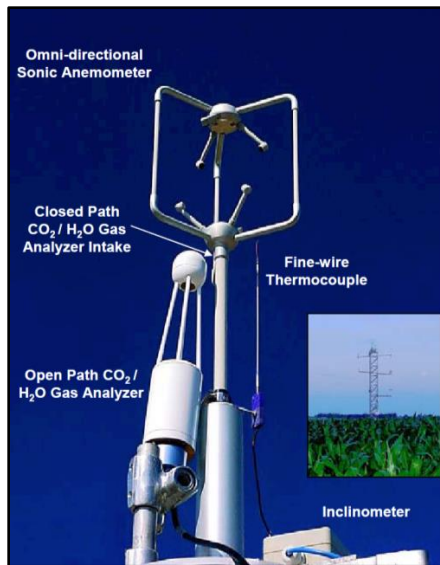


**Figure 9 - Example eddy covariance tower sensors (Burba and Anderson 2007)**

All of these sensors run at high speed, 10-20 Hz, to catch very small eddies in the atmospheric boundary layer. The CO<sub>2</sub> flux over an area is calculated, in short, by measuring how much gas is carried upwards by this turbulence compared to how much gas returns back down on these eddies; the net difference is the amount of carbon dioxide being emitted from the area. Flat terrain is a requirement for this system; changes in density caused by altitude changes interfere with the calculations and the algorithms also work on the assumption that flow is uniform, but turbulent. The range of these systems is affected by variables including the terrain, mounting height, and weather, and can measure from between 50-500 m upwind. These flux levels are averaged over at least 30 minutes and, despite the varying nature of the data, the end result is a very reliable measurement of the flux of CO<sub>2</sub> over a large area. A shortfall of this system, however, in addition to the terrain restrictions, is its ineffectiveness at night. The diurnal cycle, illustrated in Figure 10, is the heating of Earth during the day and cooling at night, causing turbulent atmospheric mixing between the heating layers throughout the day and calmer stratification of the layers during the night. This lack of wind and turbulence remove some of the key components of eddy covariance measurements causing the system to not measure reliably at night. This atmospheric mixing should also be taken into consideration for any aerial measurements as the

time of day will greatly affect the concentrations and dispersion of CO<sub>2</sub> (Burba and Anderson 2007).

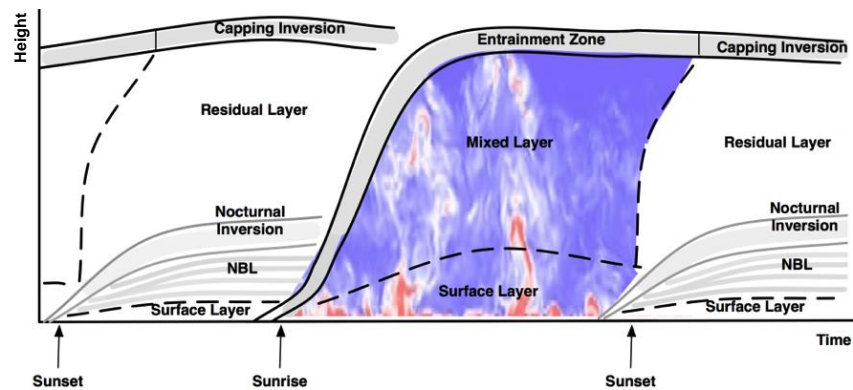


**Figure 10 - Diurnal cycle of Earth's atmosphere (Clark, et al. 2013)**

A novel method being used to detect leaks from carbon sequestration sources is the introduction of tracer gas into the CO<sub>2</sub> being injected underground. These tracers, often gases that are not ordinarily found in the environment, are very easily detectable as opposed to the difficulty of measuring fluctuating CO<sub>2</sub> levels and determining if they came from natural variation or a carbon sequestration leak. Gases commonly used include sulfur hexafluoride (SF<sub>6</sub>) or a perfluorocarbon tracer (PFT). If these gases are detected it makes it very clear that carbon dioxide is leaking from the storage site. A disadvantage of this system, however, is that these tracer gases may not disperse in the atmosphere the same way as CO<sub>2</sub>, meaning that while they can be very helpful in detecting a leak, they may not be useful in quantifying the leak. These gases also may react with minerals and liquids underground and not escape as easily as carbon dioxide. Natural tracers also occur in the CO<sub>2</sub> such as methane, radon, and carbon isotopes which are found in manufactured CO<sub>2</sub> but not natural carbon dioxide, but introducing unique gases is likely the most effective method if possible. Work is currently being done to develop new types of tracer gases which will better mimic the movement and dispersion of CO<sub>2</sub> so both gases travel to the same places in similar quantities (US Department of Energy 2012).

#### D. ATMOSPHERIC PLUME MODELING

To know where to expect the CO<sub>2</sub> concentrations, it is helpful to develop mathematical models of the gas in the atmosphere. There are multiple ways to model plumes, but a good straightforward method involves modeling the plume as a constant 3D source much in the same way as pollutants from a smokestack would be modeled. This type of modeling consists of two main components, diffusion and advection as shown in Figure 11. Diffusion is the tendency of concentrations of a gas or liquid to disperse over time. This is governed by Equation 1 as shown below which consists of the gradient of the product of the diffusivities (D) and spatial change of the concentration as well as factors for the velocity (v) and decay ( $\lambda$ ) (Holzbecher 2012).

### Equation 1 – 3D Gaussian diffusion

$$\frac{\partial c}{\partial t} = \frac{\partial}{\partial x} D_x \frac{\partial c}{\partial x} + \frac{\partial}{\partial y} D_y \frac{\partial c}{\partial y} + \frac{\partial}{\partial z} D_z \frac{\partial c}{\partial z} - v \frac{\partial c}{\partial x} - \lambda c$$

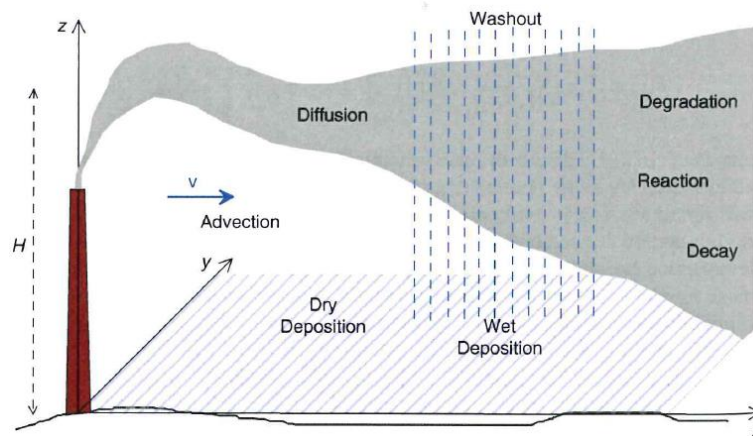


**Figure 11 - Illustration of basic components of plume model from a smokestack (Holzbecher 2012)**

When combined with advection, the movement due to the wind, and some decay, this produces a form of Gaussian model as shown in Equation 2 and illustrated in Figure 12 which is based upon a Gaussian distribution of the gas as opposed to uniform distribution. The standard deviations,  $\sigma$ ,



and  $\sigma_x$ , are therefore major components in determining the shape of the plume (Vaz and Ferreira 2008).

**Equation 2 - Gaussian plume model**

$$c(x, y) = \frac{Q}{\pi v \sigma_y \sigma_z} \exp\left(-\frac{1}{2} \left( \frac{y^2}{\sigma_y^2} + \frac{H^2}{\sigma_z^2} \right)\right)$$

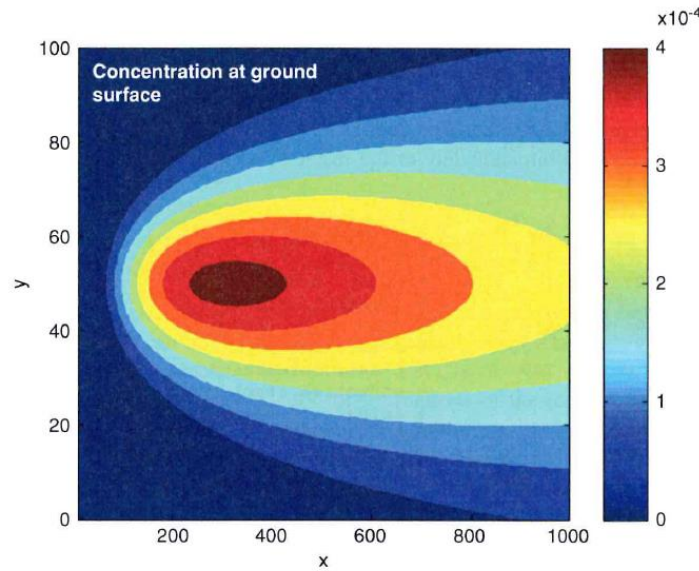


**Figure 12 - Sample Gaussian plume model in XY plane below the release point (Holzbecher 2012)**

## **II. LITERATURE REVIEW**

### **A. MANNED AIRCRAFT TESTING**

Manned aircraft have often been used for atmospheric carbon dioxide measurement. One such pair of examples are the Gulf of Tehuantepec Experiment (GOTEX) and Carbon in the Mountains Experiment (ACME) performed by the National Science Foundation (Campos, et al. 2005). Both of these tests were flown in 2004 aboard a U.S. C-130 military transport aircraft operated jointly by the National Science Foundation and National Center for Atmospheric Research. The purpose was to measure CO and CO<sub>2</sub> in the atmosphere released by fossil fuel combustion. The aircraft was equipped with a LI-COR 6252 analyzer aboard, a benchtop NDIR gas sensor. The sensor was

modified with temperature and pressure regulation for use in the operating environment. The flow rate and drying systems were improved over the previous system setup to improve the time response. Air flowed through the system at 2 SLPM and at 400 mB. The dryer system consisted of a naifon dryer and a cryo trap to lower the dew point to -30 °C (which was required to stop ice particles that formed and were ingested). The CO<sub>2</sub> system was regularly calibrated in flight using reference gases of 360, 370, and 395 ppmv. During the GOTEX experiment data was recorded at 1 kHz in back-to-back 2 minute segments and a 0.3 s median filter was applied. During the ACME flight data was recorded at 25 Hz continuously and a 1 s filter was applied. Both sets of data were then downsampled to 5 Hz. The results were then validated by comparing them to the newest standards for atmospheric gas levels developed by NCAR as well as against flask samples. Overall, the mean difference was found to be only 0.2 ppmv.

#### B. UAS TESTING OF ENVIRONMENTAL LEVELS

An early test of measuring atmospheric carbon dioxide levels using unmanned aircraft was conducted by the National Institute of Environmental Studies in Tsukuba, Japan in 2000 (Watai, et al. 2006). They put a measurement system aboard a 28 lb gas powered pusher propeller kite plane as shown in Figure 13. Air was brought into the system through a pump and intake tube and went through a chemical desiccant before reaching the LI-COR LI-800 NDIR CO<sub>2</sub> sensor.

Airflow was kept constant at 0.15 LPM and at 0.12 MPa as measured by a Honeywell AWM series flowmeter and controlled by a pair of thermal valves. The system took 1 Hz measurements of CO<sub>2</sub> level, temperature, and pressure. The total device weight was 7.7 lbs.



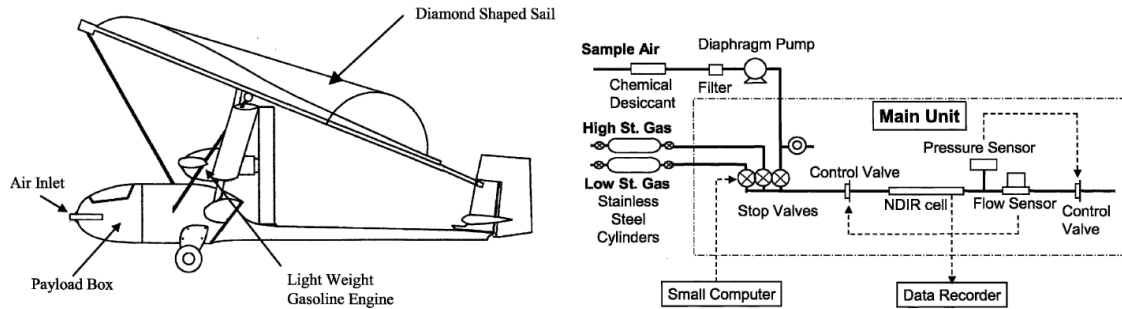


**Figure 13 - Early atmospheric CO<sub>2</sub> measurement UAS and sensor system schematic (Watai, et al. 2006)**

The system constantly performed in-flight calibrations to ensure the accuracy of the measurements. Two sample gases, a high concentration (393 ppm) and low concentration (349 ppm), were carried onboard in pressurized steel canisters. These gases were measured five times on the ground before launch to ensure their accuracy. In flight, the measurement cycle would sample the high concentration gas for 30 s, followed by the low concentration gas for another 30 s, and then perform five minutes of atmospheric measurements. It was found that the chemical desiccant used decreased the CO<sub>2</sub> levels by 0.18 ppm and ambient temperature drops of 10 °C would decrease levels by an additional 0.21 ppm. The main issue they encountered was with pressure fluctuations affecting the flow rate at altitudes above 4000 m. It was found that the response time of the system was on average 20 s based upon delays in expected changes of CO<sub>2</sub> levels during altitude changes. The results of the testing showed that carbon dioxide begins the day stratified with high concentrations near the ground (~380-390 ppm) and as the temperature increases throughout the day causing turbulent mixing of the atmospheric layers the gas level became ~360 ppm by around 9:00-11:00 am when the layers were fully mixed. At lower altitudes (200-600m) the CO<sub>2</sub> level was between 360-370 ppm and at higher altitudes (650-1800 m) the levels were closer to 360 ppm. At high altitudes late in the day a small increase in levels was detected, determined to likely be from the ocean air bringing in more CO<sub>2</sub>.

### C. UAS TESTING OF SIMULATED LEAK SOURCE

A more recent test with the specific purpose to detect CO<sub>2</sub> emissions from carbon sequestration sites was performed by Australian National University in Canberra (Poppa, et al. 2013). They determined that for a leak to be detected by a ground station against the background levels of CO<sub>2</sub> (~390 ppm) at a distance of 1 km away, the leak would have to be at least 20 tons/day. To provide an additional method of measurement, they developed an unmanned helicopter to measure CO<sub>2</sub> levels. This was based on their previous work in which they made a quadcopter to measure gas levels. The quadcopter was equipped with a Dräger X-am5600 personal gas monitor (using infrared and electrochemical sensors to detect multiple gases). They performed wind tunnel tests to determine the best placement of the sensor for accurate readings with high response. It was tested in a passive configuration (simply mounted to the exterior out of the prop wash), semi-active (airflow through the rotors directs air into an intake tube connected to the sensor), and active setup (in which the tube is in the free-stream flow and a pumps bring air into the sensor). The active was found to be the best system, measuring 66% of the actual CO<sub>2</sub> concentrations. Each air sample was taken by hovering over a location for 20 s to fully measure the values and then each data point was added to a heat map for visualization of potential leaks.



**Figure 14 - Helicopter UAS for carbon sequestration leak detection (Poppa, et al. 2013)**

For the improved helicopter aircraft pictured in Figure 14, they investigated using laser-based remote sensing methods and even tested out a short range methane detection laser on a remote control car, but ultimately it was determined that the aircraft would have to fly too close to the ground because the lasers that could be carried have such a short range. Previous subsurface tests showed that when releasing 100 kg of CO<sub>2</sub> per day the CO<sub>2</sub> level 20 m away from the release site would be only around 10 ppm above ambient. An issue that the system faced is that because it is a helicopter, the rotors mixed the air so the CO<sub>2</sub> levels recorded just represented an average for the area. The aircraft was fitted with a Vaisala GMP343 diffusion sensor which has an accuracy of  $\pm 3$ ppm and a response time of 2 s if the filter is removed. The sensor was mounted on a gimbal on a T-Rex 700E helicopter. Tests were performed to see if the probe was accurate in motion; a concern was that the moving air would reduce temperatures and pressure and affect the gas readings. To do this, the sensor was placed outside of the window of a moving car to see if velocity correlated with CO<sub>2</sub> readings. It did not, showing that the temperature changes from the airflow did not affect the measurements and the heating probe's purpose was likely to prevent moisture from accumulating on the optics.

For the flight test portion the helicopter flew 2 m over the emission source. The filter was reattached on the sensor, but although it decreased the response time, the downwash from the rotors was expected to increase the flowrate enough to compensate. Each time the aircraft flew over the CO<sub>2</sub> release source the sensor detected CO<sub>2</sub> spikes as shown in Figure 15 but each subsequent pass detected decreased levels which was assumed to be because the downwash of the blades dispersed the gas. The leak rate was set to be equivalent to 100 kg/day and the helicopter measured spikes of up to 460 ppm compared to the background levels of 375 ppm. Future work will include mounting laser altimeters to the aircraft to fly at consistent altitudes in a grid pattern to develop a CO<sub>2</sub> distribution map for the area, similar in many ways to the work of this project.

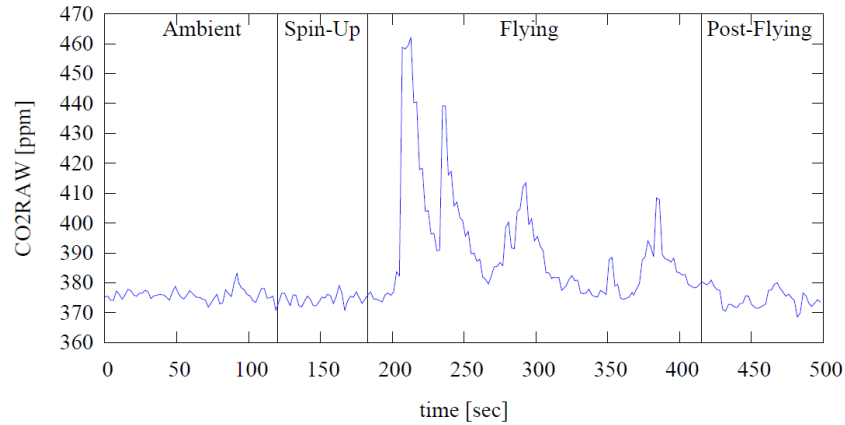


**Figure 15 - CO2 levels recorded by helicopter UAS (Poppa, et al. 2013)**

#### D. SURFACE LEVEL CARBON ISOTOPE MEASUREMENTS

Ground tests to map CO<sub>2</sub> levels have previously been performed such as those at the Zero Emissions Research and Technology test site operated by the University of Montana (Spangler, et al. 2010). These tests (Krevor, et al. 2010) measured carbon isotope  $\delta^{13}\text{C}$  – a natural tracer in the anthropogenic CO<sub>2</sub> which was pumped underground and not present in the same quantities in biogenic carbon dioxide. The sensor used was a Picarro Wavelength Scanned Cavity Ringdown Spectroscopy (WS-CRDS) unit. This sensor was part of a 60 lbs system on a cart which pumped air in from 9” off of the ground at 150 mL/min (providing a 4s residence time in the optical cavity). The CO<sub>2</sub> levels and GPS location were recorded at 1 Hz while the system was pushed around the simulated sequester source at roughly 1-2 m/s. The simulated source released CO<sub>2</sub> from a 1-3 m deep 100 m horizontal well at a rate of 0.2 tonnes of CO<sub>2</sub> per day for 30 days; a rate similar to a commercial sequestration site leaking at 0.001% to 0.01% annually. Each pass was approximately 5 m apart; an example of the raw data from the measurement path is shown in Figure 16. The data was then broken down into 10 m x 10 m grids and Keeling plots were made showing the ‰ of  $\delta^{13}\text{C}$ . The results were then mapped at 1 m resolution, interpolated using triangulated linear interpolation, and outliers showing a change greater than 10 ppm/s were omitted. This produced a map of the area showing the ratio of the isotopes of CO<sub>2</sub>. It was found

that areas on this map showing an isotope ratio indicative of anthropogenic CO<sub>2</sub> were located along the pipeline where leaks were occurring. It was estimated that taking measurements at a similar rate using a motorized vehicle would allow coverage of 40-85 km/day which would take 2-4 weeks to cover the 1000 km traverse of a 100 km<sup>2</sup> commercial sequestration project.

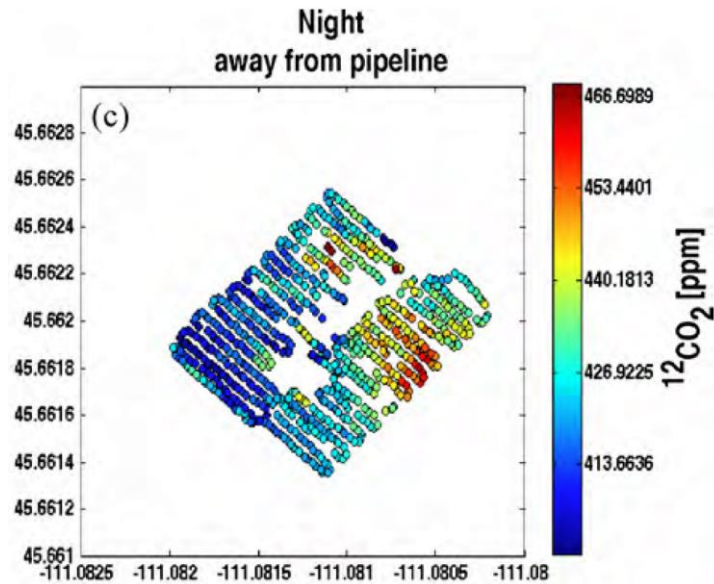


Figure 16 - Raw measurements of <sup>12</sup>CO<sub>2</sub> at ZERT field site (Krevor, et al. 2010)

#### E. NDIR SENSOR COMPARISON STUDY

Various studies have been performed previously to compare and validate various non-dispersive infrared CO<sub>2</sub> sensors. One such study was performed by the University of Shizuoka in Japan (Yasuda, Yonemura and Tani 2012). NDIR sensors are very stable and resist interference from pollutants, but can be affected by temperature, pressure, and length of use as this study found.

Five diffusion-type NDIR sensors were compared including the Vaisala GMM222C, SenseAir K-30, ELT S100, KCD AN100, and GE Sensing T6615. The output of these sensors was first measured by placing the sensors in a test chamber successively filled with nitrogen based reference gases between 0-1810 ppm. The gas flowed into the box at 1 LPM and the sensors were powered for 30 minutes before measurements to allow for warm-up. Recordings were taken at

various temperatures and periods of time after first use (up to 306 days). The sensors were calibrated by creating an offset as well as coefficient of correction for the temperature, pressure, and number of days operated and the RMS error was then minimized using these values. Field measurements were also taken using a handheld unit based upon an ATmega2560 microcontroller which logged the CO<sub>2</sub> levels, humidity, temperature, and GPS location to an SD card. These measurements were taken inside of a classroom and compared against those of a LI-COR 6262.

It was found that both the number of days and temperature increased the required correction factor. The K-30 required the least correction and that correction was uniform across all of the K-30 models tested. When compared with the measurements of the LI-COR 6262, the K-30 with the correction factor applied displayed a RRMS difference in CO<sub>2</sub> values of 3.5%. There was a linear relationship between the length of use and correction required for times up to one year. The response time of the sensors did not show any correlation with the length of use or temperature.

## CHAPTER III

### EQUIPMENT DESIGN AND TEST SETUP

#### I. SENSOR SYSTEM

The heart of this project is the sensor system that detects the carbon dioxide and logs its values and the other various data that is required to identify a plume. Though it is possible to control and log data from some of these sensors through the autopilot, it was chosen to make the sensor system an entirely self-contained system. Though does take up some more space and weight, this method allows for a variety of benefits that are particularly helpful when developing a prototype electronics system: the system can be removed easily to be installed in another aircraft (such as the Firebird) or used outside of the aircraft for ground tests, it offers more expandability to add additional sensors or rearrange components, all sensor types can be used (the Pixhawk does not easily allow serial communication, only I2C and analog), it is easier to program and change programming compared to the Pixhawk (which requires custom drivers and changing the firmware to communicate with additional sensors), and there is less chance of interfering with the autopilot (whether through affecting its processing or changing its programming).

The sensor system was based upon an Arduino microcontroller to handle all of the communications and processing. A SenseAir K-30FR was chosen as the CO<sub>2</sub> sensor to detect gas levels. The 3D position was obtained from a GPS unit for latitude and longitude as well as a

pressure altimeter for altitude. Other sensors included a flowmeter, temperature/humidity sensor, and pressure sensor. All of this data was logged to an SD card connected to a board that includes a real-time clock to provide a timestamp of each run. All of these systems run off of 5V power that can easily be provided by the Arduino's built in regulator with the exception of the flowmeter which requires 10V. Powering this sensor involved integrating a voltage step-up circuit to boost the voltage. This system can be easily powered by a 2S (7.4V) lithium-polymer battery and is primarily contained in two modular plastic enclosures for protection and ease of handling. One enclosure, called the data box, contains the Arduino, SD card, and altimeter. The second enclosure, the sensor box, contains the CO<sub>2</sub> sensor with pass-through tubing, 10 V voltage circuit, pressure sensor, and temperature/humidity sensor. The boxes are connected through a standard RJ-45 ethernet cable, chosen because it is a widely available cable and provides eight wiring channels. External to the boxes are the GPS and flowmeter. The system, shown in Figure 17, was designed to be modular and low-cost, achieving a final cost of <\$500.

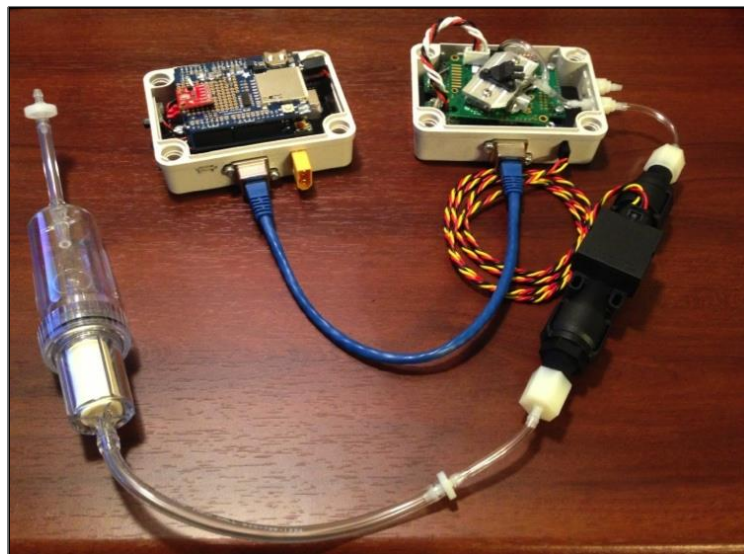


**Figure 17 - CO<sub>2</sub> sensor system enclosures, flowmeter, and water filter**



## A. ARDUINO MICROCONTROLLER

The “brains” of this sensor system is an Arduino microcontroller. The Arduino has become hugely popular for custom electronics in the last several years due to its ease of programming and very low cost. Because of this popularity a large variety of sensors and shields are produced specifically for Arduino that are built to mount straight to the microcontroller board and have space and connections for quick, easy prototyping. In addition, many of these sensors include example code that can be easily adapted into my programming, saving time and troubleshooting that can be spent developing the rest of the system instead. The Arduino can be powered off of 5V USB power but also has a built in regulator. This regulator takes 6-20V input power (recommended 7-12V due to overheating concerns if overpowered and voltage fluctuations if undepowered) and provides up to 1A of power to the microcontroller and its attached sensors (though this is thermally limited – a lower input voltage such as ~7V allows for maximum current output). Because of this, the system will be powered by a 2S 1000mAh battery as shown in Figure 18 that provides between 8.4V (fully charged) and 6.6V (safe point to consider depleted) with a nominal voltage of 7.4V.



**Figure 18 - Sensor system battery**

Arduino manufactures a variety of microcontroller boards, but by-and-far the most common is the Arduino Uno R3. The Uno is their medium-sized board at 2.7”x2.1” and contains 14 digital I/O pins, 6 analog input pins, one UART serial communications channel (shared with the USB), and a replaceable ATmega328 processor chip. This chip has 32 KB of onboard memory (used for the

bootloader and program storage), 2 KB of SRAM, and 1 KB of EEPROM. In addition to the mentioned serial communications channel, the board is also capable of SPI and I2C communications with the sensors. I2C is particularly helpful because it allows for multiple devices and sensors with unique addresses to be connected to only one pair of pins. If additional UART serial channels are needed, built-in code called SoftwareSerial is provided which can enable software serial communications on pairs of the 14 digital I/O pins.



**Figure 19 - Arduino microcontroller**

Two of the big benefits that come with the Arduino are the shields and libraries that are tailor-made for the microcontroller. Shields are stackable prebuilt circuit boards that are designed to plug directly into the top of the Arduino to easily attach and switch between various electronics systems. These shields provide a huge array of ready-made systems uses such as SD logging, communications, displays, and sensors that eliminate much of the painstaking circuit design. Libraries, likewise, are premade sets of code that can be added to an Arduino's programming to provide new functions such as communication (like the aforementioned SoftwareSerial), new software commands, and generally streamline common parts of programming such as writing to SD cards or controlling motors; leaving more time and effort to be spent on developing the parts of code that are more important.



**Figure 20 - Arduino board with example Bluetooth shield**

The Arduino Leonardo is a new board that is produced by Arduino that is in many ways an update of the Uno R3. The Leonardo has the same form-factor and pinout of the Uno, which allows for all of the shields built for the Uno to be used with the Leonardo as well. Some new features include changes to six of the digital I/O pins that allow them be used for that purpose or reconfigured as additional analog inputs. The most notable new feature, however, is a new processing chip, the ATmega32u4. While this chip is not replaceable as the processor on the Uno is, it has built-in USB communications, which allows for the serial communications pins to be used at the same time as the USB. This processor also includes 2.5 KB of SRAM memory as compared to the 2 KB on the Uno. Because of these two features, the Arduino Leonardo was chosen as the microcontroller board for the sensor system. As will be discussed later, it was found that the chosen GPS works best using hardware serial communications (as opposed to SoftwareSerial) and the additional 0.5 KB of SRAM is necessary to allow for the program to run smoothly.

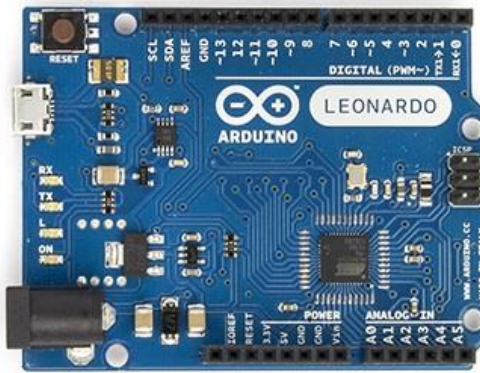


**Figure 21 - Arduino Leonardo**

There are some issues with the Leonardo that made wiring and programming more difficult, however. It is a newer board and still has bugs and not widely documented changes that have already been worked out on the more mature Uno. One such change is that only certain (and not as many) digital pins can be used for SoftwareSerial, whereas all of the digital pins on the Uno could be configured for either serial TX or RX. The SCL and SDA pins for I2C communications were also moved, which frees up the two analog pins that served dual-duty, but also does not match the wiring on many shields. In addition, many libraries that work on the Uno (such as the SD card library) are not compatible with the Leonardo which necessitated modifying or updating the libraries. While none of these issues were any problem to fix once they were known, they did make for difficult troubleshooting and resoldering many connections and would be good to take note of for anyone wishing to work with the Leonardo in the future.

## **B. CO<sub>2</sub> SENSOR**

The carbon dioxide sensor is the core component of the sensor system. It needs to be lightweight with a small form factor but with high response time being one of the most important features followed by accuracy and cost. The response time is critical because the aircraft will be traveling at a relatively high rate of speed and it is desired to fly in a continuous path instead of hovering over points for several minutes to fully detect the CO<sub>2</sub> levels. Two of the major types of carbon

dioxide sensors are non-dispersive infrared (NDIR) and electrochemical. Though there are different variations, NDIR sensors all work on the basic principle of light absorption or spectroscopy. CO<sub>2</sub> gas absorbs light with a wavelength of 4.26 μm so infrared light is shined through a cavity filled with the gas sample. A light detector fitted with a 4.26 μm filter then measures how much light makes it through the cavity to determine how much was absorbed by the CO<sub>2</sub>. When comparing datasheets NDIR sensors nearly always had quicker response times, much longer lifespans, and lower drift over time when compared to electrochemical sensors.

NDIR sensors come in a wide variety of shapes and sizes. In general larger and more expensive sensors have much higher accuracy than smaller systems, as would be expected. Previously mentioned sensors such as the Picarro WD-CRDS (which uses more advanced spectroscopy) and LI-COR 6252 or the CAI ZRE used in later testing all have much higher quality detection equipment and often include reference gas chambers for live calibration, but are designed to be bench or rack mounted and are large, weigh 20+ lbs (Picarro's flight-ready model weighs 70 lbs), and cost several tens of thousands of dollars.

There are, however, a range of smaller, relatively lower cost sensors that offer lower, but decent, measurement ranges and accuracy which are ideal for this application. Of these, they are separated by the two major methods in which the air sample reaches the sensor chamber: diffusion and flow-through. Diffusion models have the sensor chamber directly exposed but have a filter membrane which protects the chamber while still allowing air through. Designed to simply passively fill with the ambient air over time, these type are generally the most common and used for mounting in ductwork or to monitor gas levels as they slowly change in rooms or in test chambers. Flow through models, on the other hand, have attachments for tubing for flow to force air through the sensor chamber. Often based on diffusion models but with flow-through attachments added (as is the case with the Sensair K-30 series and Vaisala GMP343) these have





much quicker response times simply due to the high exchange rate of the air through the sensor chamber.

After searching extensively, several potential sensors were identified that fit the requirements for measurement range, accuracy, response time, and cost. Based on these factors, primarily response time, all of the sensors evaluated were NDIR flow-through models. They all specified low noise digital readings and were generally unaffected by humidity, pressure, and temperature ranges except in extreme cases. Some included pressure and humidity sensors to correct for these situations, but will not be necessary in the planned operating ranges.

The Senseair K-30 FR sold in the U.S. by its supplier, CO2meter.com, is a variation of the standard K-30 sensor with a measurement rate of 2 Hz instead of the 0.5Hz on the standard model. It is capable of both analog and digital output (via UART or I2C). It is very small and lightweight, only a 57 x 51 x 14 mm circuit board though it would require some type of housing. It has a quick warmup time of one minute and the option to attach a cap to turn it into a flow-through model. The U.S. supplier also provides an Arduino library and example LabVIEW code to ease its integration into the datalogging systems. It provides a very good combination of cost and decent accuracy and has been selected by the chemistry department for deployment in the network of low-cost ground sensors.

Another model is the LiCor Li-820, a pared down version of the \$18,000 Li-7200 used on LiCor's well-known range of eddy covariance towers. Though it boasts an impressive accuracy and response time, it unfortunately is rather large at 2223 x 1525 x 762 mm and 2.2 lbs and high cost. In addition, the size and interior design of the sensor chamber leads to worries that it could be damaged during rough landings of the aircraft.

**Table 1 - CO<sub>2</sub> Sensor Comparison**

Sensor Model/Image	Range	Accuracy	Response Time	Cost
Senseair K-30 FR 	0-5,000 ppm	±30 ppm + 3% of reading	2 sec @ 0.5 LPM	\$219
LiCor LI-820 	0-20,000 ppm	±< 3% of reading	0.5 sec @ 1 LPM	\$3900
Vaisala GMP343 	0-20,000 ppm	±5 ppm + 2% of reading	8 sec @ 1.2 LPM	\$3090
Vernier CO <sub>2</sub> Sensor 	0-10,000 ppm	±100 ppm	120 sec	\$249

The Vaisala GMP343 was another promising sensor found. Available in both flow-through and diffusion models, it is advertised as designed for rugged use which is favorable for use in an aircraft. It has low noise,  $\pm 3$  ppm, very good accuracy, and a small size of 188 x 55 x 55 mm and 360 g, but a relatively low response time in comparison to the other sensors as well as high cost.

Finally, the Vernier CO<sub>2</sub> Sensor was included in the comparison because it was already available on-hand. It is a diffusion type sensor however, and the response time is typical of the type. It also has a very low accuracy and overall isn't viable for the project. Table 1 summarizes the comparison of the important specifications of these four sensors. It is important to note that the response time is the T<sub>90</sub>, the time to reach 90% of the CO<sub>2</sub> level, and is based on certain flowrate points provided by the manufacturer, but these times will vary as the flowrate changes.

Based on these specifications and the features discussed previously, the Sensair K-30FR was chosen as the CO<sub>2</sub> sensor to be used in the aircraft system. The primary factors included the response time, cost, and size. Its accuracy is not as good as that of the more expensive systems, but for the purpose of detection and not quantification of CO<sub>2</sub> levels it was considered acceptable. In addition, the findings by Yasuda, et al. provide a useful body of knowledge of this sensor's limitations and the corrections required.

### C. SD LOGGING SHIELD & REAL TIME CLOCK

While it would be desirable to have a real-time feed of the CO<sub>2</sub> levels and other data, integrating a transmitter into the system would have large power requirements, be difficult to get the range required, and can have reliability issues. Instead it was decided to log all of the data to an SD memory card onboard the aircraft. It is a hassle to remove the memory card and download the data after each flight of the aircraft, but this method is simpler and more reliable. An Adafruit Data Logging shield for Arduino was chosen to interface with the SD card. Being a shield allows



it to be easily attached to the Arduino, as previously covered, and it includes a large empty prototyping area that allows for the attachment of other sensors and provides an area for the wiring to the other parts of the system. The shield accepts standard size SD cards which, using an adapter, allows for all sizes of SD cards to be used (as opposed to many SD boards that only include a slot for micro SD cards). SD card capacity or read/write speed is not an issue since simple text files are being written at a rate of ~2 Hz. A 2 GB micro SD card (one of the smallest capacities readily available) was fitted which, despite its small capacity by today's standards, can hold an estimated 102 days of continuous logging (17 million data points) which will clearly not be a limiting factor in the system's testing.

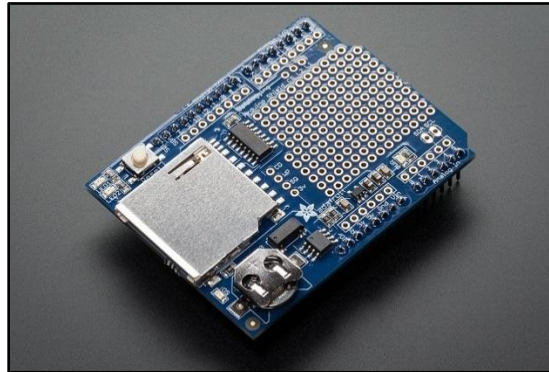


**Figure 22 - Adafruit Data Logging shield**

The shield also includes a real-time clock (RTC) to allow putting a time and date stamp on all of the data. Whereas the Arduino can only measure the time since it began receiving power, the RTC includes a battery to maintain the date and time while the system is powered off. While the date and time is available from the GPS timestamp as well, the RTC provides good redundancy for when the GPS does not have a connection such as when running tests indoors and in the basement wind tunnel.




The Adafruit shield has free available example code on how to get the SD logging and RTC clock running that was easily adapted to work for the CO<sub>2</sub> datalogging system. It also includes an update to the standard Arduino SD library. As previously mentioned, the Leonardo has changes

that make it difficult to use with some of the standard Arduino libraries, but the Adafruit update allow for the SD library to work smoothly with the shield despite the Leonardo's different wiring.

#### D. GPS RECEIVER

A GPS Receiver is needed for the system to record the position latitude, longitude, altitude, and time. The GPS needs good accuracy as well as an update rate as fast as or faster than the system's logging rate (2 Hz). Several GPSs were considered and are compared in Table 2.

**Table 2 - GPS comparison**

			
	<b>3DR uBlox GPS</b>	<b>3DR MediaTek GPS</b>	<b>SparkFun Venus 10920</b>
<b>GPS Chip</b>	uBlox LEA-6H	MediaTek MT3329	Venus638FLPx
<b>Advertised Accuracy</b>	2.5 m	<3 m	2.5 m
<b>Sensitivity</b>	-162 dBm	165 dBm	-165 dBm
<b>Update Rate</b>	5 Hz	10 Hz	20 Hz

All three GPSs compared fit the requirements of update rate and good accuracy. Ultimately, the 3DR uBlox GPS was chosen because it is the same that is used with the aircraft's autopilot and already available on hand. It was also released as the replacement to 3DR's MediaTek GPS so its performance is likely at least somewhat improved over that model. Additional features include a plastic housing which makes it more suitable for externally mounting on the aircraft as well as an

onboard battery which allows for warm and hot starts – which somewhat to dramatically decrease the time required for a satellite lock (depending on how recently the GPS was powered).

#### E. ALTIMETER

Though the altitude is available from the GPS, it was decided to add a pressure altimeter improved accuracy. This also provides redundancy in case there is no GPS signal (and likewise, the GPS altitude serves as backup in case there are issues with the altimeter). A Sparkfun SEN-11084 breakout board was chosen. It is built around a Freescale Semiconductor MPL3115A2 pressure transducer with a resolution of 1.5 Pa which is equivalent to 0.3 m (1ft) of altitude. This board communicates to the Arduino using I2C communications which is helpful since it allows for multiple sensors to be connected to the same channel.

As with most of their products, Sparkfun provides example code that allowed for the altimeter to be easily integrated into the system's programming. During testing it was found that the altimeter has an error where it would stop outputting data after running for extended periods of time. Further troubleshooting indicated it is some sort of power issue since battery power delayed the onset of or eliminated the problem (compared to USB). Sparkfun tech support had not heard of a similar issue and was unable to assist, but ultimately, because using the battery caused the error to not appear until after around 30 minutes of continuous operation (longer than a typical flight time) and the GPS altitude was available as backup, it was decided that the issue was not worth rebuilding the system with a new altimeter.



**Figure 23 - Sparkfun MPL3115A2 Altimeter Board**

## F. FLOWMETER

At the most basic level, a flowmeter is needed to indicate whether air is properly flowing through the system during flight, or whether blockage or some other cause is affecting the performance. More importantly however, it was determined that the flowrate affects the CO<sub>2</sub> sensor's response time (which will be further discussed in later chapters). Because there are several seconds of delay between when an air sample enters the system and when it is detected by the gas sensor, an accurate flowrate is needed to determine what the delay time is and correlate that CO<sub>2</sub> level to the GPS coordinates from when it was picked up several seconds previously. Based upon conversations with the supplier of the K30 FR, a flowrate of 1 LPM or above was expected for the quickest response times. Based upon this an electronic flowmeter was found with performance falling in that general range. Most flowmeters were a manifold design for ductwork and only one flow-through model was found with a low enough flow range (before falling into the category of micro-flow of just a few hundred mLPM).



**Figure 24 - Honeywell AWM5101VN flowmeter**

The Honeywell Sensing and Control AWM5101VN was chosen; it uses a venturi type flow housing to flow directly past a microbridge flow chip which measures the flowrate in a way similar to a hotwire probe. It has a 0-5 SLPM range with a linear analog output of 1-5 V so it can easily be interfaced with the Arduino by reading the voltage values through the analog input pins. The response time is 60 ms and at maximum flowrate the pressure drop is 0.25" H<sub>2</sub>O. The unit's rugged design can withstand 100 G impacts so it can withstand being mounted in an aircraft. A threaded inlet and outlet allow for nozzles to be fitted to attach to the desired tubing size. The total weight is only 60 g but the housing is 6.4" long so careful consideration is needed for the sensor's location in the aircraft. It also requires 10 V excitation which will require an increase in the 5 V system voltage.

## **II. CO<sub>2</sub> FLIGHT TEST CONFIGURATION**

The sensor system is one half of the project, but the unmanned aircraft is what makes such large area measurement possible. The unmanned aircraft needs to be capable of carrying the sensor system and performing the leak detection mission. Developing a unique composite airframe offers benefits such as customizing the interior spaces for the CO<sub>2</sub> system layout and tailoring the aircraft's performance to the planned mission profile, and although OSU excels at aircraft development such as this, it was decided that a commercial-off-the-shelf aircraft would be the best choice for the scope of this project. This is to be a proof-of-concept technology demonstrator and using a COTS airframe allows for the focus to be on system development and testing whereas designing and constructing a custom aircraft is worthy of its own dedicated design project.

Part of that system development is to include the CO<sub>2</sub> intake system design. This is a critical part of the sensor system design that warrants just as much testing as the sensors themselves because it determines the flowrate and quality of air samples that are seen by the system. Being an





unmanned aircraft also requires an autopilot which must be integrated into the system and tested for reliable autonomous operation. This autopilot will not only assist the remote human pilot in flight and provide live telemetry, but will enable the aircraft to perform preprogrammed search patterns so the flight profile is consistent and accurately covers the desired search area.






#### A. AIRCRAFT

The test aircraft most importantly needs to fit the CO<sub>2</sub> sensor system. This requires a large payload volume and the capability to carry a payload (in addition to battery) of at least 2 lbs. Good mounting points are also desired for components such as the intake tube, antennas, and video cameras. The aircraft needs to either be a pusher or twin engine type to allow clean airflow to enter the sensor system (wing mounted intakes were decided to require too much tubing that would decrease the response time). An electric aircraft is also desired due to electric propulsion systems being simpler, more reliable, having smaller space requirements, and not posing potential issues that could damage the electronics systems such as vibration and fuel leaks. Because it is a technology demonstrator, performance is not critical although it needs to be able to perform testing competently – including stable flight and a preferred endurance of 20+ minutes. Several aircraft were researched that fit these criteria as shown in Table 3.

After evaluating all of these options, it was decided to select the Skywalker X-8 as the aircraft platform primarily because of its low cost and large amount of interior volume (all easily accessed through its large main hatch) as shown in Figure 25. The aircraft is a flying wing with two elevons and no rudder. It is constructed of EPO foam and breaks into a fuselage section and two wings for easy transport. Structural support is provided by two 10 mm composite tube spars which slide through the fuselage and into each wing. The X-8 has a wing area of 8.6 ft<sup>2</sup> and empty airframe weight of 2.6 lbs. The recommended takeoff weight is 7.7 lbs but this will be studied through further calculations and testing.

**Table 3 - Airframe selection**

Aircraft	Mfg.	Span	Material	Price	Notes
Skyhunter 		5.9 ft	Foam	Airframe: \$110 ARF: \$225	5 lbs payload
Skywalker X-8 		7 ft	Foam	Airframe: \$160 ARF: \$265	5 lbs payload
Rooney 	Hangar 18	7.2 ft	Fiberglass fuselage, fiberglass foam core wings	Airframe: \$1200 ARF: \$1500	Similar to O2 with more fuselage space; roughly 2-4 lb of payload
O2 	Hangar 18	7.2 ft	Fiberglass fuselage, fiberglass foam core wings	Airframe: \$900 ARF: \$1200	1 hour electric flight times with 2-4 lb payload

Maja 	BormaTec	6 ft or 7.2 ft	Foam	Airframe: ~1 hour \$269 ARF: electric flight \$810 with ~3 lb payload
VAMP 	BormaTec	6 ft	Foam	Airframe: ~2.2 lb \$160 payload ARF: \$674
Jackaroo 	Attopilot	5 ft	Fiberglass	Airframe: ~1 hour \$2770 electric flight ARF: with ~4 lb \$3450 payload
Techpod 	Hobby UAV	8.5 ft	Foam	Airframe: 5 lb flight \$160 weight, 2.2lb ARF: of payload \$899
Penguin BE 	UAV Factory	10.8 ft	Composite	Airframe: 110 minute \$17650 flight with 6 lb payload





**Figure 25 - Stock Skywalker X-8 internal area**

The aircraft was equipped with an autopilot system to allow autonomous navigation as well as assist the human pilot by providing in-flight telemetry. Three low-cost hobby grade autopilots were considered, the 3DR Ardupilot Mega 2.6, the 3DR Pixhawk, and the Blackswift Swiftpilot. The Blackswift is a commercial autopilot which costs \$1700 and could be considered above hobby grade. Unfortunately, the ground station software is tablet based and was not ideal for the planned mission use. In addition, bugs in the software of the Swiftpilot made the Pixhawk the favored choice. The \$450 3DR Pixhawk is the successor to the Ardupilot Mega 2.6 and is capable of running the APM firmware of the Ardupilot or the newer Pixhawk firmware. It was chosen to run the APM firmware because the ground station software, Mission Planner, is more stable and feature-rich than the software for the Pixhawk firmware, QGroundControl. One important feature of Mission planner is its ability to produce automated waypoint grids to allow for the aircraft to fly in multi-altitude grid patterns while surveying an area.

Two X-8 aircraft were used in flight testing, one hand-launch version and one equipped with landing gear as shown in Figure 26. The aircraft were electric powered with two 4000 mAh batteries. The aircraft were equipped with the intake tube for the CO<sub>2</sub> flow system and the airspeed Pitot tube protruding from the nose of the airframe. In addition, the aircraft was

equipped with a first person video (FPV) camera to assist pilot navigation. Full details of the aircraft configuration are provided in Appendix A.

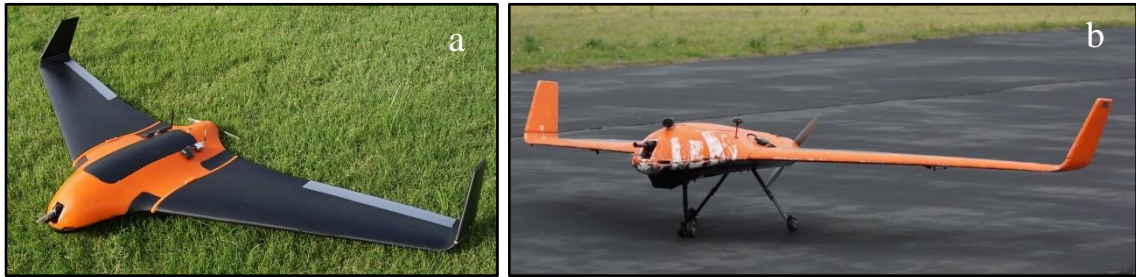


**Figure 26 - X-8 test aircraft: configuration 1 (a) and 2 (b)**

## B. CO<sub>2</sub> FLOW SYSTEM

A key part of the interior layout of the aircraft is the flow system to deliver the sample air to the CO<sub>2</sub> sensor system. The system consists of an intake tube on the front of the aircraft (shown in Figure 27), a particle filter, water trap/hydrophobic filter, flowmeter, the CO<sub>2</sub> sensor, and the exit ducting. Several different variations of intake tube were considered. The original consisted of a thin-walled stainless steel pipe with 0.135" inside diameter – sized to fit in the mounting gland alongside the Pitot tube while having roughly twice the area as the smallest portion of tubing (the 3/32" diameter CO<sub>2</sub> sensor inlet and exit) to provide a good flowrate. Several other options were considered to increase the flow rate including mounting a 1" or 2" funnel to the stainless steel intake tube or replacing it with a 1/2" copper pipe with the end widened by a flaring or swagging tool. Following the intake tube is a 150 micron particle filter from CO2meter.com to prevent dust, ash, and debris from entering the system. This is followed by a water trap/hydrophobic filter, also from CO2meter.com, to prevent water from entering the system. The supplier specified that the readings of the K-30 are not affected by moisture in the atmosphere except in the case when the moisture level is high enough for condensation to form in the sensor chamber causing it to not be able to read; because of this a moisture filter is recommended, but not necessary if flight

conditions allow it. Next is the Honeywell flowmeter as previously described. This is in turn connected to the sensor box containing the K-30 FR CO<sub>2</sub> sensor.



**Figure 27 - Nose mounted air sample intake, Pitot tube, and FPV camera**

As for the exit flow from the box, several variations were studied. One option consisted of piping the exit flow from the sensor directly onto the temperature/humidity sensor inside of the sensor box in order to record the atmospheric data. If a flowrate increase is required, however, there is the option to connect the exit tubing to flow out of the back of the aircraft through an exit duct. This duct, consisting of a 1" or 2" diameter plastic funnel will be placed in a low-pressure region which is expected to provide suction to increase flow through the system without need for a pump. Locations for this exit duct include mounting a 1" funnel in the blunt rear of the aircraft next to the motor, a location in which the air flowing from the system into the low-pressure region should provide a moderate decrease in the pressure drag, or mounting a 2" exit funnel on the trailing edge of the wing, a location which would add additional drag but also likely provide more suction for an increased flowrate. Figure 28 illustrates the flow system layout as well as its possible components and configurations.

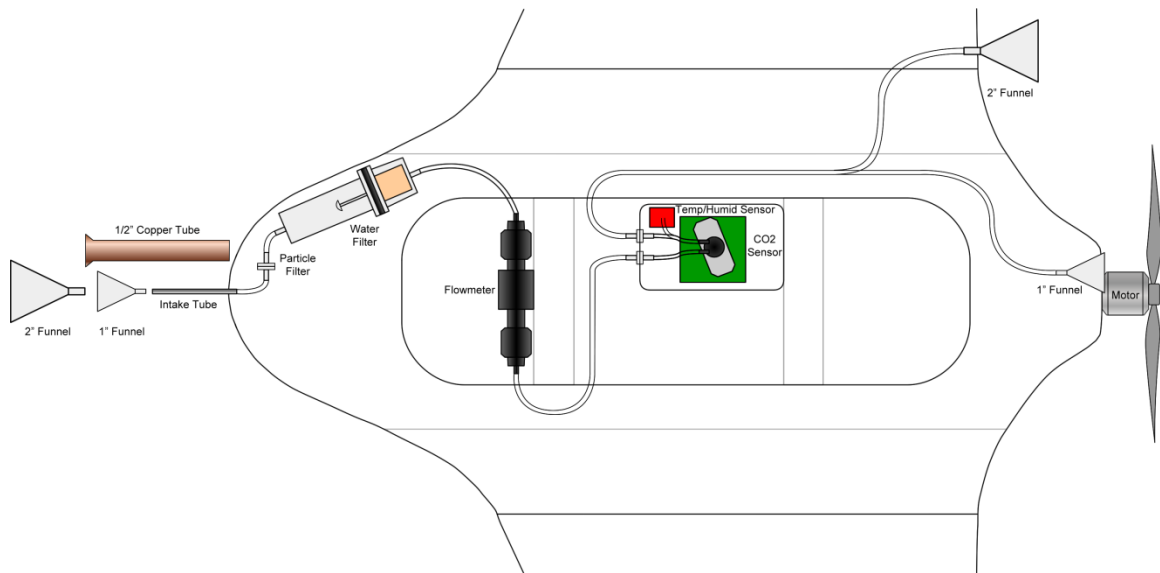


**Figure 28 - Air sample flow system and configurations**

### **III. CONTROLLED BURN FLIGHT TEST CONFIGURATION**

The opportunity arose to perform test flights over controlled rangeland burns. Because fire produces carbon dioxide over a large area, this was seen as an opportunity to test in an environment vaguely similar to a carbon sequestration leak source (at least, in comparison to CO<sub>2</sub> released from a small tank source). The test flights were being performed by another student in the lab as part of a study of how best to observe wildfires using unmanned aircraft so firefighters could most effectively fight the blaze. To collect CO<sub>2</sub> data during these tests the sensor system had to be fitted into his aircraft in addition to the systems which were already installed. The fires were mostly performed by Oklahoma State's Fire Ecology program in the department of Natural Resource Ecology & Management on plots of generally 100+ acres.

#### **A. AIRCRAFT**

The fire observation UAS, dubbed the Firebird and shown in Figure 29, is based around the hand-launched Skyhunter aircraft which was previously evaluated. In addition to an autopilot (an Ardupilot 2.6) and electric propulsion system, the aircraft was extensively outfitted with video

systems for fire observation. This included an infrared camera manufactured by DRS technologies mounted to the side of the aircraft, a FPV camera mounted to the nose, and a GoPro HD camera mounted to the nose hatch; all of these cameras were mounted at a downward angle for ground observation while in level flight. In addition, wireless video transmitters for the infrared and FPV were equipped as well as onboard digital video recorders for these two cameras.



**Figure 29 - Firebird UAS being launched by its developer**

## **B. CO<sub>2</sub> SYSTEM CONFIGURATION**

To perform CO<sub>2</sub> tests during the fire flights the sensor system, including sensor box, data box, flowmeter, GPS, battery, strobe, and tubing had to be fitted in the narrow fuselage of the Firebird. The boxes were squeezed in tandem in the fuselage connected with a 0.5 m Ethernet cable. The flowmeter was placed atop the Ethernet cable with the battery nestled below and the strobe mounted beneath; leaving just enough room for the digital video recorders in the nose. The highest flowrate tubing configuration which could be fitted was equipped. This included the 0.135" ID intake tube with the 1" intake funnel attached, the particle filter (very important with the smoke and ash), no water filter, and a 2" exit funnel mounted on the trailing edge of the wing

just between the aileron and edge of the prop arc. The entire system configuration is shown in Figure 30.

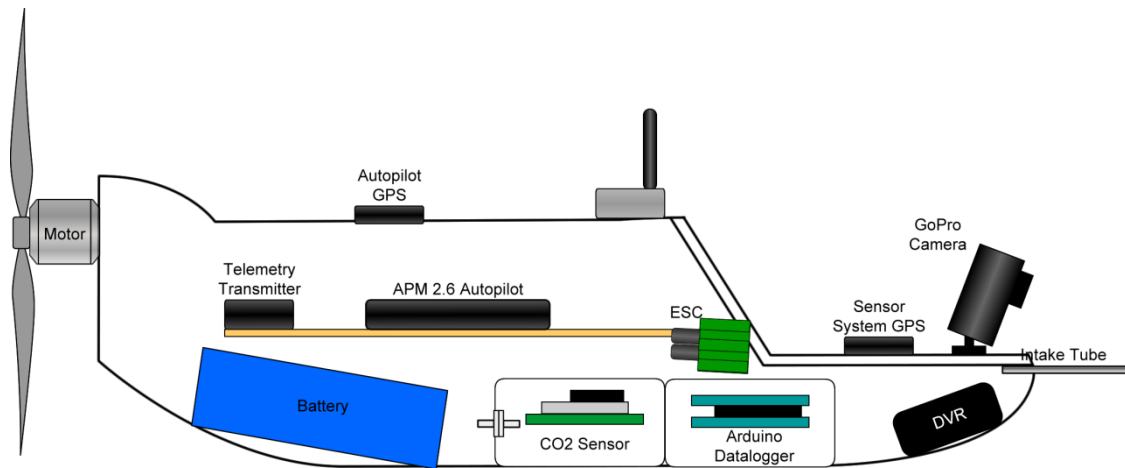


Figure 30 - Firebird internal layout

### C. CONTROLLED BURN LOCATIONS

The burns were performed on OSU owned land roughly eight miles west of Stillwater, OK during the burn season which generally ran from early February to late March when green vegetation began growing. The dryness and lack of vegetation during this time means that background CO<sub>2</sub> levels should be generally low and consistent. As mentioned, most burns were in the 100+ acre range (commonly 160 acres/1/4 square mile as shown in Figure 31) and performed by OSU's Fire Ecology program although one was several square miles and performed by a professional company, Chloeta Fire. The burns were only performed if winds were acceptably low (~5 mph) so notification that a burn was happening was only given up to 24 hours in advance. Winds also determined the burn pattern and their direction would change at any time before the burn, so flight plans had to be developed at the launch site and often while already in the air.





**Figure 31 - Portion of 160 acre controlled burn**

#### **IV. GROUND TEST CONFIGURATION**

##### **A. CO<sub>2</sub> CALIBRATION SYSTEM**

To verify the output of the K-30 FR sensor, it first had to be calibrated by comparing it to a known gas level. The sequestration team from the chemistry department had already developed a test setup that they use to verify their own sensors (including the K-30). The system, as shown in Figure 32, uses a California Analytical Instruments ZRE sensor to measure the levels of gas. The ZRE is a benchtop NDIR analyzer that can detect a variety of gases including CO, CO<sub>2</sub>, CH<sub>4</sub>, SO<sub>2</sub>, and NO. It has a repeatability of 0.5% and noise of less than 1% of full scale. The system is supplied by a tank of pure nitrogen (N<sub>2</sub>) and a calibrated tank of 2960 ppm CO<sub>2</sub> with N<sub>2</sub> filler. An Omega FMA5400 mass flow controller controls the flowrate of each of the gases which are mixed to produce the desired percentage of CO<sub>2</sub>. This tubing system then flows into the ZRE analyzer and test cell. To test the aircraft CO<sub>2</sub> system, the CO<sub>2</sub> sensor was attached in-line with the tubing, and the full system, including the flowmeter and particle filter, was used to log the CO<sub>2</sub> levels for comparison to the ZRE sensor.

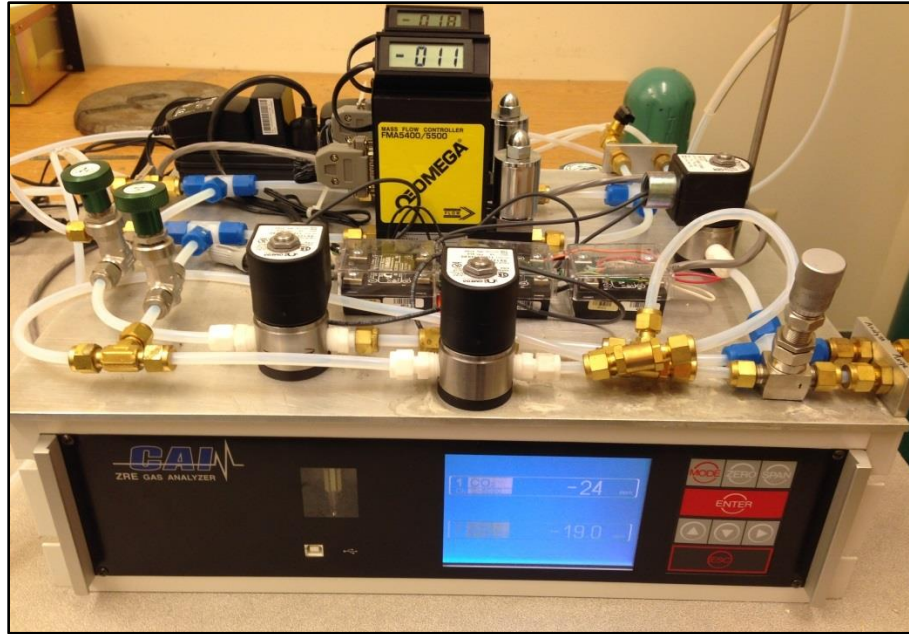


**Figure 32 - CO2 calibration system**

## **B. WIND TUNNEL SETUP**

All wind tunnel tests were performed in OSU's low speed wind tunnel. The wind tunnel includes two back-to-back test sections, one of transparent plastic, the other of plywood, with a 3'x3' cross section; with these sections the maximum airspeed is 28 m/s. The tunnel is located in the basement of the OSU Advanced Technology Research Center and is known to have some minor turbulence issues due to the inlet flow coming into the basement, but the turbulence should not be a major issue for the types of tests that are to be run. The entire fuselage of the X-8 was mounted in the tunnel on a custom Plexiglas mount. The mount, is designed to easily fix the aircraft at multiple angles of attack. The parts are laser cut and the angle of attack is etched along the slider rail at increments of 5°. The total movement range is -30° to +30° to encompass any angle of attack that the aircraft is likely to encounter. The mount can easily be adapted to any other airframe by simply replacing the four-hole mounting plates with new ones containing holes sized for the aircraft's spars.



For data analysis, the wind tunnel is equipped with a desktop computer with National Instruments' LabView software installed and an attached National Instruments NI USB-6009 DAQ. The wind tunnel speed was measured using a small pitot tube mounted in the front of the test sections. The pressure lines were connected to a Dwyer U-Tube Manometer as well as an Omega pressure transducer. The pressure transducer was powered by a CircuitSpecialists CSI530S Regulated DC Power Supply and its output was recorded by the DAQ system.

## 1. FLOWMETER TEST SETUP

The first round of wind tunnel tests was performed to measure the flowrate through the CO<sub>2</sub> sensor's air intake system as it varied with airspeed and various tubing configurations. The aircraft fuselage was mounted in the center of the tunnel and the flowmeter was wired to the bench power supply and DAQ. It was decided to use these systems to record the data instead of the onboard Arduino based system because the DAQ is much more accurate and easier to use than the aircraft's onboard sensors (though tests will be run with the Arduino system to compare its results to those of the DAQ). A simple Labview program was put together to record the voltages from the flowmeter and pressure transducer (for tunnel airspeed). The program, shown in Figure 33, also converts the voltages into the flowrate and airspeed based upon theoretical equations for reference (as opposed to calibration measurements which will be used for the final data).

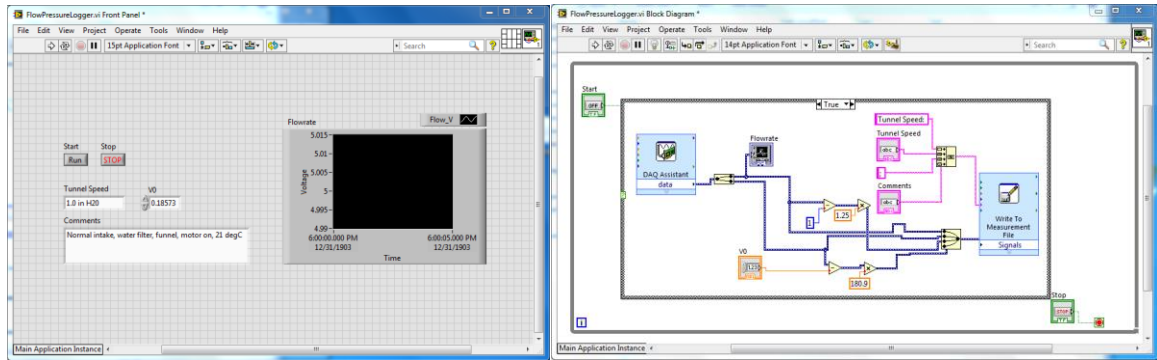


**Figure 33 - Flowrate test LabVIEW program**

The tests were performed by changing various components in the flow system and testing the flowrate of each configuration at a range of various speeds in the wind tunnel. In the first group of tests, the 0.135" ID intake tube and particle filter were the same for all configurations and combinations were made of removing the water filter and 1" exit funnel and turning the motor on, as highlighted in Figure 34.

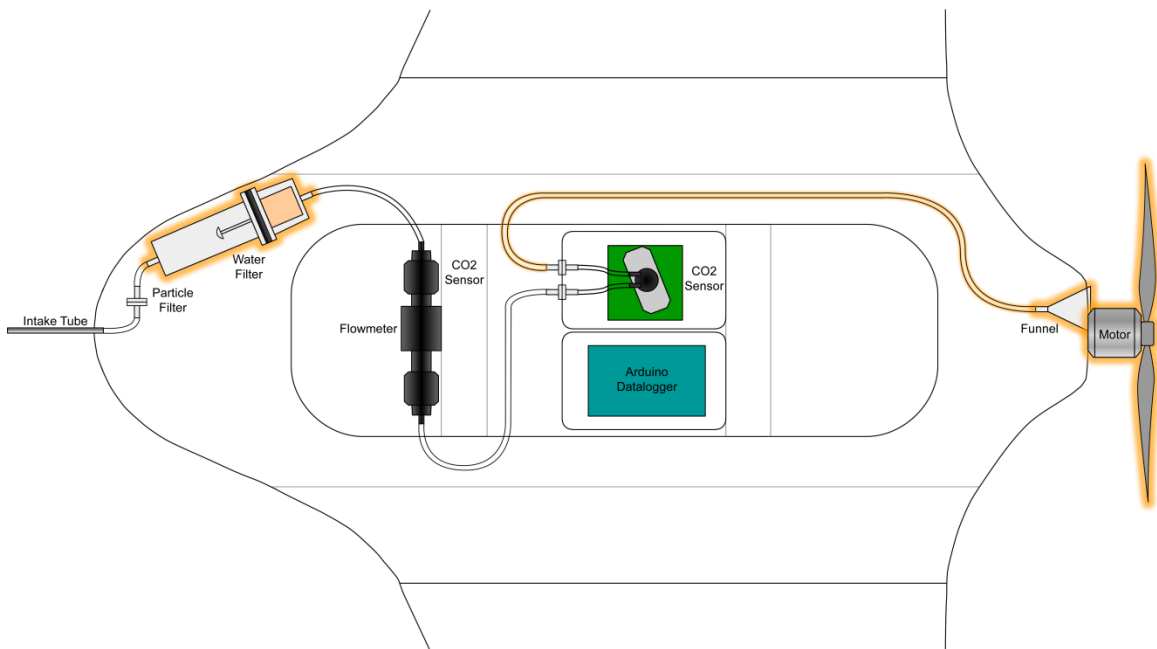


**Figure 34 - Equipment changed during first round of flowmeter tests**

## 2. CO<sub>2</sub> RESPONSE TEST SETUP

The next series of tests were designed to compare how the flowrate affected the response time of the CO<sub>2</sub> sensor. The aircraft was again placed in the center of the wind tunnel and CO<sub>2</sub> was released into the tunnel from tubing facing upstream and located 17" in front of and inline of the intake tube on the aircraft. The tubing setup consisted of the 0.135" ID intake, particle filter, flowmeter, CO<sub>2</sub> sensor, and 1" exit funnel located near the motor; the water filter was omitted and the motor was not turned on. Initial tests showed that releasing the gas from a 9 g CO<sub>2</sub> cylinder and recording the times with a stopwatch between the release and peak CO<sub>2</sub> levels on the sensors was far too inconsistent.



**Figure 35 - CO<sub>2</sub> response time test wind tunnel setup**

To remedy this, the LabVIEW program was modified to control the release of the CO<sub>2</sub> as well as log the CO<sub>2</sub> level, flowrate, and tunnel speed. The flowmeter and pressure transducer were again powered by bench supplies and recorded by the DAQ; communications to the CO<sub>2</sub> sensor through an FTDI cable were set up based upon an example provided by the sensor supplier (CO2Meter.com). An output channel of the DAQ was wired to a relay controlling a solenoid valve to release the gas. The CO<sub>2</sub> source was a 5 lb 600psig CO<sub>2</sub> tank that released the gas

through a 50 psig regulator. The LabVIEW program (shown in Figure 36) recorded the CO<sub>2</sub> level as fast as communications would allow (~6 Hz) and for each gas reading recorded the median value of the flowrate and pressure based on 100 sample points recorded at 1000 Hz. The LabVIEW program was automated so a defined number of releases (20 in most tests) separated by a delay (for CO<sub>2</sub> values to return to ambient) could be run and recorded without any additional user input.

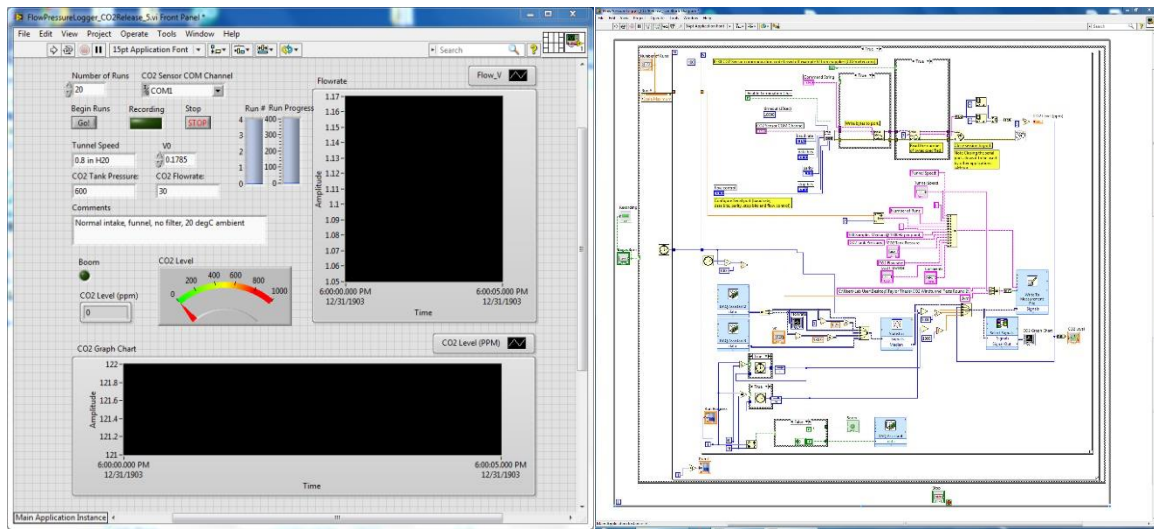
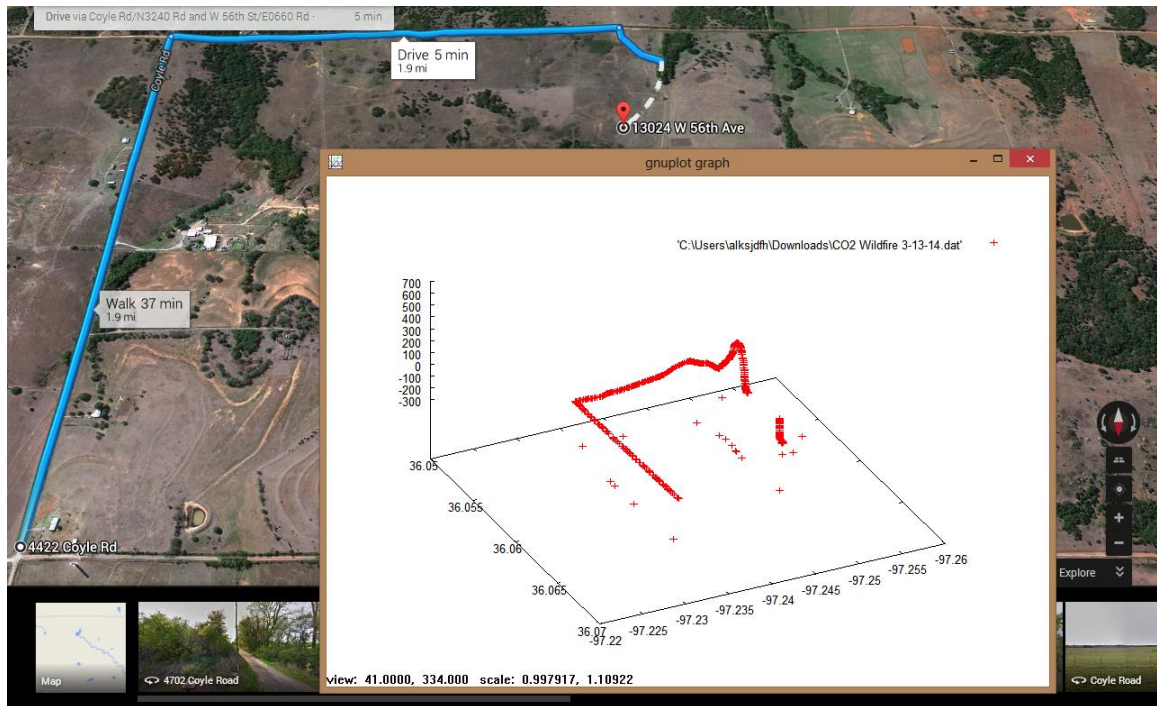


Figure 36 - CO<sub>2</sub> response time test LabVIEW program

### C. FIELD TEST SETUP

Preliminary field tests were performed to simply prove the system's basic ability to detect increased levels of CO<sub>2</sub> in the atmosphere. A very simple prototype version of the sensor system was used consisting of the Arduino Leonardo, a SD breakout board, the 3DR GPS, were similar, band the K30 FR CO<sub>2</sub> sensor. This setup could only record the latitude, longitude, and CO<sub>2</sub> level, but it was enough to prove the concept works. The intake system consisted of a 0.061" ID intake tube, the particle filter, and the water filter. The test was performed east of Stillwater in early March at one of OSU's controlled wildfire burns as previously described. The test consisted of simply holding the intake tube out of the window of a car while driving south alongside and

downwind of the burn at roughly 20 mph. Readings continued to be taken as the car drove away from the fire and then traveled north again  $\frac{3}{4}$  miles away from the edge of the burn. The results shown in Figure 37 show the values clearly rising as the vehicle traveled through the smoke and returning to ambient levels as the car drove north away from the fire, proving the viability of the system and warranting commencing testing.



**Figure 37 - Data from early field test**

## CHAPTER IV

### TEST RESULTS

#### I. GROUND TEST RESULTS

##### A. CO<sub>2</sub> CALIBRATION TEST RESULTS

The K-30 FR was calibrated to determine how closely its readings matched the actual gas levels. Nitrogen and carbon dioxide mixed gas was released through the K-30 system and the CAI ZRE in the previously described setup. The ZRE was first calibrated by setting the zero value while pumping pure N<sub>2</sub> through the system and then setting the CO<sub>2</sub> value while the 2960 ppm CO<sub>2</sub> calibrated gas was flowing through the system. The K-30 was set to run off of battery power and log to a SD card just as it would during flight. The level of the gas was increased in steps collect readings at six different gas levels. Each step lasted roughly 10-15 minutes to allow for the CO<sub>2</sub> levels (which rose quickly over several seconds but took several minutes to reach their full value) to settle and become steady state. The values from the steady state portion were then averaged and plotted to develop the trend between the readings of the ZRE and K-30 as shown in Figure 38; one standard deviation error bars are too small to be visible on the graph.

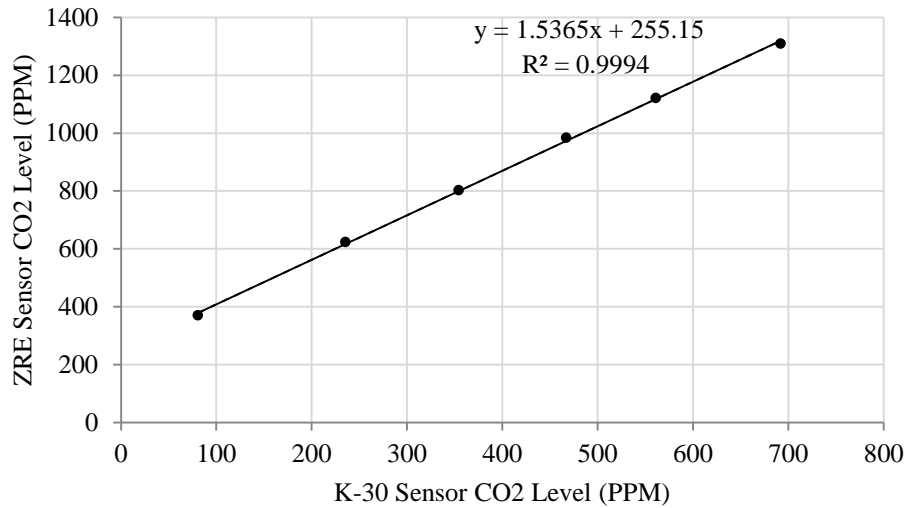


**Figure 38 - CO2 sensor calibration**

## B. WIND TUNNEL TEST RESULTS

The wind tunnel tests were run to find the characteristics of the system before the flight tests commenced. The tests were primarily run in the winter months (November-January) and because the tunnel is an open-loop design drawing outside air, the air temperatures generally ranged from 0-10 °C.

### 1. FLOWMETER TEST RESULTS

The first tests performed were the flowrate tests to determine the configuration that would provide maximum flow rate through the sensor system. A total of six configurations were compared in the first round of testing. Each configuration was run at the full range of speeds the wind tunnel was capable (0-2 in H<sub>2</sub>O or 0-68 mph) in increments of 0.2 in H<sub>2</sub>O (for 11 total speeds including 0) as recorded on the manometer from the Pitot tube. Data was collected at 1000 Hz for 5 seconds and at least two runs were performed per data point. To begin, a calibration of the pressure transducer connected to the Pitot tube was run to compare its output voltage (when being powered with an excitation voltage of 10 V) to the recorded pressure on the U-tube manometer. The data was graphed and a trendline was fitted as shown in Figure 39.

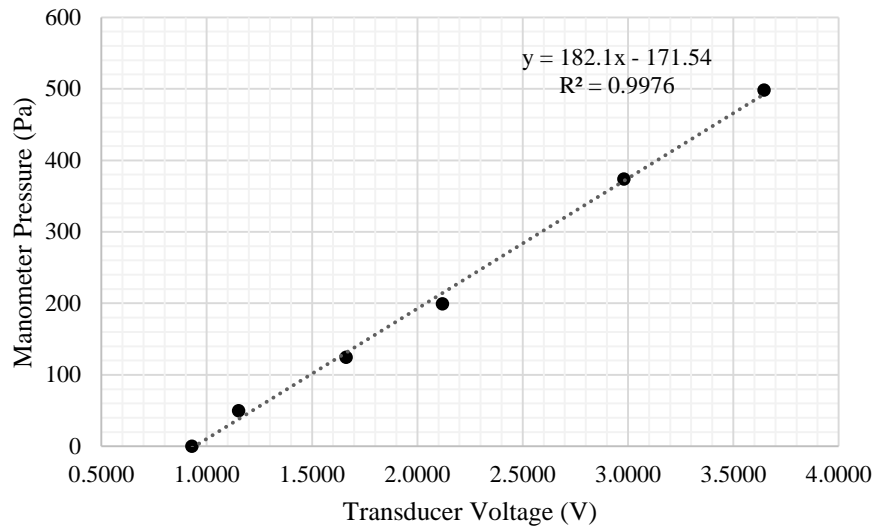


**Figure 39 - Tunnel airspeed pressure transducer calibration**

For the flowrate tests all configurations, as mentioned previously, had the same intake and particle filter. Tests were performed with the water filter installed and with the water filter removed but an equal length of tubing installed in its place. The impact of adding a 1" exit funnel at the back end of the aircraft next to the motor mount was also compared to having the air exiting the sensor box flow directly into the aircraft with no further tubing attached. The motor is also powered on during one series of tests at 66% throttle to observe the effects the increased airflow from the propeller has on the flow exiting from the funnel. For a reference, tests were also performed with everything removed except the intake tube, particle filter, and flowmeter (no CO<sub>2</sub> sensor, water filter, or exit funnel). The results of this series of tests are shown in Figure 40; error bars are too small to be visible.



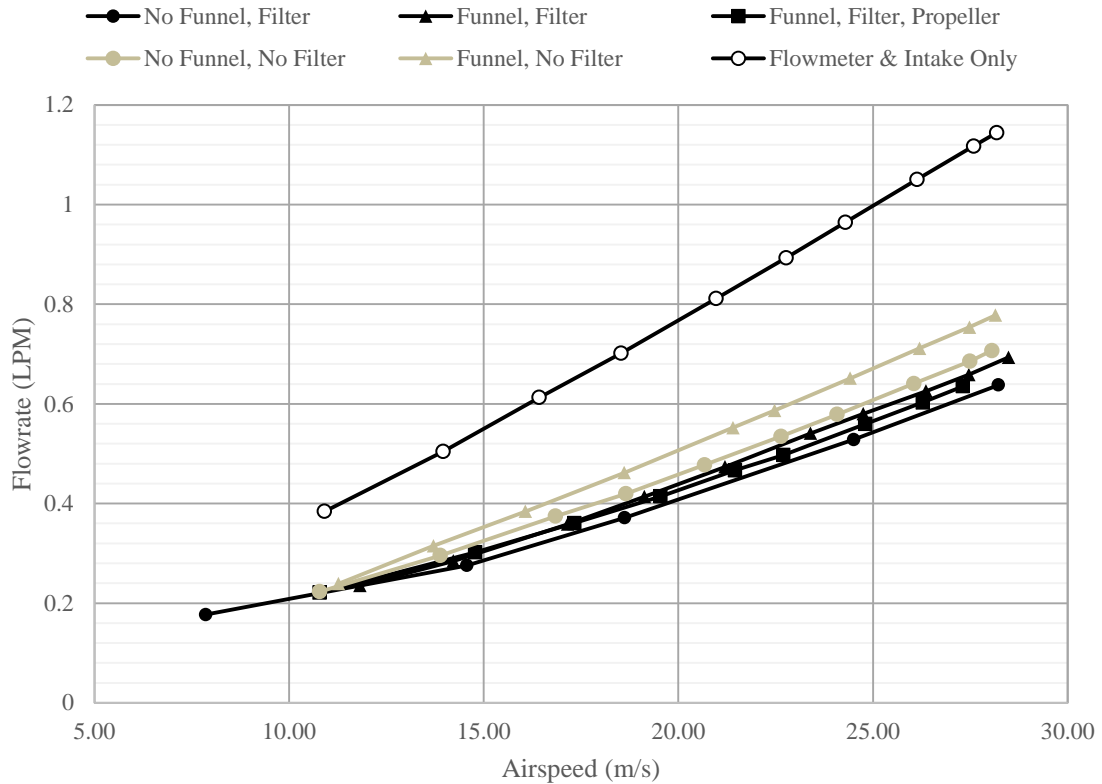


**Figure 40 - Flowrate as a result of airspeed and configuration**

Adding the CO<sub>2</sub> sensor and other systems clearly have a large impact on the flowrate, reducing it by nearly 40%. Unfortunately, the sensor clearly has to be included and there is no way to modify the flow arrangement that is built into the sensor. Removing the water filter has the next biggest impact, increasing the flow by 14% at max speeds. Although the water filter was recommended to reduce the chance of condensation in the sensor, flights are not planned to take place in high humidity environments and the filter design could add mixing to the intake air, further reducing the results, so it was decided to delete it from the test configuration. Adding the 1" exit funnel also helped improve the results, increasing the flow by 10% at the highest test speed, although having the motor running reduced this effect by up to 4.5%. This improvement was enough to decide to continue using the exit funnel and explore additional sizes and locations in the next tests.

## 2. FLOWMETER NOISE TESTS

During the flowrate testing, it was found that during the motor tests when the autopilot and onboard systems were powered the flowmeter data indicated a noticeable amount of noise even though the measurements were being recorded through an independent DAQ and power source. Moving the wiring to exit the nose of the aircraft so it was farthest from the aircraft's systems helped improve the issue, and enough data points were taken by the LabVIEW program that taking the median of the values eliminated the effect of the noise. When recording the flowrate through the Arduino's systems, however, the noise was far too severe to have quality data as shown in an example wind tunnel test in Figure 41 using the flight configuration of the sensor system (not the NI DAQ system).

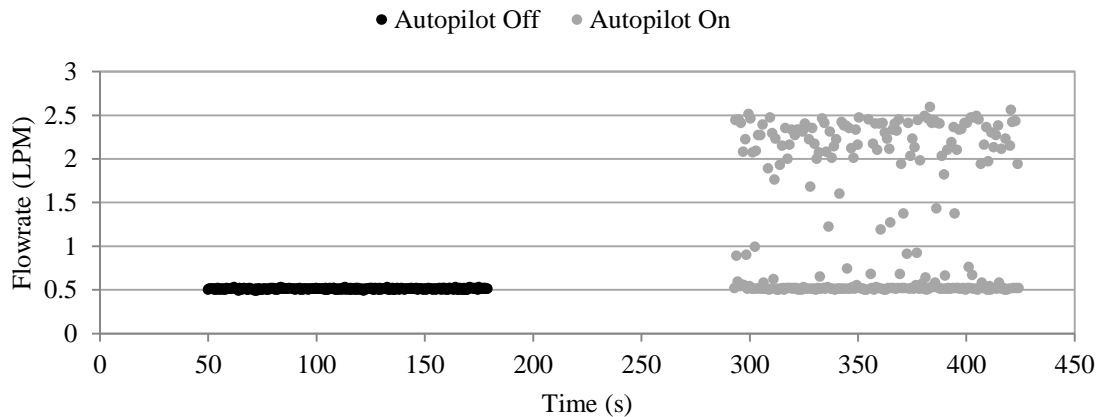


**Figure 41 - Noise comparison using Arduino system at 25 m/s in wind tunnel**

The source of noise was found through the process of elimination by removing components of the autopilot and other systems. It was found that the noise was caused by the telemetry transmitter from the autopilot. A metal shielded enclosure was developed to encase the transmitter and the antenna was moved to the aircraft wingtip. While this drastically reduced the noise level, if possible test flights will be flown without telemetry to avoid any noise issues.

### 3. CO<sub>2</sub> RESPONSE TEST RESULTS

To determine how the flowrate affected the response time of the CO<sub>2</sub> sensor, tests were next run in the wind tunnel while releasing CO<sub>2</sub> into the flow. The tests were run over a range of speeds from 0.5-2 in H<sub>2</sub>O (14-68 mph) and in increments of 0.3 in H<sub>2</sub>O of differential pressure from the Pitot tube for a total of five test speeds. Ten CO<sub>2</sub> releases were performed per test and each test was run twice for a total of 20 CO<sub>2</sub> releases per test speed. Each release was one second in duration and releases occurred every one minute fifteen seconds. The gas was released at a rate of 30 SCFH for a total release per burst of 2.1 g CO<sub>2</sub>. Tunnel temperatures at the time of testing ranged from 9-13 °C. As mentioned previously, data was recorded at a rate of ~6 Hz and for each point the median of 100 samples recorded at 1000 Hz of the flowrate and pressure voltages was recorded. A sample of two of the releases is shown in Figure 42; charts for all of the tests are included in Appendix B.

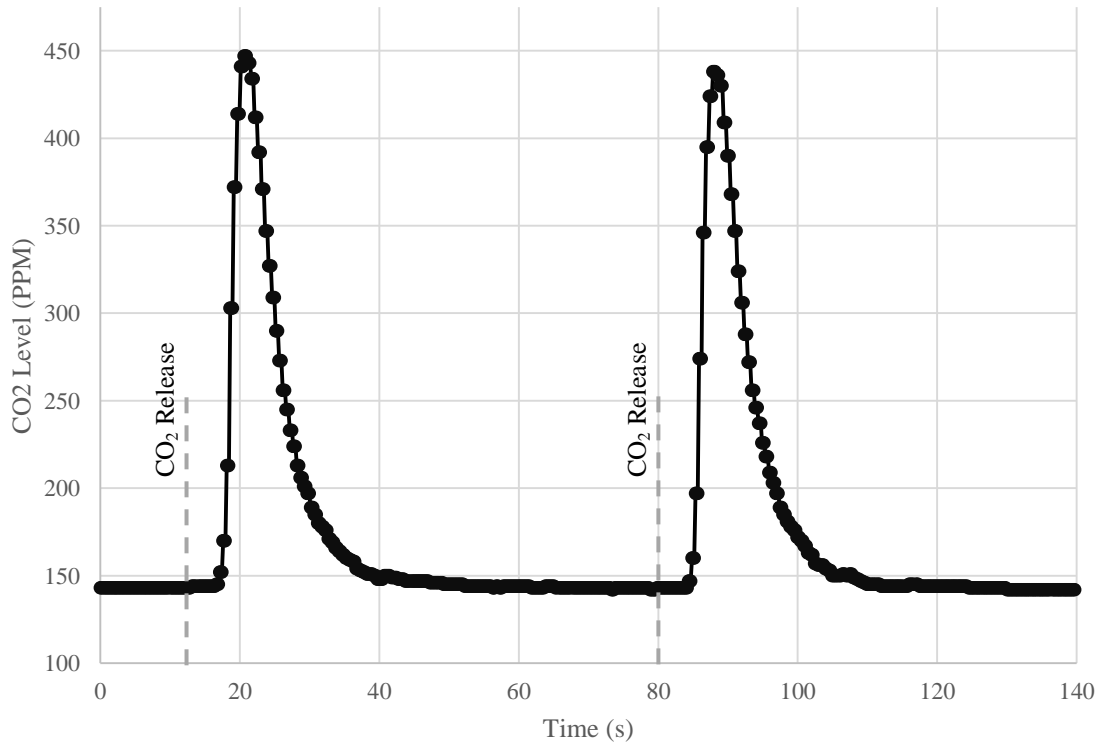


**Figure 42 - Sample CO<sub>2</sub> sensor response test at 0.435 LPM flow rate; 14.25 m/s airspeed**

From this data, the times were measured between the CO<sub>2</sub> release and both the CO<sub>2</sub> detection time (when the CO<sub>2</sub> level began to rise above ambient) and the CO<sub>2</sub> peak time. These values were then averaged and graphed vs. the median flowrate which they were recorded at. The resulting correlations for the detection time are shown in Figure 43 and the peak times in Figure 44; error bars of one standard deviation are provided. A second order polynomial line of fit was then calculated which could be later applied to flight test data.

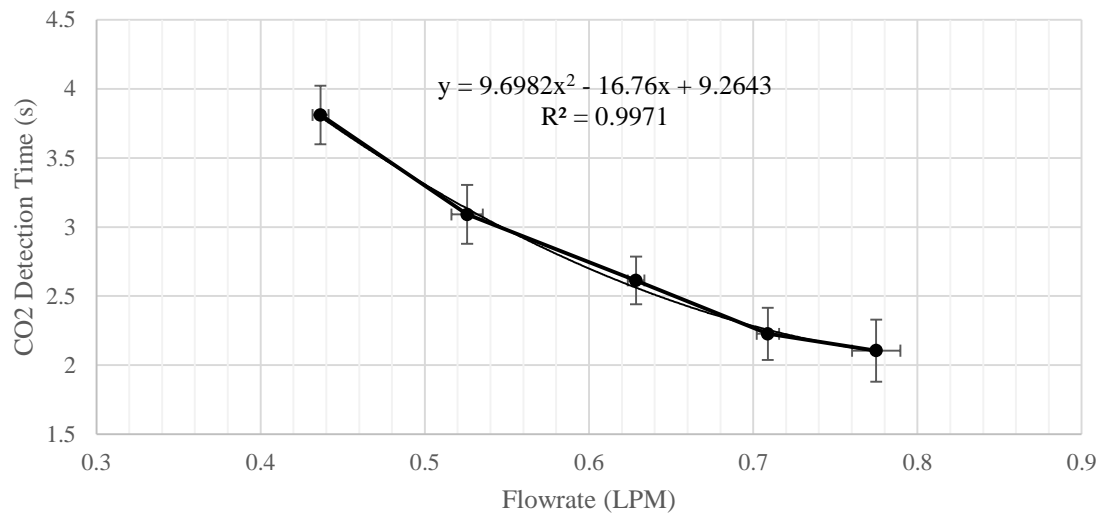


**Figure 43 - CO<sub>2</sub> detection time based on flow rate**

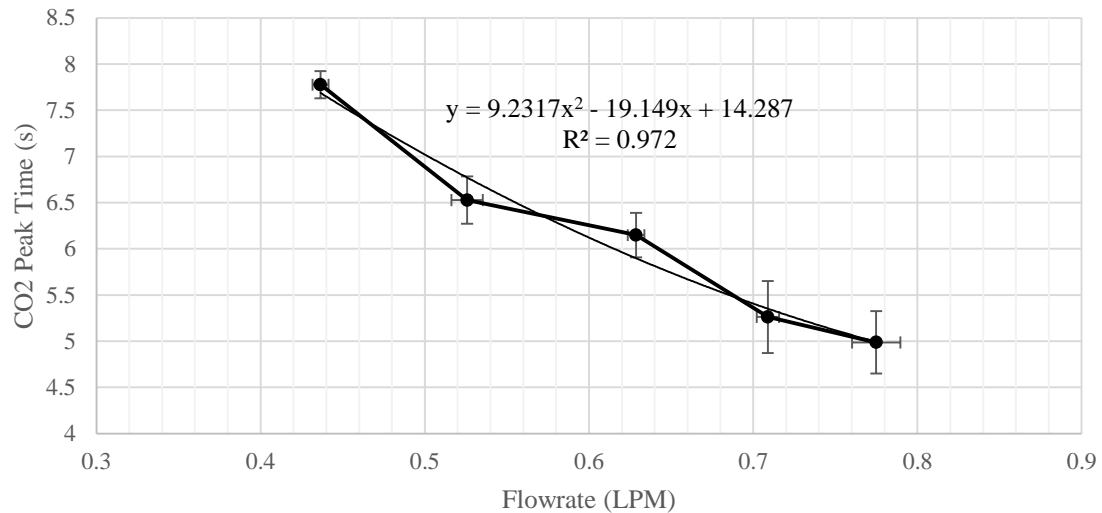


**Figure 44 - CO<sub>2</sub> peak time based on flowrate**

It took the CO<sub>2</sub> levels between 5-8 seconds to peak. These times, while not ideal for instantaneous response, are small enough to easily apply the correlation to backtrack from the CO<sub>2</sub> level to the coordinates several seconds previously when the gas entered the system.

## II. FLIGHT TEST RESULTS

### A. PRELIMINARY FLIGHT TESTS & LESSONS LEARNED

Initial flight tests to prove the airworthiness of the aircraft system were carried out at OSU's Unmanned Aircraft Flight Station. Tests were first performed with the version 1 configuration (detailed in Appendix A) of the hand-launch X-8 aircraft. Although the aircraft could fly while operating near its published maximum weight, it was too heavy to reliably launch. The success rate of launches was approximately 1 in 10. While the aircraft often skidded harmlessly along the ground during failed launches, several times it impacted the ground nose-first as shown in Figure 45, damaging the nose of the aircraft and the air intake. For this reason it was decided to upgrade to an X-8 with fixed landing gear for runway takeoff.

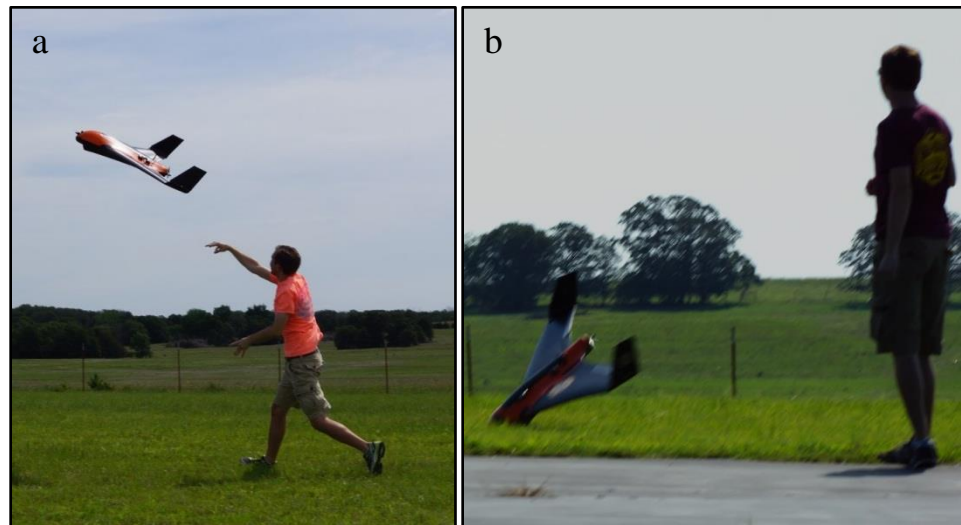


**Figure 45 - Successful (a) and failed (b) X-8 hand launch**

Due to the location of the landing gear in the new aircraft as well as experiences with the original airframe, a new internal layout was developed for the X-8 version 2 configuration (detailed in

Appendix A). Flight testing was reliably accomplished with a flight weight of 9.8 lbs. At this weight and a cruise speed of 17 m/s, the aircraft achieved a typical flight time of 22 minutes with some battery power still in reserve. During testing issues were discovered with the factory autopilot wiring causing reliability issues; details of the fixes applied are contained in Appendix A.

Tests were performed to optimize the autopilot gains and settings to best perform a typical CO<sub>2</sub> survey mission. Various grid patterns, such as those shown in Figure 46, were tested to evaluate what type of flight pattern the aircraft could reliably perform. It was found that the aircraft could perform turns as tight as 50 m. If a tighter grid is desired, such as for the planned CO<sub>2</sub> tank release tests, an interleaved grid consisting of offset 50 m grids can be used such as that shown in Figure 46 (b).

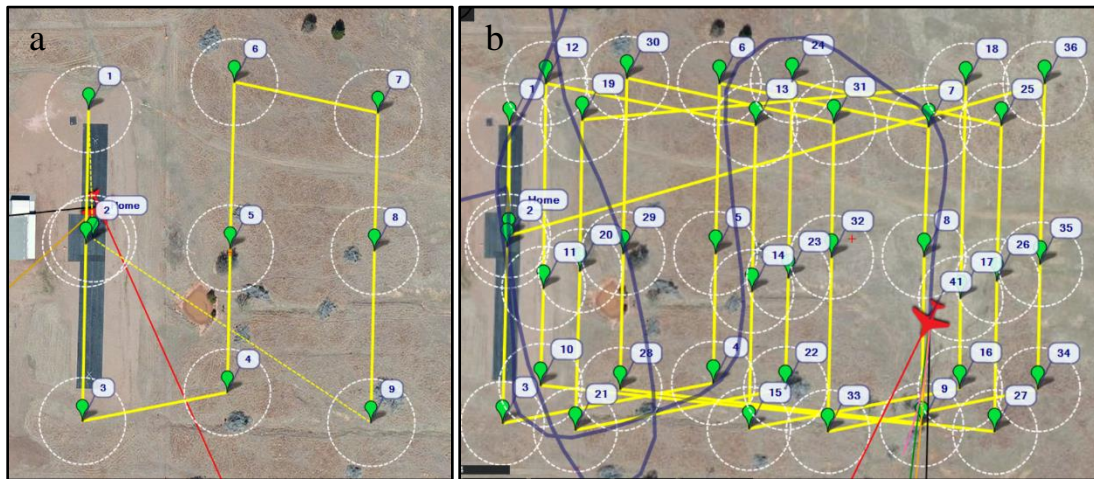


**Figure 46 - Sample grid flight paths: simple (a) and interleaved (b)**

## B. 160 ACRE CONTROLLED BURN TEST RESULTS

The first flight test performed over a controlled range burn took place on 160 acres (1/4 mi<sup>2</sup>) southwest of Stillwater, OK. The land was on a plot owned by Oklahoma State and was burned as a study by the Fire Ecology program. The burn occurred in late winter when the only live vegetation was cedar and similar trees so background CO<sub>2</sub> levels should be relatively uniform and

low. The flight configuration consisted of the CO<sub>2</sub> sensor system placed in the Firebird along with the original video recording setup; the flow system consisted of the 0.135" ID intake tube, particle filter, flow meter, CO<sub>2</sub> sensor, and the 2" exit funnel located on the trailing edge of the wing outboard of the tail booms.

Two flights were performed, each lasting about 20 minutes. The initial flank fire was started around 9:45 am on the southwest corner and the adjacent edges of the plot. The launch of the first flight occurred at around 10:20 am; at that time the winds from the nearby Oklahoma Mesonet site showed 8.3 mph at 40° azimuth. By the time of the launch the fire had grown to cover roughly the southwest quarter of the plot and was burning along the western flank as far north as the northern edge of the plot.

The first flight was set to fly a grid over the entire 160 acres at a nominal altitude of 300 ft. A benefit of flying over fires is the smoke gives a very good indication of where the winds may be blowing the CO<sub>2</sub> plume. Figure 47 shows the view from the aircraft at 300 ft on approach to the flank fire; the aircraft is approaching from the north of the plot and flying south along the eastern edge of the plot.



**Figure 47 - Flank fire as seen on approach from north**

The flight path after launch consisted of manual flight above the launch point while the data link was verified and autopilot settings were adjusted followed by switching the aircraft into autonomous waypoint-following mode to fly the grid pattern over the plot with a separation of 650 ft between each pass. Due to winds, the aircraft often could not get close enough to the southern waypoint on each leg so it performed a circle until it made it to the waypoint and continued on. The flight data was downloaded post-flight and run through a Matlab script to plot the aircraft's location with the CO<sub>2</sub> level indicated by the size and color of the points. The CO<sub>2</sub> levels were normalized by taking the ratio of the current CO<sub>2</sub> level and the minimum recorded CO<sub>2</sub> level for the plotted range. This data was then placed over a Google satellite map which was annotated with the wind speeds and fire locations for each pass based upon footage from the onboard GoPro: orange areas indicate locations that were burning when the aircraft passed over and black areas indicate areas which had already burned. The average flowrate for this flight was found to be 0.75 LPM which correlates to a 5 second delay before the peak CO<sub>2</sub> level is detected by the system, leading to the CO<sub>2</sub> data being matched with the location data from 5 s previous. The resulting flight path and normalized CO<sub>2</sub> levels are shown in Figure 49.



**Figure 48 - Firebird flight 1 launch**



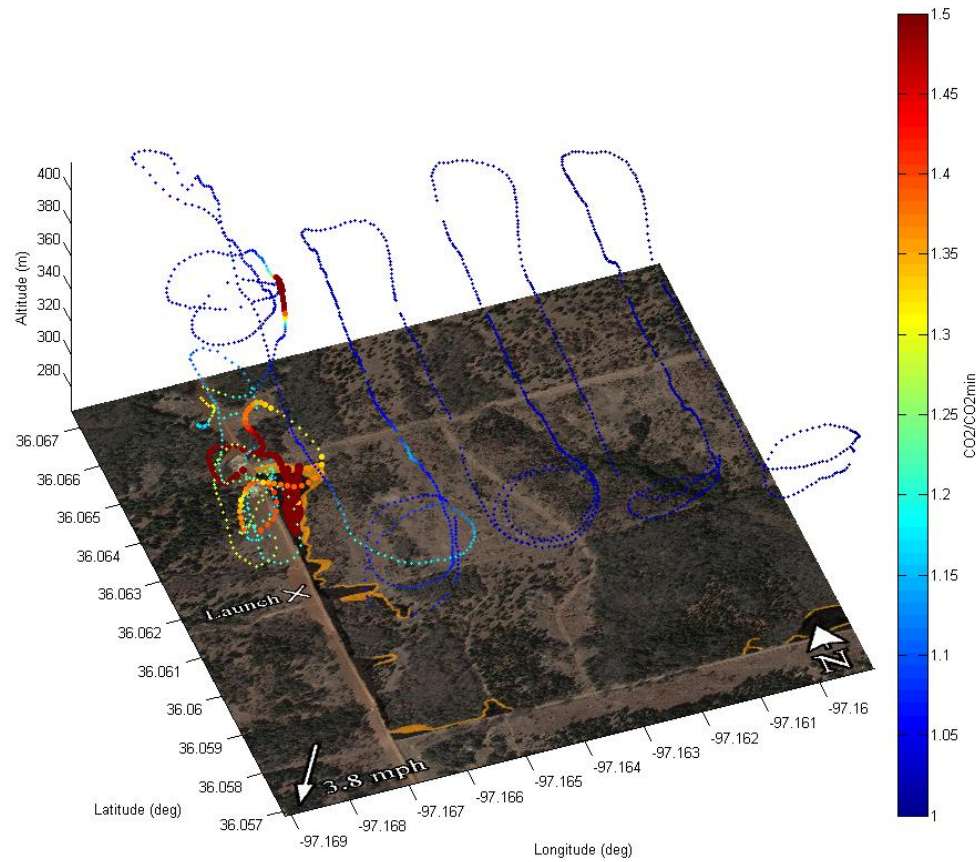


**Figure 49 - 3D plot of flight 1 path and normalized CO<sub>2</sub> levels**

The gas levels near the ground were much higher than in the air, which is to be expected since the density of CO<sub>2</sub> make it less buoyant compared to air and because the launch site, the aircraft's lowest altitudes, was inundated with smoke (and therefore likely CO<sub>2</sub>) as shown in Figure 48. Because the high ground levels wash out the gas levels recorded at 300 ft AGL during the grid pattern over the main burn plot, the range plotted was reduced to only this cruise portion of the flight as shown in Figure 50.

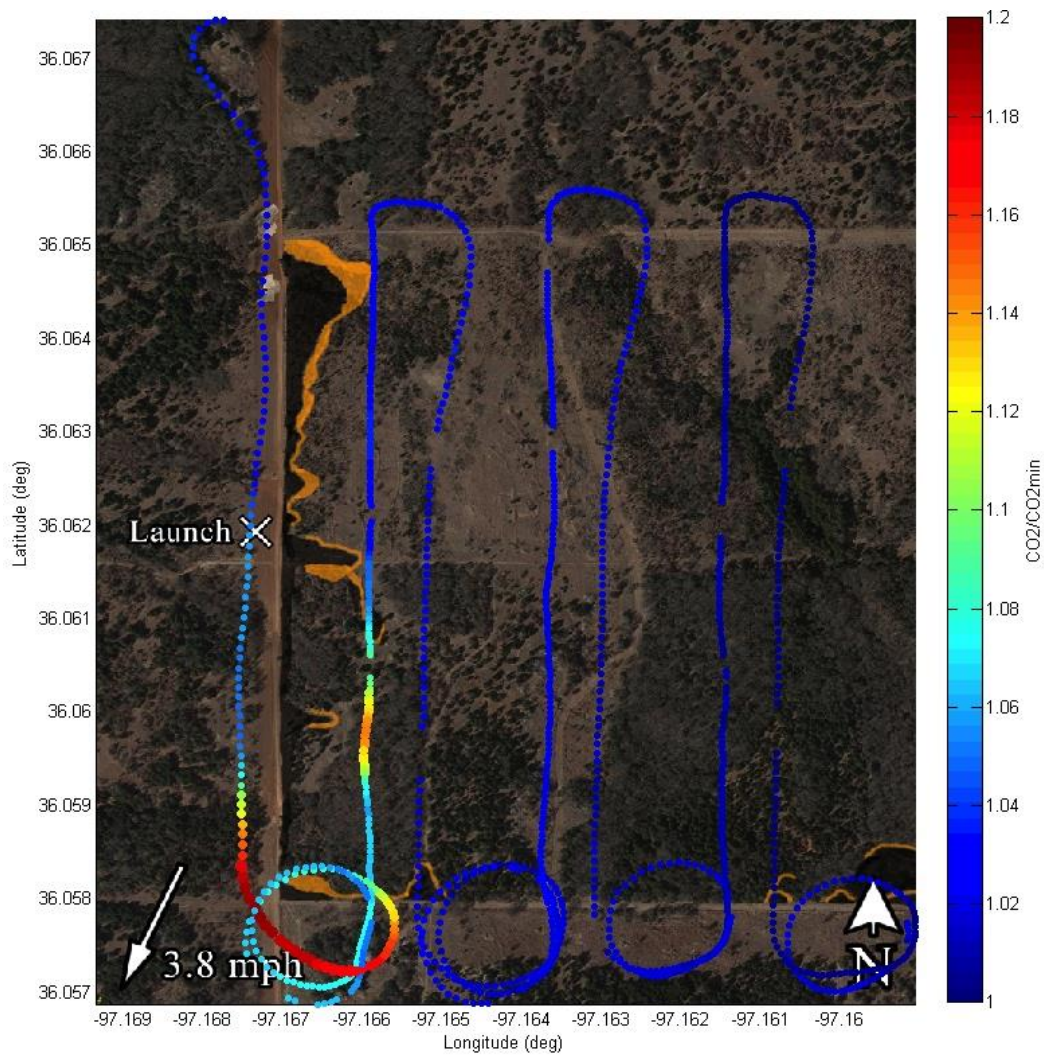


**Figure 50 - 2D plot of flight 1 path and CO<sub>2</sub> levels at nominal 300 ft altitude**

In this plot it can be clearly seen where the CO<sub>2</sub> levels are increased while flying over the fire in the southwest corner. During the circle portion the altitude changed leading to the varying gas levels when the aircraft was flying over the same points. To help further visualize the CO<sub>2</sub> concentrations over the area, the data from the full flight was interpolated using Matlab's TriScatteredInterp function which performs a linear Delaunay triangulation on the known values. The interpolation was applied to a 20 point grid over the flight range. The resulting model is shown in Figure 51. Because the fire is transient the interpolation cannot be applied to multiple passes because the data will change. It is important to note the values shown are not

measurements but calculations based upon those measurements for the purpose of simply providing visualization.

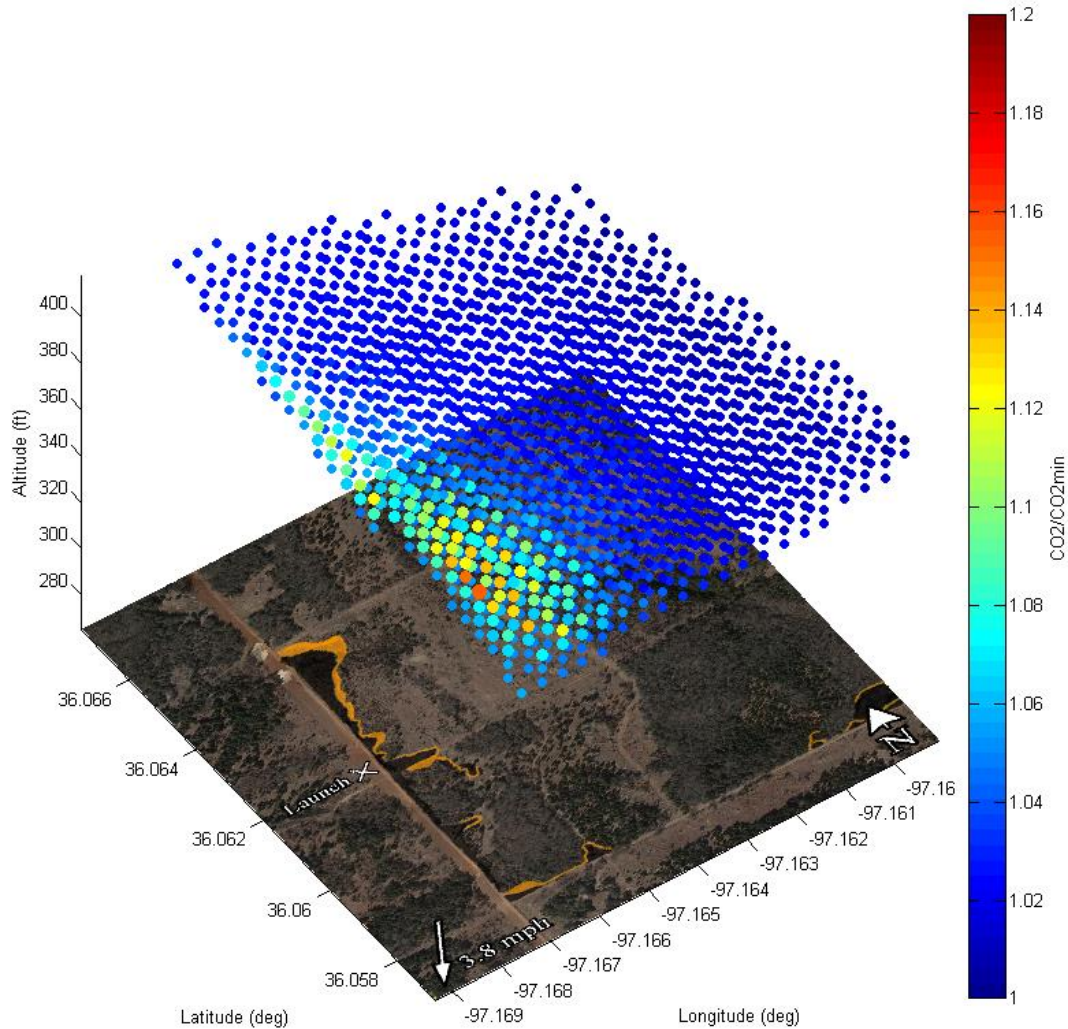


**Figure 51 - 3D interpolation of CO2 levels from flight 1**

### C. 2 MILE<sup>2</sup> CONTROLLED BURN TEST RESULTS

The next controlled range burn flight was flown over a roughly 2 mi<sup>2</sup> area north of Lake Carl Blackwell near Stillwater, OK. The burn was performed by a professional company, Chloeta Fire, to clear some OSU land for rangeland use. The area burned is shown in Figure 52 along with the aircraft launch point and several of the flight areas.



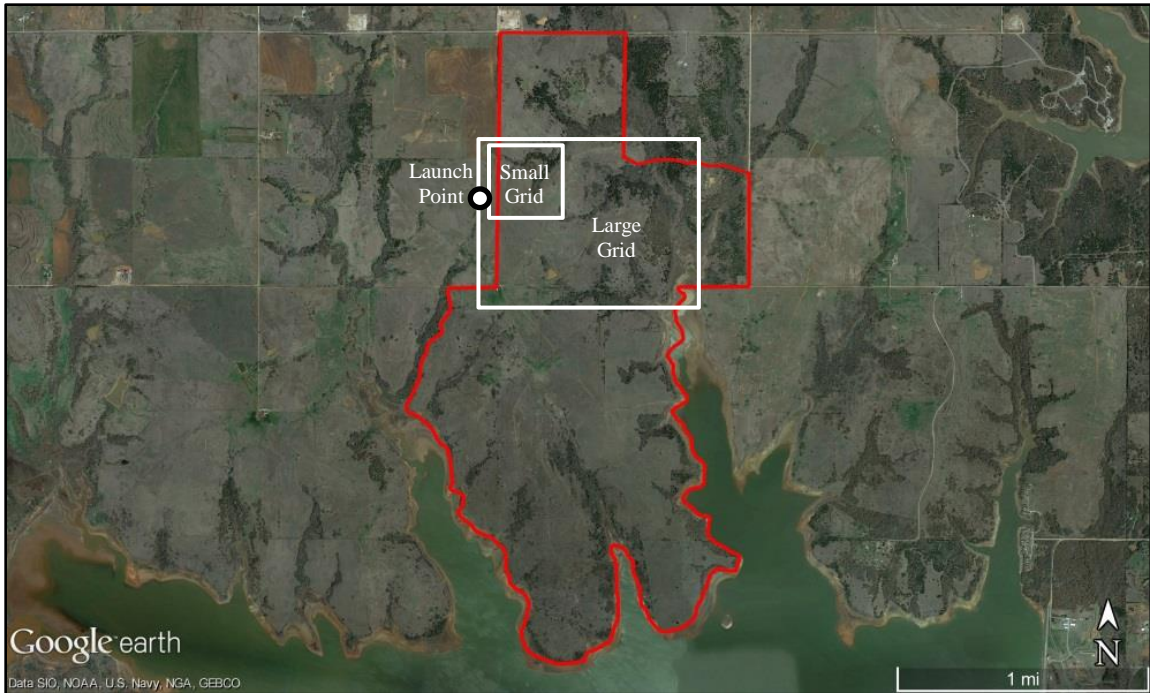


**Figure 52 - Lake Carl Blackwell burn area**

The flight test setup was similar to before with the 2” exit funnel but with the addition of a 1” intake funnel added to the 0.135” intake tube to increase the flowrate. The test took place in early spring when there were some sprigs of grass beginning in some fields, but the vegetation was mostly still dead.

The first flight occurred at 1:30 pm and did not pass over any fires – the purpose was simply to test the systems and the datalink range, record background levels, and collect imagery of fires burning in the far eastern part of the site. Unfortunately, any background and ground level CO<sub>2</sub> measured near the launch site for this and any other test is likely affected by the exhaust from the vehicle running to power the ground station. The flight lasted a little over 25 minutes and the CO<sub>2</sub> levels recorded are plotted alongside the aircraft altitude as shown in Figure 53.

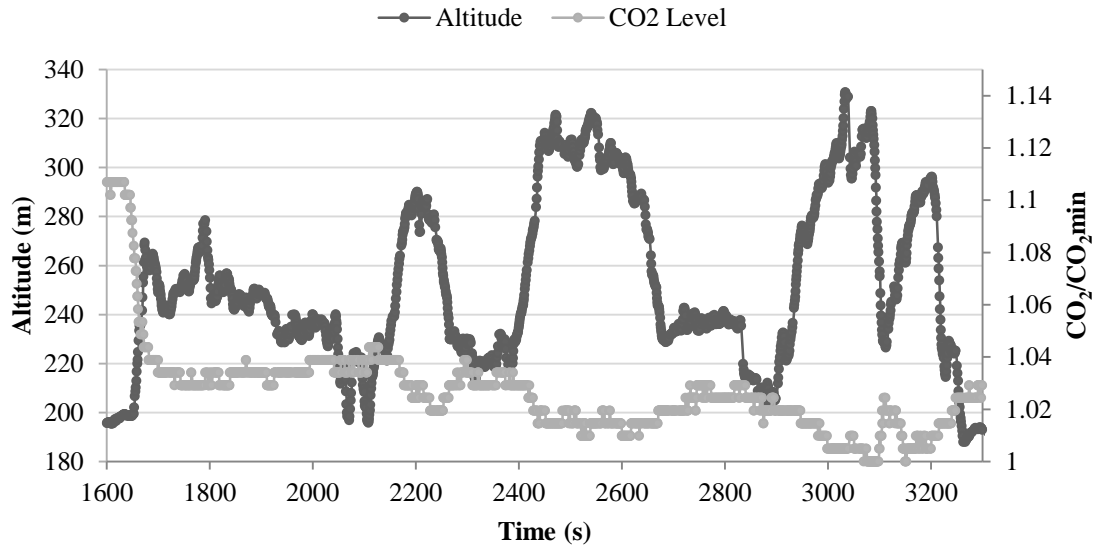


**Figure 53 - Flight 1 altitude vs CO2 level**

The gas level quickly levels off once the aircraft is in the air and has clean air flowing through the intake system; during the entire flight CO<sub>2</sub> levels are very consistent and the maximum percent increase over the lowest level recorded during the flight was 4.37%.

The second flight was launched at 3:30 pm when winds were at 6.7 mph from a direction of 347° (recorded from the 10 m tall Lake Carl Blackwell Mesonet Station) and the flight lasted 30 minutes. Shortly before the launch, a fire was started in the southwest as shown in Figure 52 and Figure 54. The flight was flown in manual mode around the launch site for short duration, followed by several passes over the fire in the southwest and a few flights to the east to try to get a view (though not fly over) the fire growing on the easternmost flank. The flight path (excluding takeoff and landing), normalized CO<sub>2</sub> levels, and the location of the burn are plotted in Figure 55. The average flowrate through the system was 0.45 LPM which correlates to a 7.5 s delay before the peak CO<sub>2</sub> levels which was included in the data.



**Figure 54 - Southwest fire during flight 2 as seen from launch point**

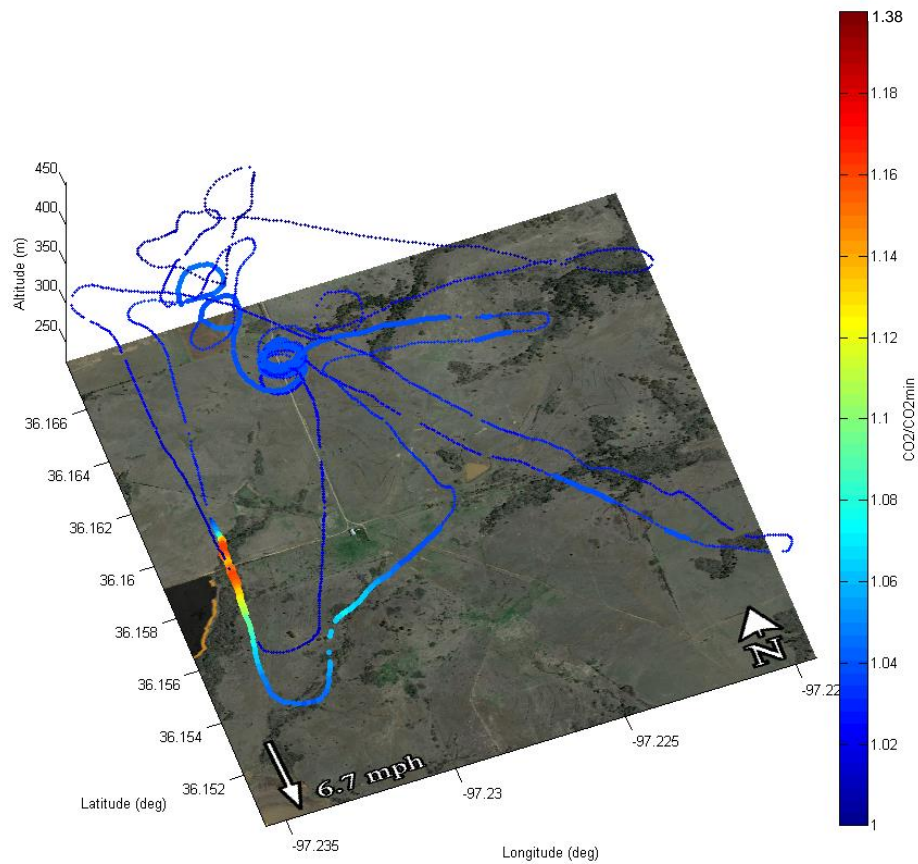


**Figure 55 - 3D plot of flight 2 path and normalized CO<sub>2</sub> levels**

The flight path shows a very clear rise in CO<sub>2</sub> levels when passing over the fire. To compare the CO<sub>2</sub> levels to the strength of the smoke plume that the aircraft was flying through, the flight video was reviewed and an arbitrary smoke level was assigned to portions of the flight quantify the strength of smoke that was seen. Figure 56 plots the first 12 minutes of the flight including the

altitude of the aircraft for reference (beginning with takeoff at 225 m MSL), the relative CO<sub>2</sub> level, and the assigned smoke level from the video. Portions of the pass are designated a-d in the chart and correspond with images from the aircraft shown in Figure 57. The smoke levels are also plotted in blue below the abbreviated flight path in Figure 58 with larger points indicating increased smoke levels. The second pass shown in Figure 55 did not detect the same rise in levels, but it occurred 12 minutes after the pass illustrated in Figure 56 - Figure 58 and review of the video showed that the smoke plume had dissipated as the fire moved further south. Including this second pass, the CO<sub>2</sub> levels after the first pass are consistently low and show a maximum percent increase over the lowest level recorded during the flight of 3.41%. In comparison, during the first pass over the fire this percent increase was 15.6% over the lowest CO<sub>2</sub> level recorded during the flight.

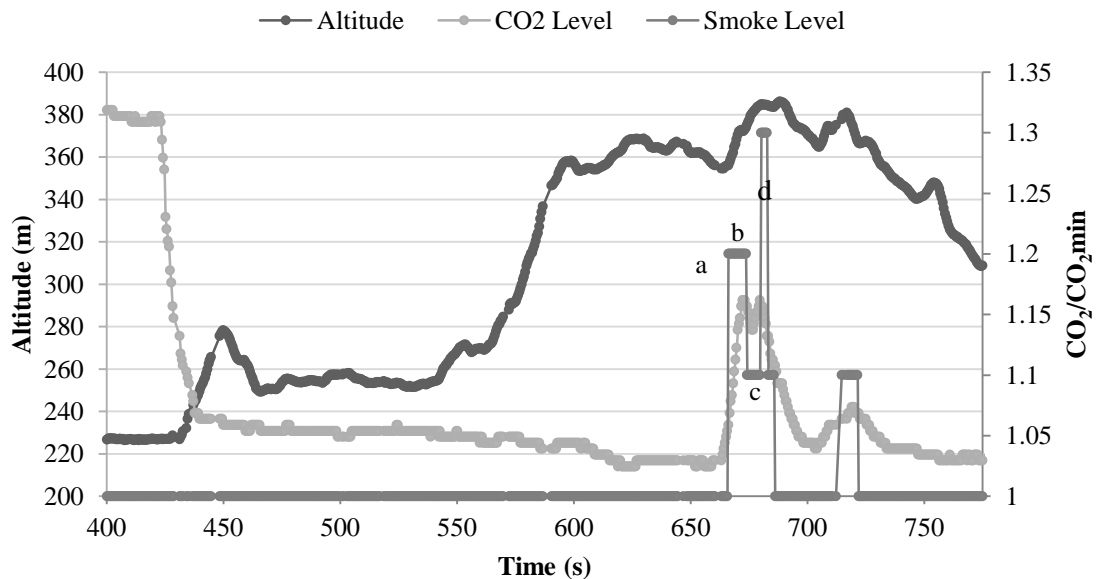


**Figure 56 - First 12 minutes of flight 2: altitude vs CO<sub>2</sub> levels and smoke levels**



**Figure 57 - Smoke seen from aircraft while passing through plume**



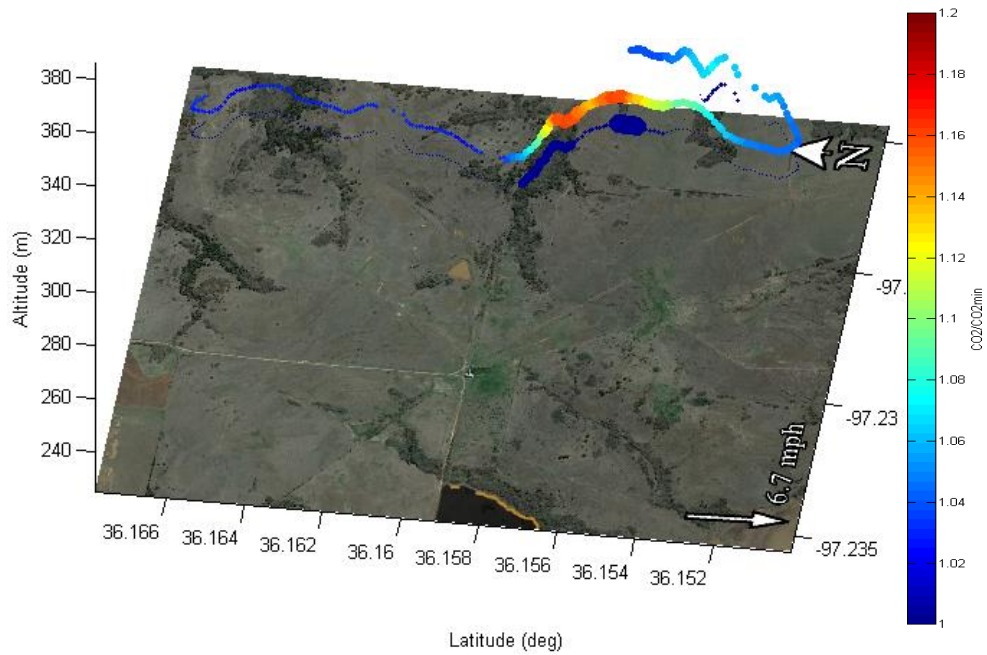


**Figure 58 - Abbreviated flight 2 path with smoke levels plotted below path**

By this point fires had also been started far to the south outside of the flight range and on another plot of OSU land being burned a mile to the west by a different company. All of these fires combined were strong enough to produce a visible plume on weather radar as shown in Figure 59

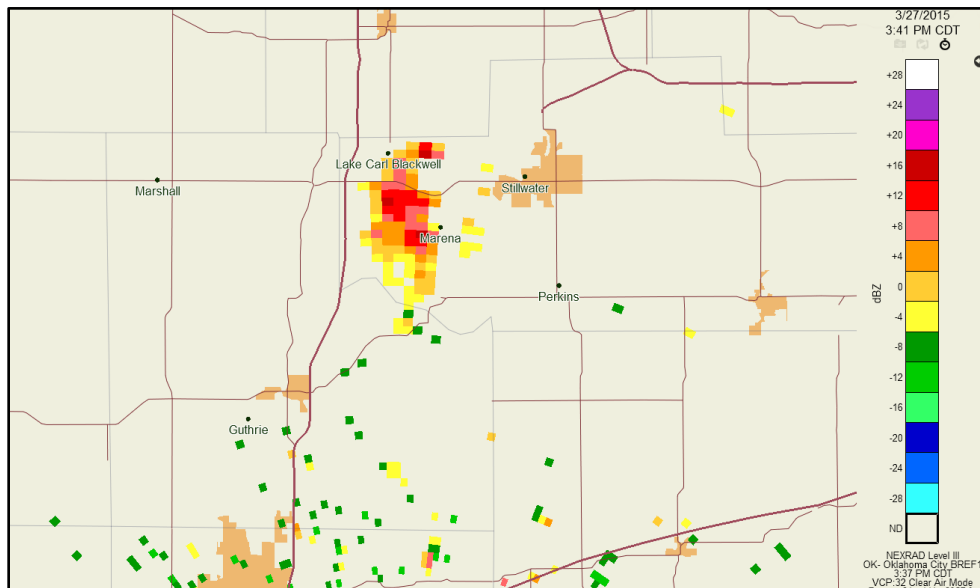


**Figure 59 - Weather radar imagery of fires**

The third flight was launched at 4:30 pm when a small fire was started just slightly northeast of the launch point (as drawn in Figure 52). The fire began small, but because the winds (7.8 mph at an angle of  $332^\circ$ ) blew it through a tall grass area, it spread very quickly to the southwest while the flight pattern was being flown above it; Figure 60 shows the fire as seen from the launch point as it began (around launch) and grew to cover most of the nearby field (four minutes later).



**Figure 60 - Flight 3 fire progression as seen from launch point**

For this flight the autopilot was set up to fly a grid over a 1200 ft wide by 1400 ft area with four passes spaced 400 ft apart and to fly the entire pattern at nominal altitudes of 100 ft, 200 ft, and 300 ft. This pattern took 8 minutes to fly, so the fire location moved quickly south during this time and changed even between each pass. Figure 61 shows the plot of the flight path (excluding takeoff) in 3D with the point color and sizes indicating the normalized  $\text{CO}_2$  levels and the general burn area and direction marked on the map. Figure 62 breaks the path down into the grid pattern at each altitude. Though it was difficult to tell with the noise, the flowrate generally ranged around 0.45 LPM during this flight that gave a 7.5 s delay between intake and peak  $\text{CO}_2$  levels which was included in the following charts.

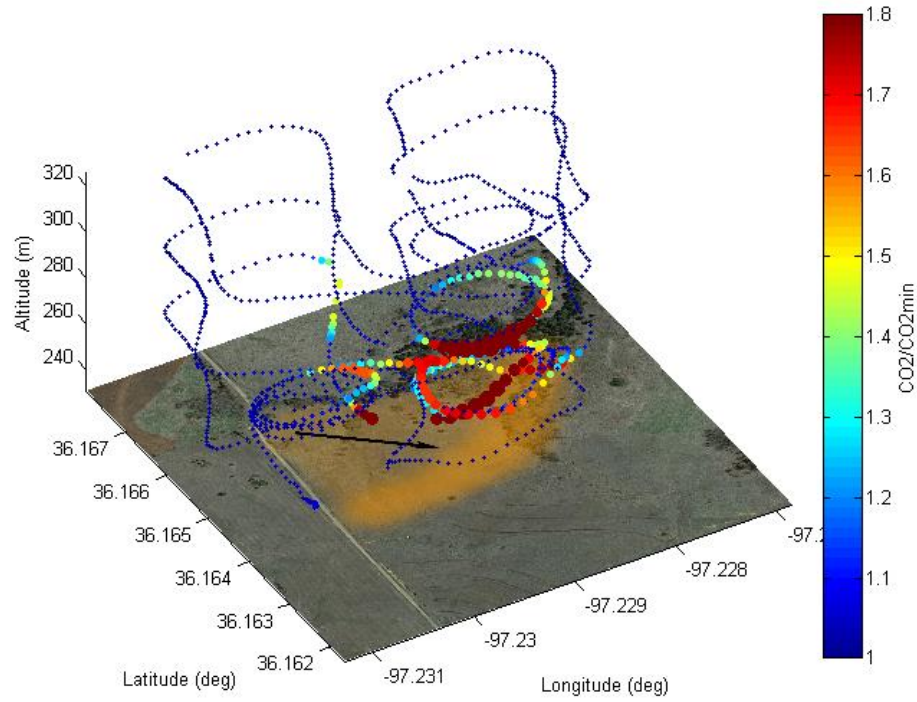


**Figure 61 - 3D plot of small grid flight 3 path and normalized CO<sub>2</sub> levels**

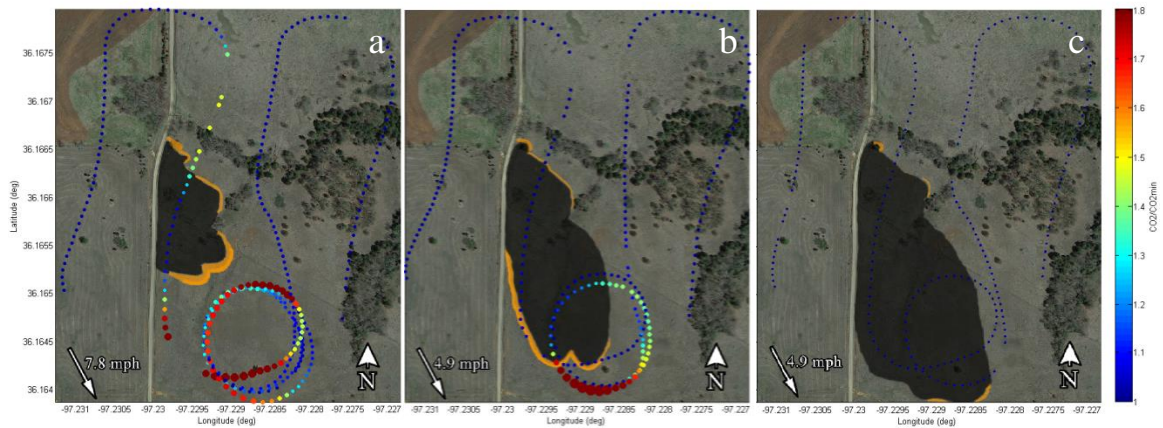


**Figure 62 - 2D plot of small grid at 100 ft (a), 200 ft (b), and 300 ft (c)**

Even though the fire was changing, the data still shows the burn front rather clearly. CO<sub>2</sub> levels were higher at lower altitudes as expected. By 400 ft the high levels detected directly beneath were hardly even detected, although this could in part be due to the fire progressing outside of the flight area.

After this small grid flight path was completed, the autopilot was programmed to fly a much larger grid pattern over the  $\frac{3}{4}$  mi<sup>2</sup> area adjacent to and to the southeast of the launch point. The grid was 4900 ft wide by 4000 ft with a grid spacing of 700 ft between passes. This grid was also set to be flown at altitudes of 100 ft, 200 ft, 300 ft, and 400 ft, but due to the size of the grid, only the 100 ft and two passes of 200 ft were accomplished during flight 3. The aircraft was landed at 5:00 and flight 4 was launched at 5:10 after replacing the batteries.

Winds at takeoff had lowered to 4.3 mph in a direction of 344°. The flight continued right where the previous flight had left off near the launch point. During this and the previous flight the fire had grown to encompass most of the observation area; the grassland areas burned quickly approaching the south and by the end of flight 4 most of the grassland areas were simply smoldering while the wooded areas mostly in the east and the southern flank were still burning (plus areas to the north and south beyond the flight grid). The aircraft unfortunately did not have enough power to complete the last 400 ft altitude grid pattern and after flying for 30 minutes was forced to make a controlled landing on the third-to-last leg of the grid. As mentioned, the grassland was already burned so the aircraft landed unharmed and could be safely retrieved. The resulting data from the large grid flight portions of flights 3-4 are shown in Figure 63. The average flowrate for this portion of both of these flights was found to be 0.37 LPM which calculates delay to factor into the data of 8.5 seconds.

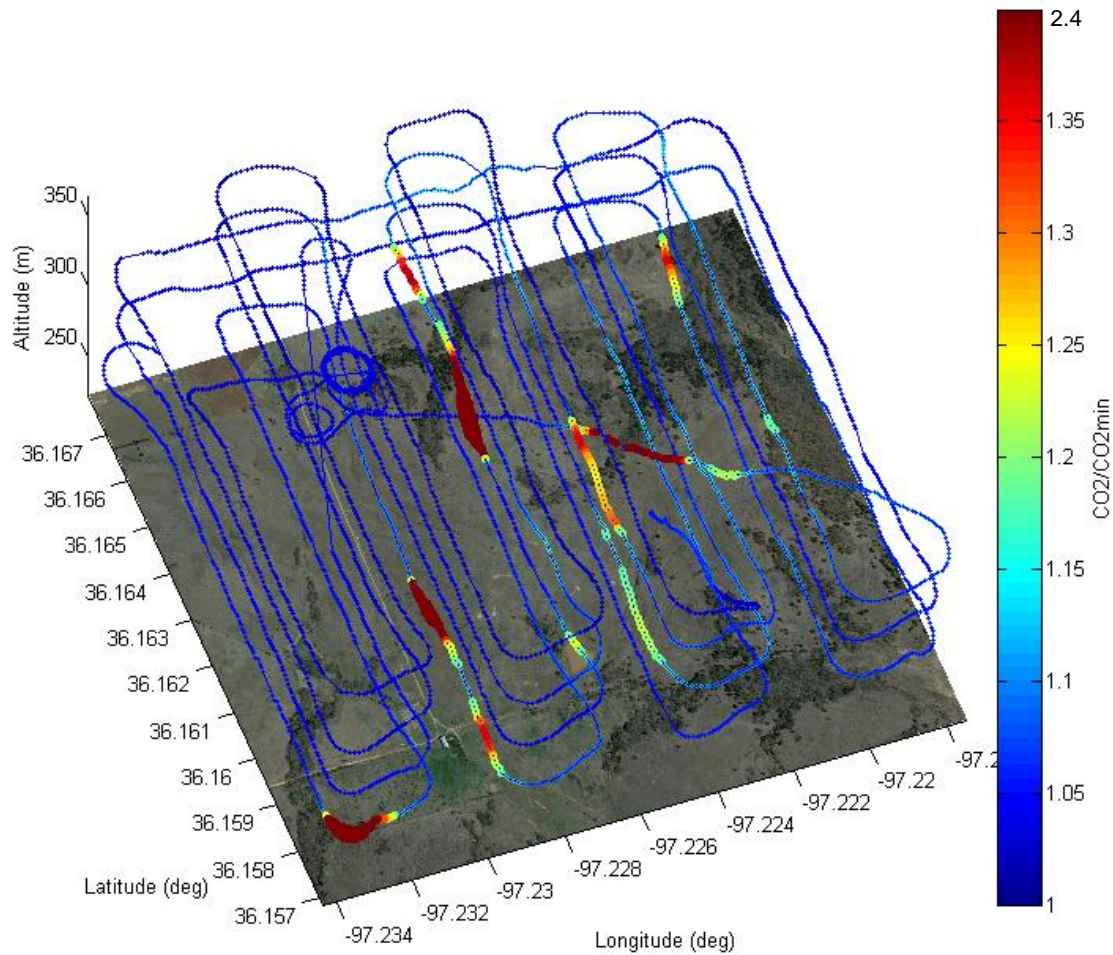


**Figure 63 - 3D plot of large grid flight 3-4 path and normalized CO2 levels**

Although the fires moved quite a bit during the flight and were burning with varying intensity with each pass, the flight data does show some clear trends. Several known fires to the south show up as increased gas levels and many of the more intense concentrations were located over groves of trees that were likely burning longer and more intensely than the surrounding grassland.



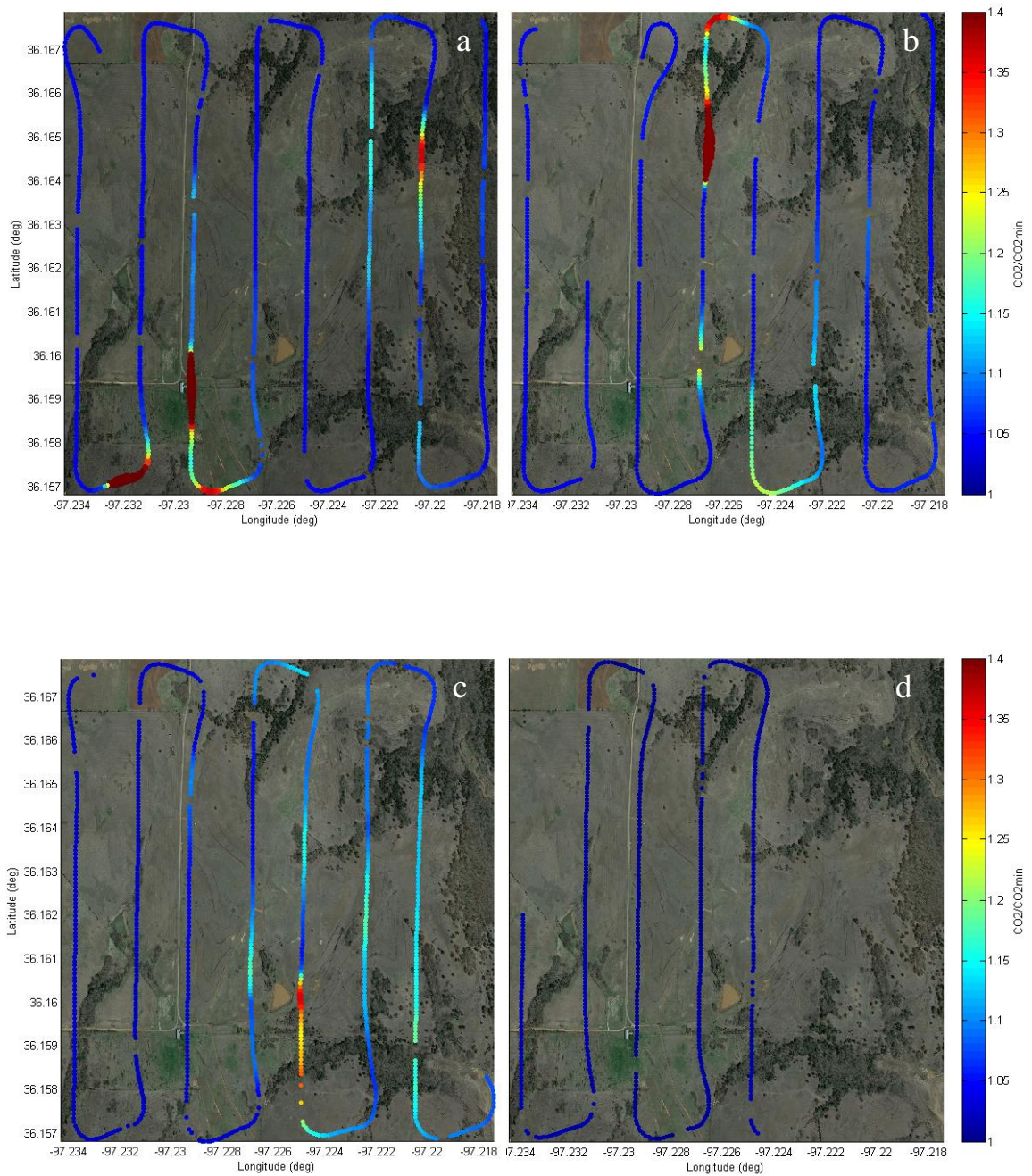


**Figure 64 - 2D plot of large grid at 100 ft (a), 200 ft (b), 300 ft (c), and 400 ft (d)**

#### D. CO<sub>2</sub> RELEASE TEST RESULT

The first controlled CO<sub>2</sub> release test was performed at the OSU airfield. The test was performed with the X-8 aircraft and the intake system consisted of the 0.135" ID intake tube and 1" exit

funnel located near the motor. A tank of CO<sub>2</sub> was connected to a nozzle mounted on a tripod to release the gas and allow the plume to disperse over the airfield. The nozzle was mounted 5.5 ft off of the ground in the setup shown in Figure 65. The CO<sub>2</sub> came from a 5 lb 600 psi tank. In an attempt to help the CO<sub>2</sub> plume rise as high in the atmosphere as possible, the tank was heated above ambient temperature by blowing a heat gun on it for 20 minutes and wrapping it in insulation filled with several pocket handwarmers. The outside temperature was 43.2 °F and winds were averaging 2 mph and gusting up to 5 mph coming from between WNW and WSW.



**Figure 65 - Airfield controlled CO<sub>2</sub> release test setup**

The aircraft was flown manually using the FPV camera instead of using autopilot so it could get as many passes as close and as quickly as possible. The tests consisted of several short bursts with direct passes over the nozzle followed by a long release while passing downwind across the plume.

The first pass was from downwind to upwind at a low altitude directly above the release point as shown in Figure 65. The CO<sub>2</sub> was released for 6 seconds at 25 SCFH (10 g of total CO<sub>2</sub> released) as the plane was on approach. The plane then looped around for a second pass. The gas was

released as the plane was again on approach and the release lasted for 30.5 s at 60 SCFH (125 g of CO<sub>2</sub> released). The plane then performed several more passes during and after the end of the release at varying low altitudes downwind to upwind. The final release consisted of releasing CO<sub>2</sub> for 12 minutes 15 seconds at 60 SCFH (3.0 kg of CO<sub>2</sub>). The gas was released for 1 min 13 s before the first pass. The aircraft passed at varying altitudes along the fenceline that was located 150 ft downwind of the release point. The entire flight path is shown in Figure 66 with an orange “X” near the runway designating the CO<sub>2</sub> release point.

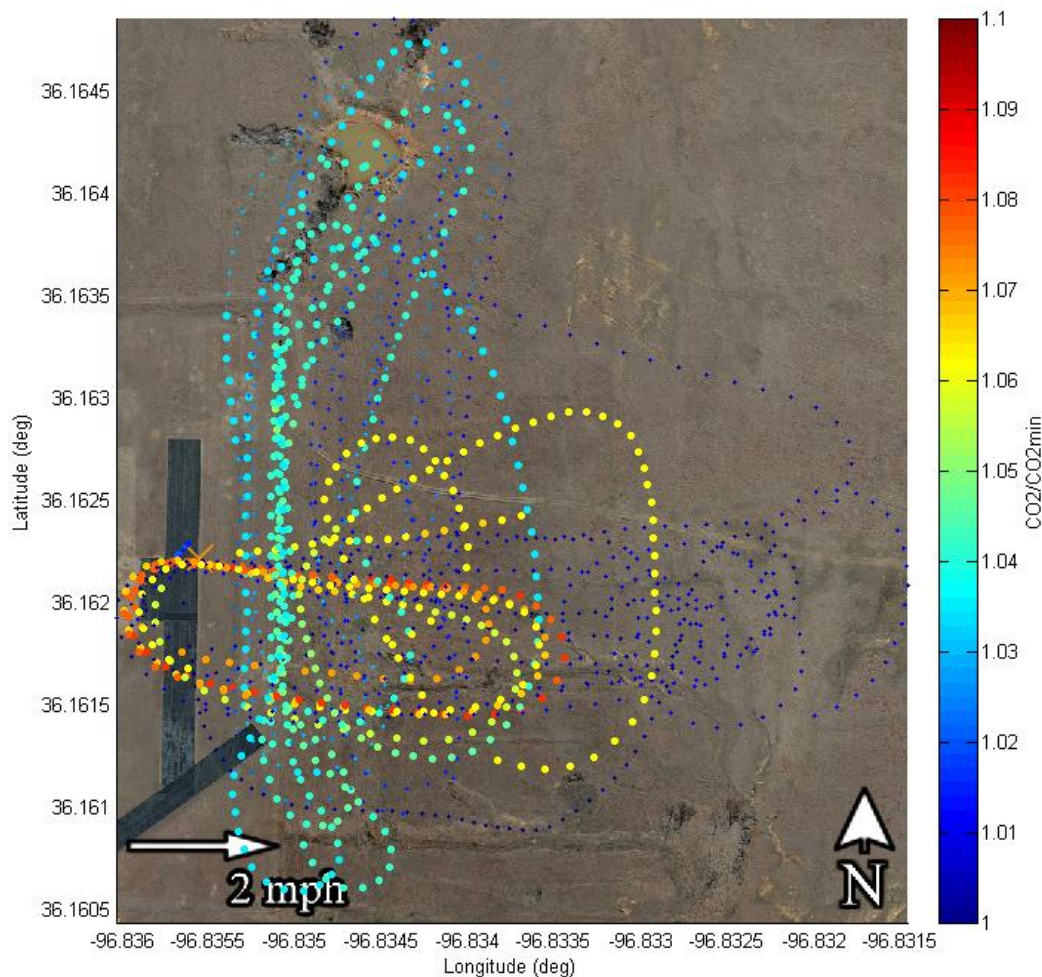


**Figure 66 - 2D plot of CO<sub>2</sub> tank release flight path**

Unfortunately, the system did not have a high enough flow rate and the passes were too short to allow the CO<sub>2</sub> levels to return to ambient between subsequent passes. This caused the CO<sub>2</sub> levels



to continue to rise each pass and created muddled data which did not give a clear image of the plume that the aircraft was flying through. This issue is best illustrated during the early downwind-upwind passes directly over the release point that are plotted in Figure 67. The passes were from east to west and the aircraft passed over the CO<sub>2</sub> release location at the western edge of the flight path, which corresponds to the bottommost peaks on the graph. The CO<sub>2</sub> levels rise at this point on each pass and remain high until rising again on the following pass.

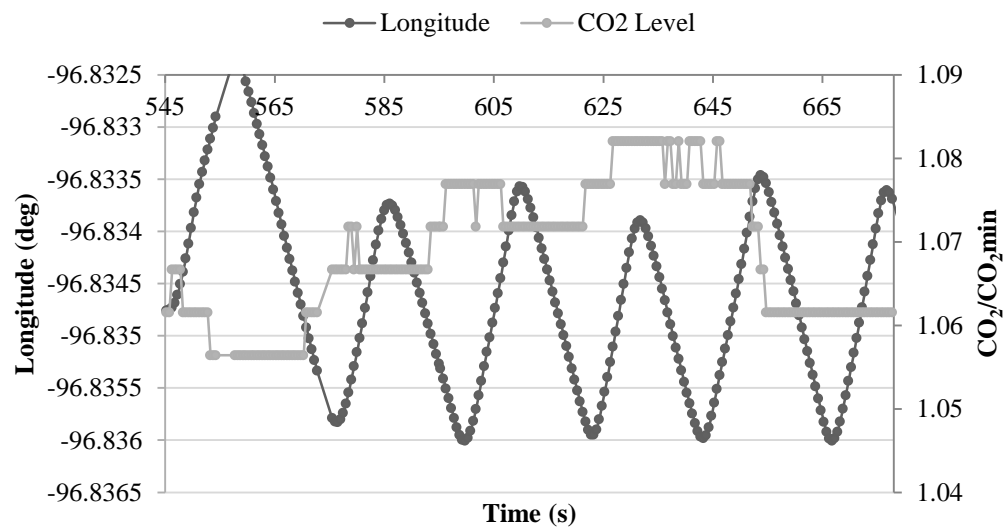


**Figure 67 - Longitude vs CO2 levels during east-west (downwind-upwind) passes over CO2 release**

The aircraft was prepared to repeat the test with a revised flow system which would provide an increased flow rate for a quicker return to ambient levels. During initial flight testing of this system, however, the aircraft suffered an electronics issue causing loss of control authority which resulted in the loss of the X-8 airframe.

#### E. SMALL PLOT FIRE TEST RESULTS

The final flight test occurred in early spring over a small plot burn performed by OSU's Fire Ecology program. The plot was only 715 yd<sup>2</sup> (0.15 acres) and located near the Fire Ecology station 5 mi west of Stillwater, OK. This burn, while much smaller, provided a good controlled

point source of fire CO<sub>2</sub> as compared to the moving widespread fires of previous tests. The sensors were again placed in the Firebird aircraft with the flow system consisting of the 2" intake funnel and 2" exit funnel. The burn occurred in early spring when there was some vegetation growing but there was still a fair amount of dead brown grass. Another student was fortunately testing another project that consisted of a trio of weather stations placed around the burn so live wind data from an altitude of 4 ft was available for the entire burn. Winds were on average 2.5 mph with a few gusts up to 5 mph in a direction of 326° during the flight.



**Figure 68 - Small plot burn**

The flight path was programmed to fly a grid pattern over the burn area at altitudes of 100 ft, 150 ft, 200 ft, and 250 ft. The grid consisted of five north-south passes which were 2600 ft long to provide plenty of clean air between passes over the fire for the CO<sub>2</sub> levels detected to return to ambient and spaced 150 ft apart. Because the aircraft could not turn tightly enough to make such close passes, a flight plan of interleaved 450 ft passes was flown. A plot on the south edge was burned before the flight, but was only smoldering by the time of launch. The flowrate during this flight averaged around 0.5 LPM which gave a resulting response time of 7 s which is included in the flight data shown in 3D in Figure 69. The fire for the plot observed was started when the grid began, but didn't become large until the second and third altitude pass. The 2D plot of the 150 ft

and beginning of the 200 ft pass is shown in Figure 70 with the burning plot highlighted in orange.

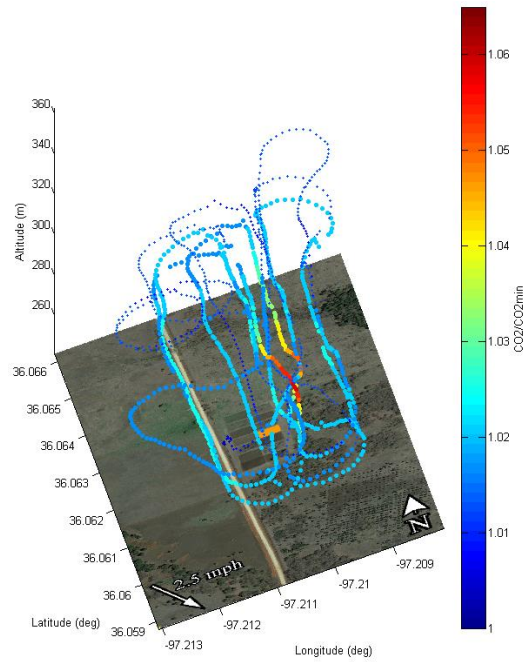


**Figure 69 - 3D plot of small plot flight path and normalized CO2 levels**

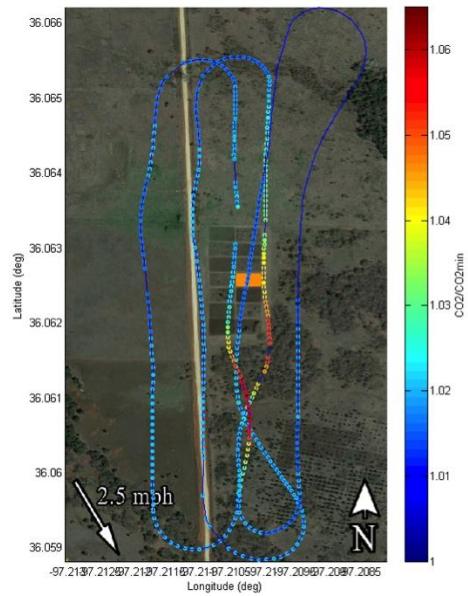


**Figure 70 - 2D plot of 150 ft small plot flight path and normalized CO2 levels**

The CO<sub>2</sub> levels very clearly increase when flying just south of the fire. This does not happen at all altitudes, but this is likely due to the changing intensity of the fire, especially during the lower altitude passes when the fire was just starting. For comparison, the model from Holzbecher was applied with the given wind speeds, a CO<sub>2</sub> diffusivity of 0.39 cm<sup>2</sup>/s, the plume originating from the plot location, and the observation point at the same altitude as the aircraft passes. The scaling values for the model do not match with the scale of the plot, so the plume model overlay in Figure 71 should be simply taken as a reference visualization of the general plume path and not a quantitative model of the CO<sub>2</sub> levels.

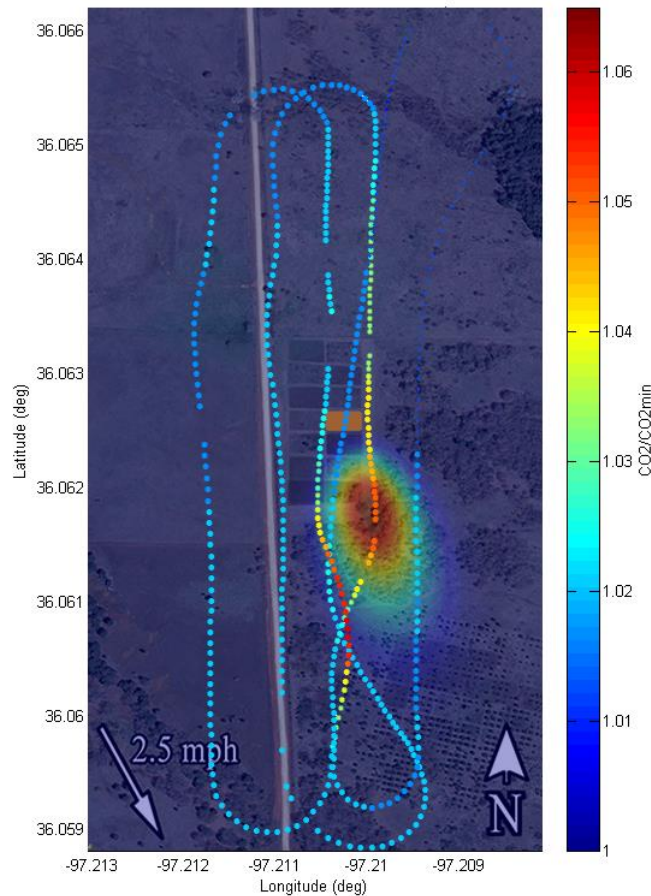


**Figure 71 - 2D plot of 150 ft small plot flight path and normalized CO<sub>2</sub> levels and sample plume model overlay**

## CHAPTER V

### CONCLUSIONS

#### I. CONCLUSIONS

The goal of this project was to develop a low-cost system to detect increased levels of anthropogenic carbon dioxide in the atmosphere. The system consists of an unmanned aircraft capable of autonomous operation as well as a flow-through sensor system which takes in-flight air samples and records the CO<sub>2</sub> level, GPS location, altitude, and flowrate. The sensor system cost less than \$500 and the complete aircraft system was developed for only a few thousand dollars.

During ground testing it was demonstrated that the K-30 FR CO<sub>2</sub> sensor requires a correction factor but has a linear output. The flow system with the best potential flow rate was identified through wind tunnel testing. Response time tests in the wind tunnel found that detection of gases took place on the order of several seconds although the time until peak detection often took roughly twice as long. It was later found that the time for the CO<sub>2</sub> levels to return to ambient was a major concern and higher flowrate systems are necessary. The first rudimentary field testing of the detection system proved promising when used to map CO<sub>2</sub> levels measured out of the window of a moving car while passing through a fire plume.

During flight testing the aircraft was flown and its layout and equipment were updated multiple times to provide high reliability and capability, adding equipment such as landing gear for higher takeoff weights and improved electronics and propulsion. The first major flight test of the gas detection system was performed aboard the Firebird aircraft and showed some very promising results in its ability to detect increased CO<sub>2</sub> levels when it flew over a 160 acre controlled burn and showed a very clear rise in gas levels when flying over the portion of the plot that was burning (Figure 50). The flight test at the airfield with a controlled release of CO<sub>2</sub> using the X-8 aircraft proved the necessity of having a high flow rate. During the test the gas levels were not able to return to ambient between passes through the plume as detailed in Figure 67, causing the CO<sub>2</sub> level to constantly increase and producing muddled data. After a controls issue resulting in the loss of the aircraft subsequent flight tests were performed aboard the Firebird aircraft.

The following flights over the large range burn at Lake Carl Blackwell helped further validate the aircraft's ability to map increased CO<sub>2</sub> concentrations. The first flight when there was no fire showed CO<sub>2</sub> levels at flight altitude to be vary only marginally with a maximum increase of 4.37%. When the second flight was flown over a distant fire (Figure 55) CO<sub>2</sub> levels were again very level (maximum increase of 3.41%) for most of the flight until passing over the burn during which they spiked up to 15.6% above the minimum level recorded during the flight. The increased levels correlated very well with the aircraft flying through the smoke plume as observed by the onboard camera as shown in Figure 56. The following flights demonstrated the issues with using a fire as a CO<sub>2</sub> source because of its transient nature of moving quickly and burning with varying intensity. This was perhaps most clearly illustrated while flying a small grid pattern over multiple altitudes during flight 3 as shown in Figure 62. What began as a point fire quickly spread and encompassed most of the flight area by the end of the grid, causing low CO<sub>2</sub> levels to be detected during early passes while increased levels were detected during subsequent passes at higher altitudes. While this did not produce a clean plume as expected from a steady-state source,

considering the wind speed and direction and the fire's burn direction the increased carbon dioxide levels did correlate rather well to the general area where the fire was burning most intensely during later passes. The transient nature of fires was illustrated even more clearly when the aircraft flew the large multi-altitude grid pattern illustrated in Figure 64 that took nearly an hour to complete. It was difficult to judge where the fire moved and grew over that large area during such a long time, but when the flight data was compared to a map of the terrain it was interesting to note that many of the areas of increased CO<sub>2</sub> levels were located over and slightly downwind of wooded areas; these areas likely burned longer and more intensely and produced a more persistent, detectable plume than the grassland areas which moved and burned out very quickly.

Finally, flight tests were performed over a sub-acre small plot burn which provided a much more controlled, predictable point source of CO<sub>2</sub> than the aforementioned rangeland burns. Although the fire did not move much during this test because the plot was so small it did again show how the changing intensity of a fire greatly affects the strength of the plume over time. Though this did cause gas levels to vary during subsequent passes at multiple altitudes, the levels shown in Figure 70 that were clearly increased above ambient all occurred where would be expected in an area slightly downwind of the plot. This location also correlated well with a Gaussian model of the plume dispersion shown in Figure 71. Ultimately, during the majority of tests the data consistently showed that increased carbon dioxide levels were detected downwind of where known fires were burning, demonstrating the system's ability to detect and map the location of carbon dioxide plumes.

## **II. IMPROVEMENTS AND FUTURE WORK**

Despite the success of the system for the desired objective, there is still plenty of opportunity for the system. One of the most important areas for improvement is the flowrate system. Attempts

were made to increase the flowrate through passive methods such as varying the design of the inlet and exit configurations of the system. While these demonstrated a noticeable improvement, they still did not provide a flowrate with a high enough sensor response time. While a few seconds delay in peak detection time is short enough to shift the data to refine the location of the detected plume, the greater issue is the time it takes for the sensor to return to atmospheric background levels. This issue was highlighted best during the controlled CO<sub>2</sub> release tests using the X-8 aircraft at the airfield. In these tests remnants of the increased CO<sub>2</sub> air sample had not fully left the system, causing the CO<sub>2</sub> levels to simply increase with each subsequent pass through the plume. Further increasing the flowrate through the system would do much to alleviate this problem, but the required increase may be beyond the reasonable capabilities of passive improvements and it may be necessary to install a pumping system onboard the aircraft.

While the system succeeded in its goal to detect increased CO<sub>2</sub> levels, further testing and improvements are required to be able to accurately quantify the gas levels detected to better characterize the plume. This type of high accuracy measurement will be necessary to detect small leak levels that may not rise but a few ppm above ambient. Improved calibration techniques will be a key part in attaining this level of accuracy, possibly including in-flight but at least pre- and post-flight calibration using reference gases as used in several previous works. In addition, further testing is needed to characterize the effects of flow rate on the values of carbon dioxide detected. This will include wind tunnel and laboratory testing to determine if the levels being detected are the actual values of CO<sub>2</sub> or if too high of a flow rate does not allow for the gas to be fully measured. Further validation of field tests would also be desired, such as comparing the atmospheric levels measured by the aircraft to a network of sensors on both the ground and at various altitudes (such as mounted to towers or balloons). More detailed mathematical plume modeling could also be a key component of these tests. Field tests would also need to utilize CO<sub>2</sub>



sources that closer mimic carbon sequestration sources that at a minimum are similar to the setup used in the X-8 airfield CO<sub>2</sub> tank release tests instead of very transient sources such as fires.

Finally, there is room for improvement to the design of the sensor system itself. The system used in this project was a prototype configuration, which, while ideal for troubleshooting and the ease of making changes, was bulky and offers plentiful potential for a reduction of size and increase in capabilities. Many autopilots (including the Pixhawk) offer the ability to modify the firmware to communicate with additional sensors through methods such as I2C. Because the Pixhawk already includes a GPS unit, altimeter, and SD logging, essentially the addition of the CO<sub>2</sub> sensor and flowmeter would allow for the elimination of nearly all of the sensor system boxes now included in the aircraft. This would remove nearly 2 lbs from the aircraft weight once the sensor system batteries and other components are included. Great care would need to be taken, however, to ensure that the additional sensor communication would not interfere with the processing capabilities of the autopilot and extensive testing would need to be performed to verify the reliability of the firmware changes. In addition to a reduction in weight and volume of the sensor system though, integration with the autopilot would also provide increased capabilities to the system. A higher logging rate may be possible as well as integration with the aircraft wireless telemetry. This wireless datalink would allow for the CO<sub>2</sub> levels to be streamed live to the ground station instead of having to wait to download the data after the flight which would allow in-flight mission changes based on areas of interest; in addition the values could then be displayed on the on-screen display of the pilot's FPV video system for increased situational awareness and flight planning. Finally, integration with the autopilot system would allow for future improvements in automated path planning as are being worked on by other teams in the mechanical and aerospace engineering department. This would allow algorithms to be applied to the data as it is recorded to make the mission more efficient by focusing the flight path on the areas of greatest interest while only sparsely covering areas with no variation in gas levels.

Future work could also include changing the gas sensor of the system to detect various other types of gases for the identification and quantification of leaks. A methane sensor could be fitted to detect leaks along natural gas pipelines or around gas storage and refining sites. Air quality measurements could be performed to detect sources of nuisance or dangerous gases over processing plants or chemical storage. Sensors could also be fitted to detect dangerous or volatile compounds in fire plumes or around disaster sites. Ultimately, there is a great amount of future potential for this system; whether through helping to improve carbon sequestration processes to reduce greenhouse gases, or through detecting gas leaks that could be potentially harmful, the combination of unmanned aircraft and atmospheric gas measurement and mapping offers the ability to save money and improve people's quality of life.

## REFERENCES

- Brake, Daniel. *Detection and Measurement of Fugitive Emissions Using Airborne Differential Absorption Lidar (DIAL)*. 10 25, 2005.  
<http://www.epa.gov/gasstar/documents/workshops/2005-annual-conf/brake.pdf> (accessed 10 12, 2014).
- Burba, G, and D Anderson. *Introduction to the Eddy Covariance method: general guidelines and conventional workflow*. Lincoln, NE: LI-COR Biosciences, 2007.
- Campos, T, S Shertz, S Hall, B Stephens, and L Husted. "Continuous Airborne Measurements of Carbon Dioxide Fluxes and Mixing Ratios and Carbon Monoxide Mixing Ratios on the NSF/NCAR C-130 Platform: Preliminary Results from GOTEX and ACME." *Seventh International Carbon Dioxide Conference*. Broomfield, CO, 2005.
- Clark, Peter, Jack Pashin, Tyler Ley, Girish Chowdhary, Jamey Jacob, and Nicholas Materer. *Surface and Airborne Monitoring Technology for Detecting Geologic Leakage in a CO<sub>2</sub>-Enhanced Oil Recovery Pilot, Anadarko Basin, Texas*. DE-FE0012173, 2013.
- Cohen, Yossi, and Daniel H Rothman. "Mechanisms for mechanical trapping of geologically sequestered carbon dioxide." *Proc. Royal Society A* 471: 20140853 (2014)..

Ethridge, David, et al. *Atmospheric monitoring and verification technologies for CO<sub>2</sub> storage at geosequestration sites in Australia*. Canberra: Cooperative Research Centers for Greenhouse Gas Technologies, 2005.

Fix, Andreas, et al. "Optical Parametric Oscillators and Amplifiers for Airborne and Spaceborne Active Remote Sensing of CO<sub>2</sub> and CH<sub>4</sub>." *Lidar Technologies, Techniques, and Measurements for Atmospheric Remote Sensing VII*, 818206. 2011.

Frankenberg, C, et al. "The Orbiting Carbon Observatory (OCO-2): spectrometer performance evaluation using pre-launch direct sun measurements." *Atmospheric Measurement Techniques*, no. 8 (2015): 301-313.

Herzog, Howard, and Dan Golomb. "Carbon Capture and Storage from Fossil Fuel Use." In *Encyclopedia of Energy*, edited by Cutler J Cleveland, 277-287. New York: Elsevier, 2004.

Holzbecher, E. *Environmental Modeling*. Berlin Heidelberg: Springer-Verlag, 2012.

Johnson, William, Kevin S Repasky, and John L Carlsten. "Micropulse differential absorption lidar for identification of carbon sequestration site leakage." *Applied Optics* 52, no. 13 (2013): 2994-3003.

Krevor, Samuel, Jean-Christophe Perrin, Ariel Esposito, Chris Rella, and Sally Benson. "Rapid detection and characterization of surface CO<sub>2</sub> leakage through the real-time measurement of  $\delta^{13}\text{C}$  signatures in CO<sub>2</sub> flux from the ground." *International journal of Greenhouse Gas Control*, no. 4 (2010): 811-815.

National Physical Laboratory. *Measurement of Challenges of Climate Change*. 8 8, 2012.  
<http://www.npl.co.uk/news/measurement-challenges-of-climate-change> (accessed 4 28, 2015).

- Poppa, Florian, Uwe Zimmer, Andrew Feitz, and Henry Berko. "Development of a Carbon Dioxide Monitoring Rotorcraft Unmanned Aerial Vehicle." *Robotics: Science and Systems (RSS) Workshop on Robotics for Environmental Monitoring (WREM)*. Berlin, Germany, 2013.
- Quatrevalet, Mathieu, et al. "CHARM-F: The Airborne Integral Path Differential Absorption LIDAR for Simultaneous Measurements of Atmospheric CO<sub>2</sub> and CH<sub>4</sub>." *25th International Laser Radar Conference*. St. Petersburg Russia, 2010.
- Spangler, Lee H, et al. "A shallow subsurface controlled release facility in Bozeman, Montana, USA, for testing near surface CO<sub>2</sub> detection techniques and transport models." *Environmental Earth Science*, no. 60 (2010): 227-239.
- U.S. Department of Energy Office of Fossil Energy. *Overview of Carbon Storage Research*. n.d. <http://energy.gov/fe/science-innovation/carbon-capture-and-storage-research/overview-carbon-storage-research> (accessed 4 26, 2015).
- U.S. Department of Energy. *Best Practices for Monitoring, Verification, and Accounting of CO<sub>2</sub> Stored in Deep Geologic Formations – 2012 Update*. U.S. Department of Energy, 2012.
- U.S. Environmental Protection Agency. *Inventory of U.S. Greenhouse Gas Emissions and Sinks: 1990-2013*. Washington, DC: U.S. Environmental Protection Agency, 2015.
- Vaz, A. Ismael F, and Eugénio Ferreira. "Air pollution control with semi-infinite programming." *Applied Mathematical Modeling* 33 (2008): 1957-1969.
- Watai, T, T Machida, N Ishizaki, and G Inoue. "A Lightweight Observation System for Atmospheric Carbon Dioxide Concentration Using a Small Unmanned Aerial Vehicle." *Journal of Atmospheric and Oceanic Technology* 23 (2006): 700-710.

Whittaker, Steve. "IEA GHG Weyburn-Midale CO2 Storage & Monitoring Project." *Regional Carbon Sequestration Partnerships Annual Review*. Pittsburg, PA, 2010.

World Meteorological Organization. "WMO Greenhouse Gas Bulletin." *World Meteorological Organization*. 9 9, 2014.

<http://www.wmo.int/pages/prog/arep/gaw/ghg/GHGbulletin.html> (accessed 4 18, 2015).

Yasuda, Tomomi, Seichiro Yonemura, and Akira Tani. "Comparison of the Characteristics of Small Commercial NDIR CO2 Sesor Models and Developmento of a Portable CO2 Measurement Device." *Sensors*, no. 12 (2012): 3641-3655.

## APPENDIX A – Additional Figures

### I. ADDITIONAL SENSOR SYSTEM DETAILS

#### A. TEMPERATURE & HUMIDITY SENSOR

Temperature and Humidity are beneficial pieces of atmospheric data to have so it was decided to add a temperature/humidity sensor to the system. A Sparkfun SEN-11295 breakout board was installed which contains a Honeywell HIH6130 digital temperature and humidity sensor. The sensor operates on 5V and communicates through I2C so it able to share the same comm channel as the altimeter. It is accurate to 4% RH and 1 °C. The layout of the sensor system was originally designed for the exit flow from the CO<sub>2</sub> sensor to blow directly onto the HIH6130 to obtain the temperature and humidity of the air in the flow system. This feature had to be eliminated, however, to attach the CO<sub>2</sub> sensor exit to an exhaust duct outside of the aircraft to increase the flowrate, which was decided to be much more important than the atmospheric data. Because of this, the temperature/humidity sensor no longer gets fresh external air and simply records the temperature inside the aircraft.



**Figure 72 - Sparkfun HIH6130 temperature/humidity board**

## **B. PRESSURE SENSOR**

A pressure sensor was also added to the system in case atmospheric pressure data was needed to develop correction factors for the CO<sub>2</sub> levels. A Honeywell ASDXACX015PA7A5 absolute pressure sensor was installed to detect the stagnation pressure in the flow tubing. The sensor has a range of 0-15 psia and a total error band of 2% of the full scale span. The sensor is digital and, like others, communicates through I2C and operates at 5 V. Ultimately, a different calibration method was used and the atmospheric pressure data was not necessary. Because the programming was already at the memory limits of the Arduino Leonardo, the code to operate the ASDX was not included and the pressure is no longer recorded.



**Figure 73 - Honeywell ASDX absolute pressure sensor**

## **A. VOLTAGE STEP-UP CIRCUITRY**

As discussed previously, the flowmeter runs off of 10 V whereas the rest of the sensor systems run off of 5 V power provided by the Arduino's regulator. Adding an external battery to power



the flowmeter was not considered a viable option because the voltage change as the battery degrades would likely affect the analog output and having separate ground sources could cause issues. Supplying the entire system with a higher voltage and adding a separate 10 V regulator to power the flowmeter was also not favorable because the 5 V regulator on the Arduino would have a high load that could cause heating issues. For these reasons it was decided to install a voltage step-up circuit to increase the Arduino's 5 V to 10 V. A Texas Instruments MC34063A switching regulator was chosen as the basis of this circuit. Table 4 from the product datasheet gives the equations to be solved to calculate the values of the various components of the circuit. Fortunately, several online calculators are available (such as the one located at <http://www.nomad.ee/micros/mc34063a/>) that will aid in computing these values. The calculations were performed to step the voltage from 5 V to 10 V with a max current of 100 mA and a frequency of 33 KHz; the resulting component values are shown in the circuit diagram in Figure 74.

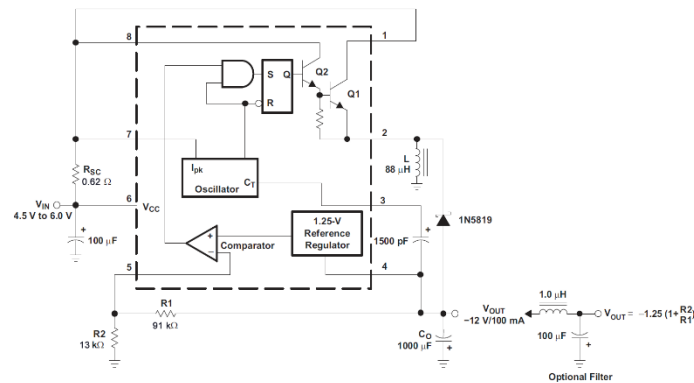


**Figure 74 - Step-up circuit diagram**

**Table 4 - Switching regulator step-up circuit calculations**

CALCULATION	STEP UP
$t_{on}/t_{off}$	$\frac{V_{out} + V_F - V_{in(min)}}{V_{in(min)} - V_{sat}}$
$(t_{on} + t_{off})$	$\frac{1}{f}$
$t_{off}$	$\frac{t_{on} + t_{off}}{\frac{t_{on}}{t_{off}} + 1}$
$t_{on}$	$(t_{on} + t_{off}) - t_{off}$
$C_T$	$4 \times 10^{-5} t_{on}$
$I_{pk(switch)}$	$2I_{out(max)} \left( \frac{t_{on}}{t_{off}} + 1 \right)$
$R_{sc}$	$\frac{0.3}{I_{pk(switch)}}$
$L_{(min)}$	$\left( \frac{V_{in(min)} - V_{sat}}{I_{pk(switch)}} \right) t_{on(max)}$
$C_o$	$9 \frac{I_{out} t_{on}}{V_{ripple(pp)}}$
$V_{out}$	$1.25 \left( 1 + \frac{R2}{R1} \right)$ See <a href="#">Figure 10</a>

It is desired for the ripple voltage to be as small as possible, but the capacitor value that determines,  $C_o$ , in the equations is very sensitive to the preferred ripple voltage and can call for very large capacitor values. In addition, the datasheet indicates that the calculated value may differ from the value required in practice, so because of this it was decided to simply test several various capacitor values to see which reduces the ripple voltage best. Capacitors of 0.047  $\mu F$ , 10  $\mu F$ , 1000  $\mu F$ , and 4700  $\mu F$  were tested. It was found that the 10  $\mu F$  capacitor reduced the ripple the most, to 38 mV (76 mV peak-to-peak). For all of these tests, and the final circuit, the optional filter (included in Figure 74) was also included to further reduce the ripple voltage. The final circuit provided a steady 10 V  $\pm$ 38 mV and was integrated into the sensor system as shown in Figure 75.

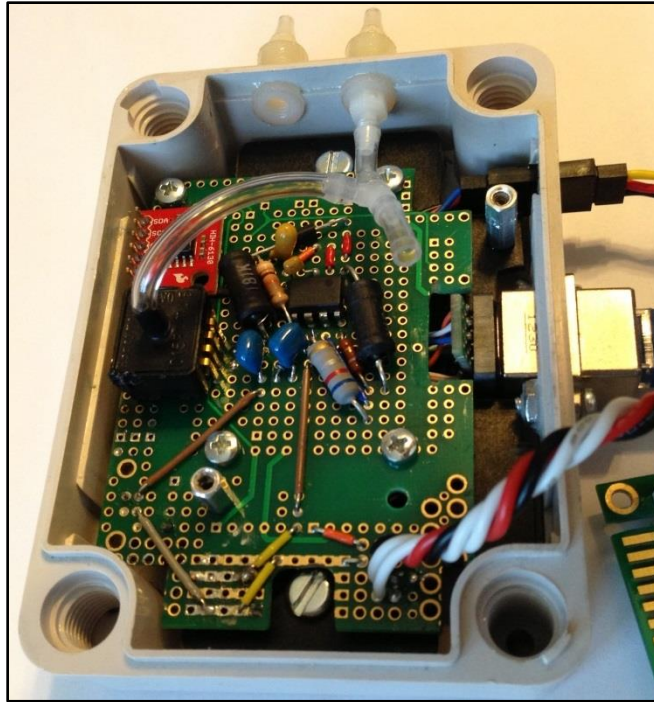


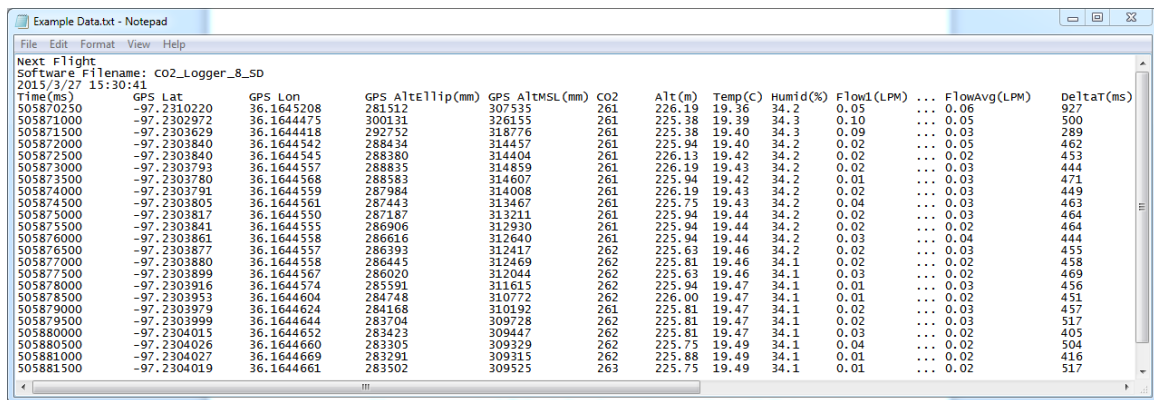
**Figure 75 - Voltage step-up circuit**

#### A. PROGRAMMING

Arduino microcontrollers are typically programmed with the Arduino IDE compiler software. Arduino programming is based on C/C++ and is fairly simple for beginners to learn. As mentioned previously, many libraries and examples are available online to simplify the programming. Because programming is not the main focus of this project, the output of the working datalogger is, the code was mostly assembled using examples provided by the various manufacturers. The code was edited to remove unused features and save space, modified to work at the desired recording rate and with the designed wiring setup, and log the outputs to the SD card. The code was divided into sections for each sensor with a header denoting each section for easy reference and editing as well as to include the citation for the original source of the code.

Arduino code consists of two main sections – the setup block which is run once when the system is first turned on (when the Arduino receives power) followed by the loop block which runs continuously while the Arduino is powered. In addition, blocks can be included for whatever

subprograms are desired. The general layout of the sensor system code begins with the setup block in which communication with the sensors is initialized, the log file is created on the SD card, and the header is added to the log file which includes the time stamp, software version, and column headers. The loop section logs the data continuously by accessing the subprograms for each of the various sensors and stores the values on the SD card as a tab delimited text file. The values logged from the various sensors are: the GPS time (measured in increments of 0.25 S), latitude, longitude, GPS altitude above the theoretical Earth ellipse, GPS altitude above mean sea level, CO<sub>2</sub> level, pressure altimeter altitude, temperature, relative humidity, ten analog readings of the flowmeter, the average of the flowmeter values, and the time in milliseconds that it took to run that iteration of the loop. The text file is closed after each run of the loop so no matter when the system is turned off only one data point at most is lost. If the time for the loop iteration is less than 250 ms then the program waits the remainder of the time to make a nominal data logging rate of 4 Hz. In practice, the sensors take varying amounts of time to communicate, especially the GPS and CO<sub>2</sub> sensor, and the actual time per iteration is a little below 500 ms, giving an effective logging rate of closer to 2 Hz. An example of the output log file is shown in Figure 76 (with some flowmeter readings omitted for brevity).



Time(ms)	GPS Lat	GPS Lon	GPS AltEllip(mm)	GPS AltMSL(mm)	CO2	Alt(m)	Temp(C)	Humid(%)	Flow1(LPM)	FlowAvg(LPM)	DeltaT(ms)
505870250	-97.2310220	36.1645208	281512	307535	261	226.19	19.36	34.2	0.05	...	0.06
505871000	-97.2302972	36.1644475	300131	326155	261	225.38	19.39	34.3	0.10	...	0.05
505871500	-97.2303629	36.1644418	292752	318776	261	225.38	19.40	34.3	0.09	...	0.03
505872000	-97.2303840	36.1644542	288434	314457	261	225.94	19.40	34.2	0.02	...	0.05
505872500	-97.2303840	36.1644545	288380	314404	261	226.13	19.42	34.2	0.02	...	0.02
505873000	-97.2303793	36.1644557	288835	314859	261	226.19	19.43	34.2	0.02	...	0.03
505873500	-97.2303780	36.1644568	288583	314607	261	225.94	19.42	34.2	0.01	...	0.03
505874000	-97.2303791	36.1644559	287984	314008	261	226.19	19.43	34.2	0.02	...	0.03
505874500	-97.2303805	36.1644561	287443	313467	261	225.75	19.43	34.2	0.04	...	0.03
505875000	-97.2303817	36.1644550	287187	313211	261	225.94	19.44	34.2	0.02	...	0.03
505875500	-97.2303841	36.1644555	286906	312930	261	225.94	19.44	34.2	0.02	...	0.02
505876000	-97.2303861	36.1644558	286616	312640	261	225.94	19.44	34.2	0.03	...	0.04
505876500	-97.2303877	36.1644557	286393	312417	262	225.63	19.46	34.2	0.02	...	0.03
505877000	-97.2303880	36.1644558	286445	312469	262	225.81	19.46	34.1	0.02	...	0.02
505877500	-97.2303899	36.1644567	286020	312044	262	225.63	19.46	34.1	0.03	...	0.02
505878000	-97.2303916	36.1644574	285591	311615	262	225.94	19.47	34.1	0.01	...	0.03
505878500	-97.2303953	36.1644604	284748	310772	262	226.00	19.47	34.1	0.01	...	0.02
505879000	-97.2303979	36.1644624	284168	310192	261	225.81	19.47	34.1	0.02	...	0.03
505879500	-97.2303999	36.1644644	283704	309728	262	225.81	19.47	34.1	0.02	...	0.03
505880000	-97.2304015	36.1644652	283423	309447	262	225.81	19.47	34.1	0.03	...	0.02
505880500	-97.2304026	36.1644660	283305	309329	262	225.75	19.49	34.1	0.04	...	0.02
505881000	-97.2304027	36.1644669	283291	309315	262	225.88	19.49	34.1	0.01	...	0.02
505881500	-97.2304019	36.1644661	283502	309525	263	225.75	19.49	34.1	0.01	...	0.02

Figure 76 - Example data log file

In practice, the system simply starts logging whenever the SD card is inserted and power is provided to the board. The log file is appended with new data (beginning with the header section

written during the setup code block) each time the system is run and data is only removed from the SD card when the card is inserted in a computer and the log file is manually deleted. For each run of the sensor system (each flight, windtunnel run, etc) a new section is added by just turning the power off and back on again to write a new header including the timestamp of when that run began. Because the SD card has a capacity to log for a very long time as previously discussed, the battery is essentially the only limit to the length of time that the system can log.

Most of the bugs in the programming were removed during testing, but a few remain with workarounds that were determined to have a negligible impact on the quality of data. It was found that recording the analog measurements immediately after the Arduino communicated through I2C added a large amount of noise. This was corrected by reading the analog data last and putting in a 75 ms delay before taking the readings. Because analog readings can naturally be noisy, the flowrate was also recorded ten times so the data could be averaged. There is also an issue (likely due some sort of power issue according to the manufacturer) in which the CO<sub>2</sub> sensor returns readings on the order of 4.3 billion PPM. If readings this high are returned, the code polls the CO<sub>2</sub> sensor one more time before moving on. This leads to these high readings being rare enough to delete those data points in post-processing and still have reliable data; the largest gaps observed have only been 3-4 data points. There is also the previously discussed issue with the altimeter after long continuous runs, but this problem is corrected by just starting a new data run and the GPS altitude is available as backup. Finally, while not necessarily a bug, is important to note that the CO<sub>2</sub> sensor has a warmup time before it begins outputting accurate data and the GPS can take several minutes to obtain a satellite lock on a cold start, so it is recommended to run the sensor for several minutes before running tests (roughly 5 minutes, though 20+ minutes – the drive time to the test sites – was common).

## II. AIRCRAFT CONFIGURATION DETAILS

### A. AIRCRAFT CONFIGURATION VERSION 1



**Figure 77 - X-8 Test Airframe 1**

The first X-8 used for testing (Figure 77) was a custom version sold by FPV Model that came with a preinstalled faux carbon fiber covering on its outer surfaces. This covering, essentially a large sticker, did provide some modest amount of increased protection to help hold the foam together in the event of a crash, as proven later during flight testing. Also included were plastic mounting plates with innovative slide-lock rails to attach the wings. The stock aircraft is designed to be hand launched, with grips molded into the underside of the fuselage, and to perform belly landings on flat terrain. The manufacturer recommended center of gravity of the aircraft coincided with the rear of the side grips as shown in Figure 78.

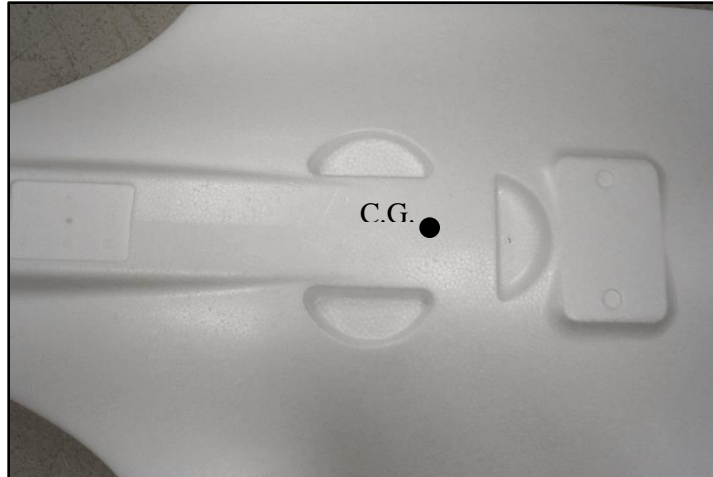


**Figure 78 - X-8 center of gravity location**

The propulsion system came from a premade kit sold by FPV Model specifically designed for the X-8. The kit consisted of a SunnySky x2820 KV920 brushless outrunner motor, a Hobbywing FlyFun 60A electronic speed controller, a pair of Henge MD933 micro-size servos for the control surfaces, and an 11x7" propeller (which was later replaced with an APC thin electric 12x6"). It was decided to power this system with 4S (14.8 V nominal) lithium-polymer battery packs because this voltage will provide the best mix between power and endurance (as compared to longer lasting 3S or higher powered 5S packs). It was found that two Turnigy 4000 mAh 4S batteries would fit the expected allowed weight for batteries (at 0.96 lbs each) and when run in parallel provide 8000 mAh of energy. The data for the motor and 12x6" propeller was calculated using the propulsion calculator at [ecalculator.com](http://ecalculator.com) – a commonly used RC propulsion resource with an extensive catalog of motor data. The aircraft flight data is based on generic assumptions, but the propulsion system numbers are generally rather good for an initial estimate. The data is shown in Figure 79 and shows a static thrust of 120.4 oz (though this slightly overpowers the motor) at a maximum current of 58.39 A.



Remarks:

• max. power over the limit of the motor. Please check the max. power limits defined by the manufacturer!

Battery		Motor @ Optimum Efficiency		Motor @ Maximum		Propeller		Total Drive		Airplane	
Load:	7.30 C	Current:	27.39 A	Current:	58.39 A	Static Thrust:	3414 g	Drive Weight:	1164 g	All-up Weight:	4000 g
Voltage:	14.15 V	Voltage:	14.37 V	Voltage:	13.88 V		120.4 oz		41.1 oz		141.1 oz
Rated Voltage:	14.80 V	Revolutions*:	12140 rpm	Revolutions*:	10930 rpm	Revolutions*:	10930 rpm	Power-Weight:	216 W/kg	Wing Load:	50 g/dm²
Capacity:	8000 mAh	electric Power:	393.5 W	electric Power:	810.7 W	Stall Thrust:	2645 g		98 W/lb		16.4 oz/lb
Energy:	118.4 Wh	mech. Power:	352.9 W	mech. Power:	698.1 W		93.3 oz	Thrust-Weight:	0.85 : 1	Cubic Wing Load:	5.6
Flight Time:	8.2 min	Efficiency:	89.7 %	Efficiency:	86.1 %	Thrust @ 56.4 km/h:	1488 g	P(in) @ max:	864.2 W	est. Stall Speed:	33 km/h
Mixed Flight Time:	10.2 min			est. Temperature:	75 °C	Thrust @ 35 mph:	52.5 oz	P(out) @ max:	698.1 W		20 mph
Weight:	840 g				167 °F	Pitch Speed:	100 km/h	Efficiency @ max:	80.8 %	est. Speed (level):	90 km/h
	29.6 oz						62 mph				56 mph
						Tip Speed:	628 km/h			est. Speed (vertical):	- km/h
							390 mph				- mph
						specific Thrust:	4.21 g/W			est. rate of climb:	6.7 m/s
							0.15 oz/W				1310 ft/min

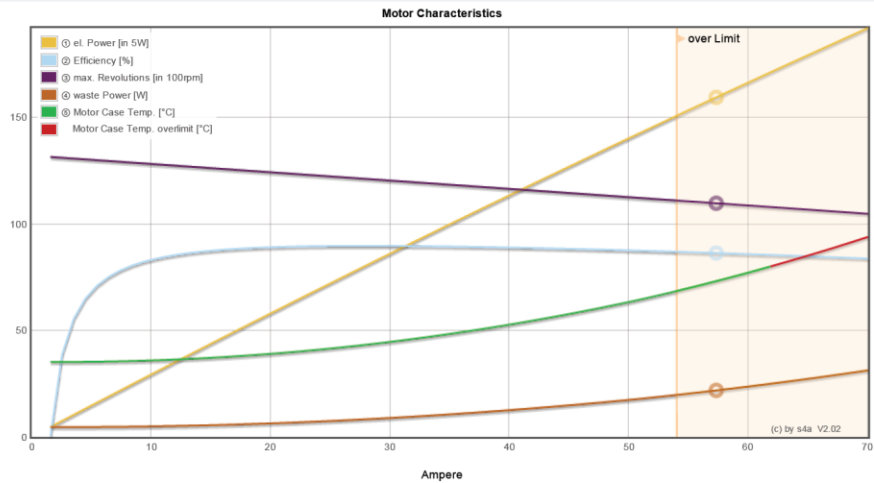
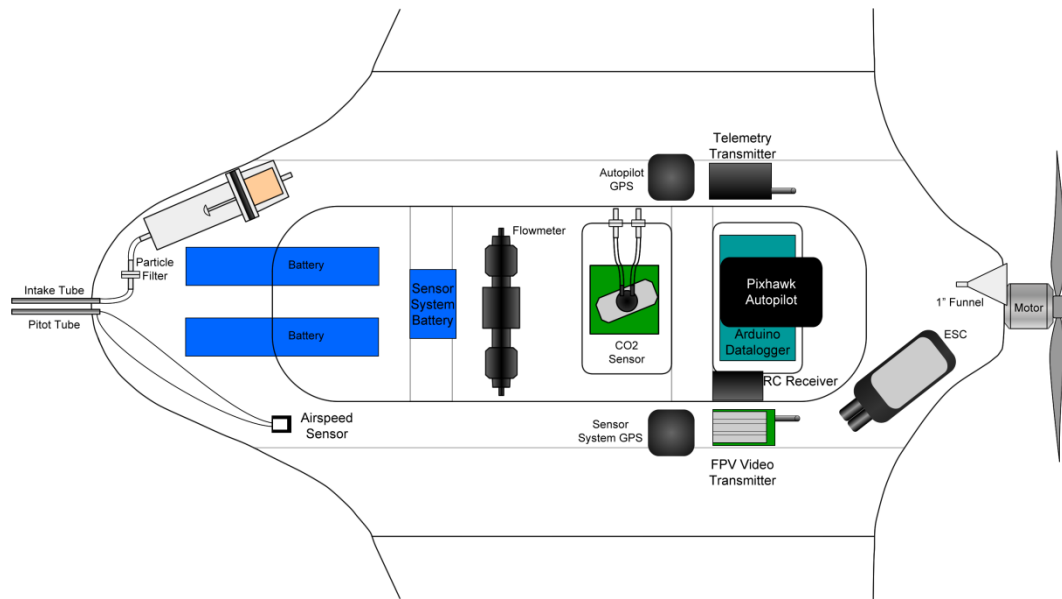


Figure 79 - SunnySky motor and 12x6" prop propulsion calculations

The general layout of the aircraft began with the batteries, the heaviest component, located in the nose to balance the C.G. and because this location gave the most room for travel in case the C.G. needed to be shifted; there was room to locate one battery in the mid compartment in case further C.G. travel was needed. The flowmeter and sensor box were located in the mid compartment, with the autopilot mounted atop the data box in the rear compartment. All GPS receivers and radio transmitters were located outside of the hatch and the ESC was located in the rear corner near the motor. The aircraft's RC receiver was mounted in the aft as well with the antennas mounted at a 90° angle in protective tubing. The internal layout is shown in Figure 80 below.





**Figure 80 - X-8 Aircraft 1 internal layout**

The front of the aircraft has an area which is conveniently notched to accommodate video cameras and other objects which require a flat mounting surface as shown in Figure 81. A mounting plate was added and a two wire cord grip from McMaster-Carr was attached. While designed to provide a liquid-tight pass through for electrical cables, this cord grip is ideal for mounting the pitot tube and CO<sub>2</sub> system intake tube because the rubber gland can be tightened to hold the tubing to protrude straight from the nose of the aircraft and if they need to be removed the gland can simply be loosened with a wrench. To assist the pilot in flying the aircraft more accurately and at a longer range, a first person video (FPV) camera system from 3DRobotics was installed. The camera was mounted to the nose beneath the intake tubes and the video transmitter was installed externally on the rear of the aircraft as mentioned previously.



**Figure 81 - Nose mounted FPV camera, CO<sub>2</sub> intake, and pitot tubes**

## **B. AIRCRAFT CONFIGURATION VERSION 2**



**Figure 82 - X-8 Test Airframe 2**

After initial tests of the first airframe, various areas of improvement were found, enough to warrant outfitting a new, upgraded airframe. The most critical issue with the first airframe was that it was already operating at the weight limit of what can safely be hand-launched, resulting in the majority of launch attempts being aborted. It was decided that landing gear was necessary for

safe and reliable operation of the aircraft. Another X-8 aircraft, already assembled with landing gear, was generously donated by a partner lab at OSU. The second X-8 is a standard model with bare EPO outer surfaces (without the extra covering). The landing gear is sold by FPV Model and is a tricycle style with a servo controlled steerable nose gear and A-frame rear gear. As opposed to the plastic slide-lock mounts attaching the wings on the previous aircraft (which were found to easily break in crashes forcing duct tape to be substituted as a wing attachment method) the wings on this aircraft were attached with simple plywood plates that were attached with screws; a method which, once the plates were fitted with T-nuts and reinforced with thin metal, was hoped to be more reliable. A very large amount of flex in the wings was also noticed in test flights of the first aircraft, so carbon fiber strips were glued vertically into the skins of the wings – one fore and one aft on the top surface and one centered on the bottom – to increase the wing stiffness.

A new motor was already installed on the aircraft when it was received. The Turnigy Aerodrive SK3 - 4240-740kv is a larger motor (42mm vs the previous 35mm), meaning it can handle more power, although it spins slower at 740 kV (no load rpm/volt) but with more torque. An APC thin electric 12x6” prop was originally fitted and later upgraded to a 13x6.5”. According to the calculations from eCalc, as show in Figure 83, this propulsion combination provides slightly less thrust, 106 oz static, but at 45 amps, a 15 amp power reduction. If increased thrust is found to be required, a higher pitch prop such as a 13x8” can be fitted. A new ESC was found, a high-quality Castle Creations Pheonix Ice 50, which provides a maximum of 50 amps (though Castle Creations ESCs are known from experience to easily handle higher-than-spec loads) as well as in-flight datalogging of voltage, amperage, temperature, etc. for a better post-flight propulsion analysis. Though this ESC, like most, provides a battery eliminator circuit (BEC) to provide 5 V power to power the aircraft’s control servos and receiver, it was decided to install a separate dedicated Castle Creations BEC to bypass the ESC for increased reliability in the event of an ESC failure.

<b>Remarks:</b>									
<b>Battery</b>		<b>Motor @ Optimum Efficiency</b>		<b>Motor @ Maximum</b>		<b>Propeller</b>		<b>Total Drive</b>	
Load:	5.65 C	Current:	19.46 A	Current:	45.23 A	Static Thrust:	3015 g	Drive Weight:	1173 g
Voltage:	14.29 V	Voltage:	14.29 V	Voltage:	13.62 V		106.3 oz		41.4 oz
Rated Voltage:	14.80 V	Revolutions*:	9901 rpm	Revolutions*:	8753 rpm	Revolutions*:	8753 rpm	Power-Weight:	151 W/kg
Capacity:	8000 mAh	electric Power:	278.0 W	electric Power:	615.7 W	Stall Thrust:	2336 g		69 W/lb
Energy:	118.4 Wh	mech. Power:	252.2 W	mech. Power:	533.8 W		82.4 oz	Thrust-Weight:	0.68 : 1
Flight Time:	10.6 min	Efficiency:	90.7 %	Efficiency:	86.7 %	Thrust @ 56.4 km/h:	1055 g	P(in) @ max:	669.3 W
Mixed Flight Time:	11.5 min			est. Temperature:	63 °C	Thrust @ 35 mph:	37.2 oz	P(out) @ max:	533.8 W
Weight:	840 g				145 °F	Pitch Speed:	87 km/h	Efficiency @ max:	79.7 %
	29.6 oz						54 mph		
						Tip Speed:	545 km/h		
							339 mph	est. Speed (vertical):	- km/h
						specific Thrust:	4.90 g/W		- mph
							0.17 oz/W	est. rate of climb:	5.3 m/s
									1048 ft/min

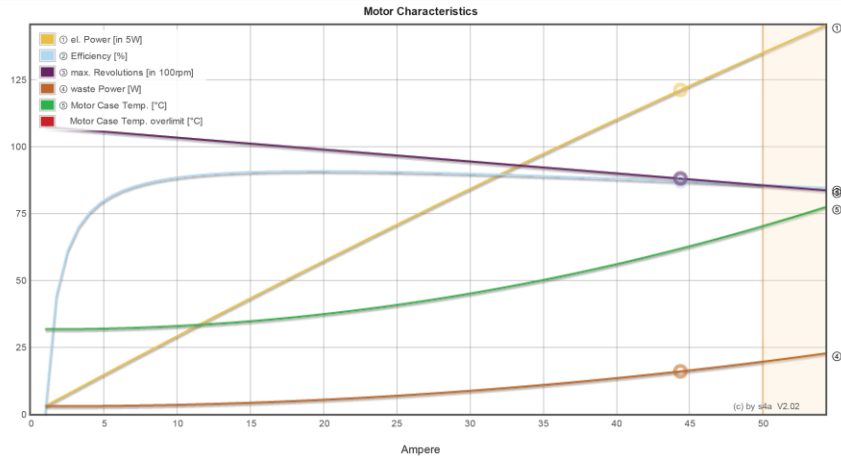


**Figure 83 - Turnigy motor and 13x6.5" prop propulsion calculations**

For this new aircraft, new features and equipment were added which necessitated a reconfigured layout. The FPV system was replaced by an improved system manufactured by Fat Shark. The camera was replaced by a Fat Shark camera and movable mount which consisted of a pair of servos so the camera could pan vertically and horizontally. The transmitter is designed to connect to Fat Shark goggles for an improved pilot view of the video feed, though this system does require a spotter for the aircraft in case video connection is lost.

The batteries were left in the nose of the aircraft (the midsection location was found to be unnecessary) and the autopilot telemetry transmitter was moved to the nose section in an EMI protected enclosure (to be detailed later). The autopilot was mounted in a custom enclosure (also to be detailed later) which required both of the CO<sub>2</sub> system components, the data box and sensor box, to be located in the midsection. The GPS receivers were moved forward as well to avoid possible magnetometer interference from the electric motor. The LED strobe for the sensors was mounted beneath the midsection and the FPV video transmitter was relocated internally in the

midsection as well with the antenna protruding through the fuselage. The final aircraft layout is shown in Figure 84; the additional wiring, enclosures, systems, and landing gear mounts caused for the interior space to be cramped, but manageable if organized.

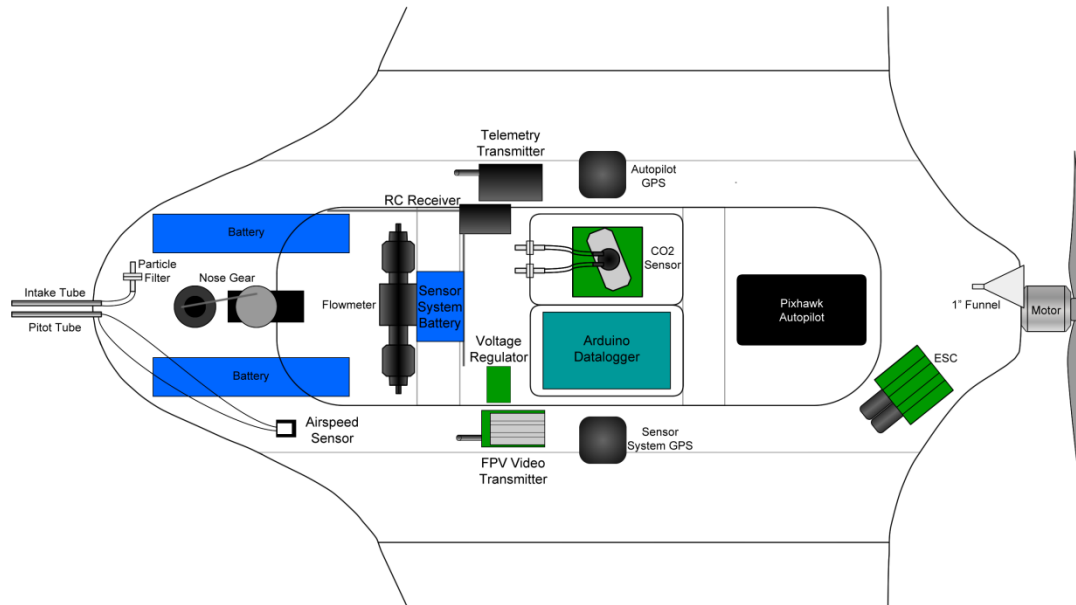


**Figure 84 - X-8 Aircraft 2 internal layout**

### C. AIRFIELD



**Figure 85 - Oklahoma State Unmanned Aircraft Flight Station**

All flight tests were performed at Oklahoma State's Unmanned Aircraft Flight Station (Figure 85) located 12 miles east of Stillwater, OK. The station is equipped with a 600 ft north-south runway and 350 ft crosswind runway, a hangar, and control room. It is located at an elevation of 1032 ft and surrounded mostly by grassland. A live feed is available through the tower-mounted weather station for updated local weather data.

### III. AUTOPILOT WIRING IMPROVEMENTS

It was found through flight testing that the stock wiring for the autopilot was not durable. The high gauge wire (~32 AWG) broke easily leading to several lost flight test days when autopilot components did not work. In addition, the DF13 connectors on the Pixhawk are very fragile and care must be taken when unplugging cables from the autopilot so as to not ruin the connectors which cannot be fixed or replaced (essentially ruining the autopilot). To correct this, new wiring was developed. Precrimped 28 AWG wires were purchased and placed in DF13 connector

housings. To additionally strengthen the wires where the crimp met the housing, the location which most often broke, the wires were potted in epoxy as shown in Figure 86. The wires were then wrapped in abrasion resistant sleeving and heat shrink to keep them organized, although this did add some stiffness to the cables. To avoid repeatedly disconnecting the DF13 connectors to avoid damage, in-line disconnects were added to the wires using Molex SL rectangular connectors. This allows components to be disconnected without unplugging the DF13 connections from the Pixhawk or components. The final cable is shown in Figure 87. Finally, to provide strain relief on the Pixhawk connections, and to hold in place some of the connections which were already damaged, a housing was developed to encase the Pixhawk which essentially acted as a strain relief backshell, as shown in Figure 88 and Figure 89.

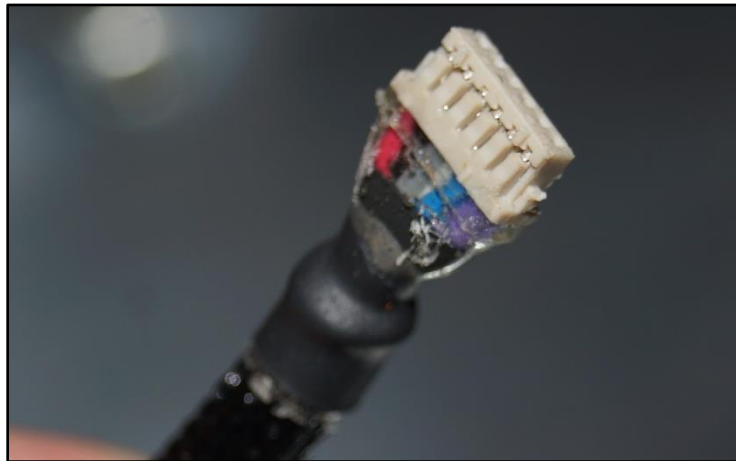


**Figure 86 - Epoxy potted DF13 connectors**

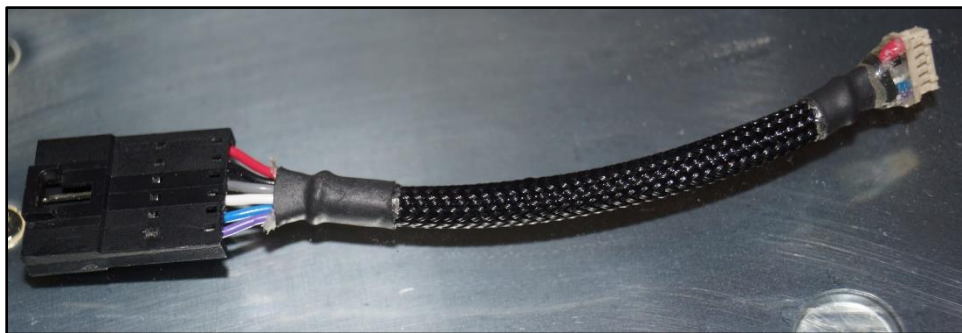


**Figure 87 - Improved autopilot cable**



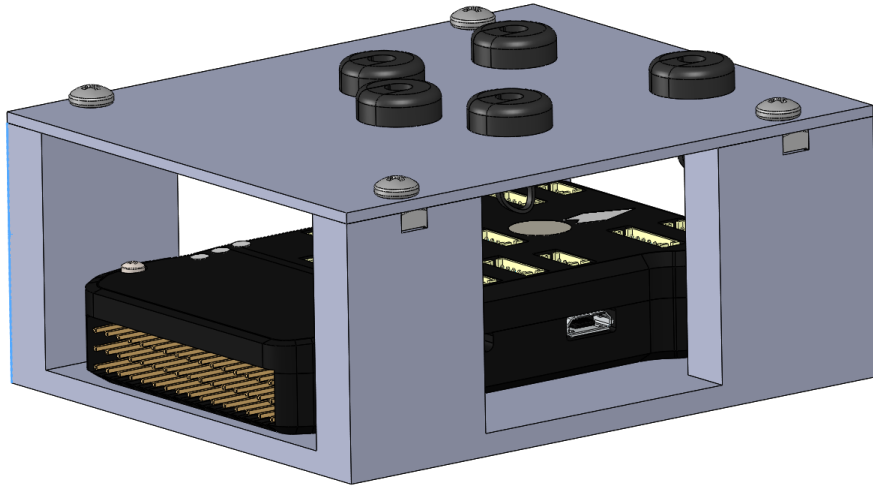


**Figure 88 - Pixhawk strain relief enclosure**

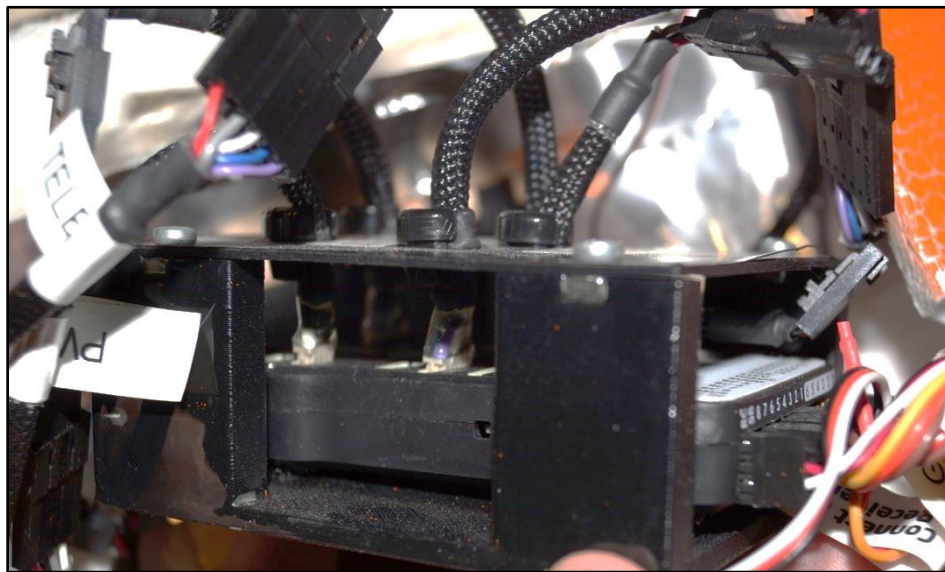
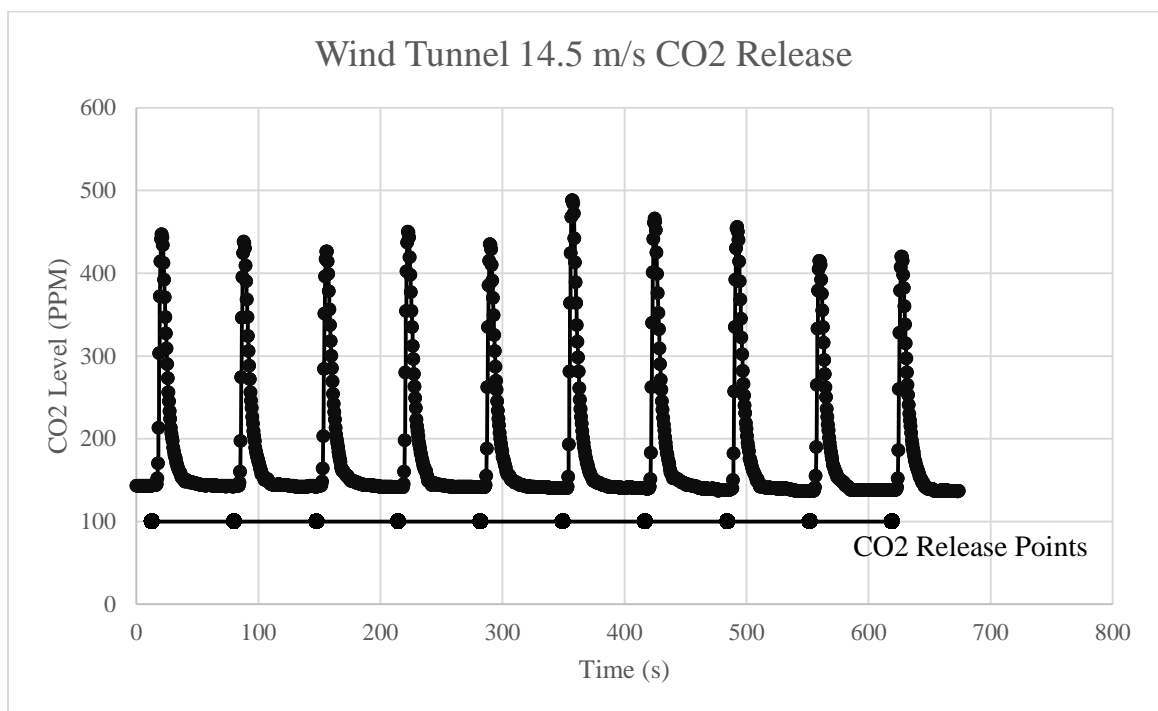


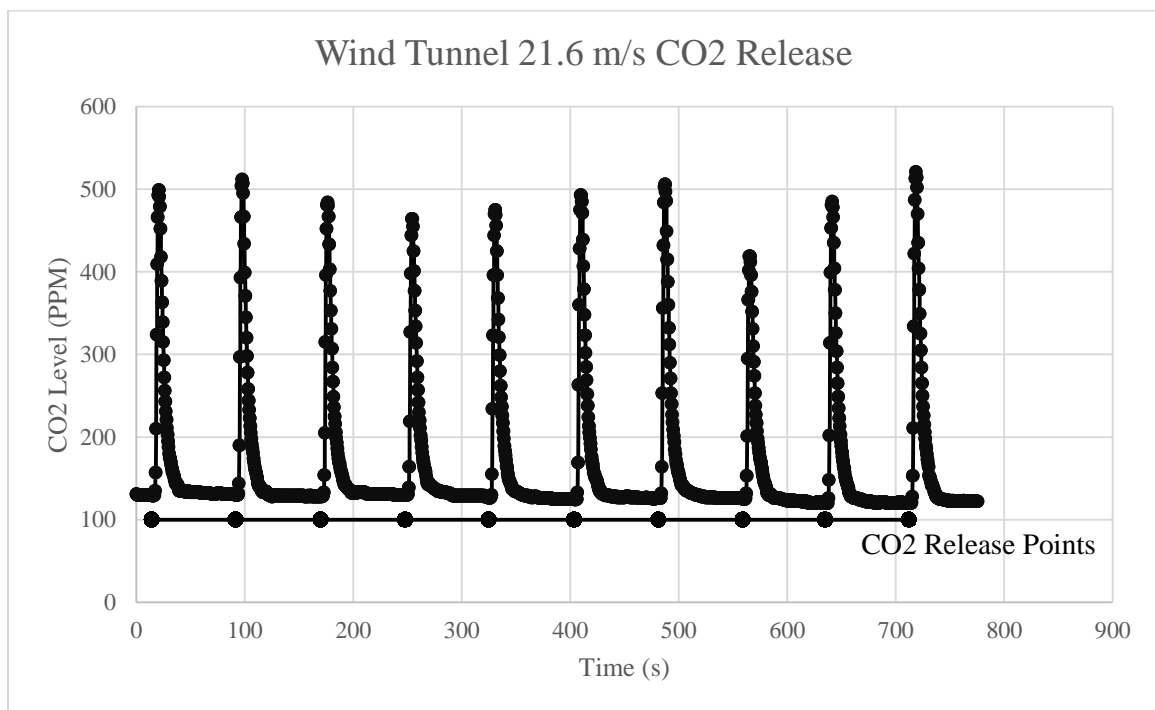
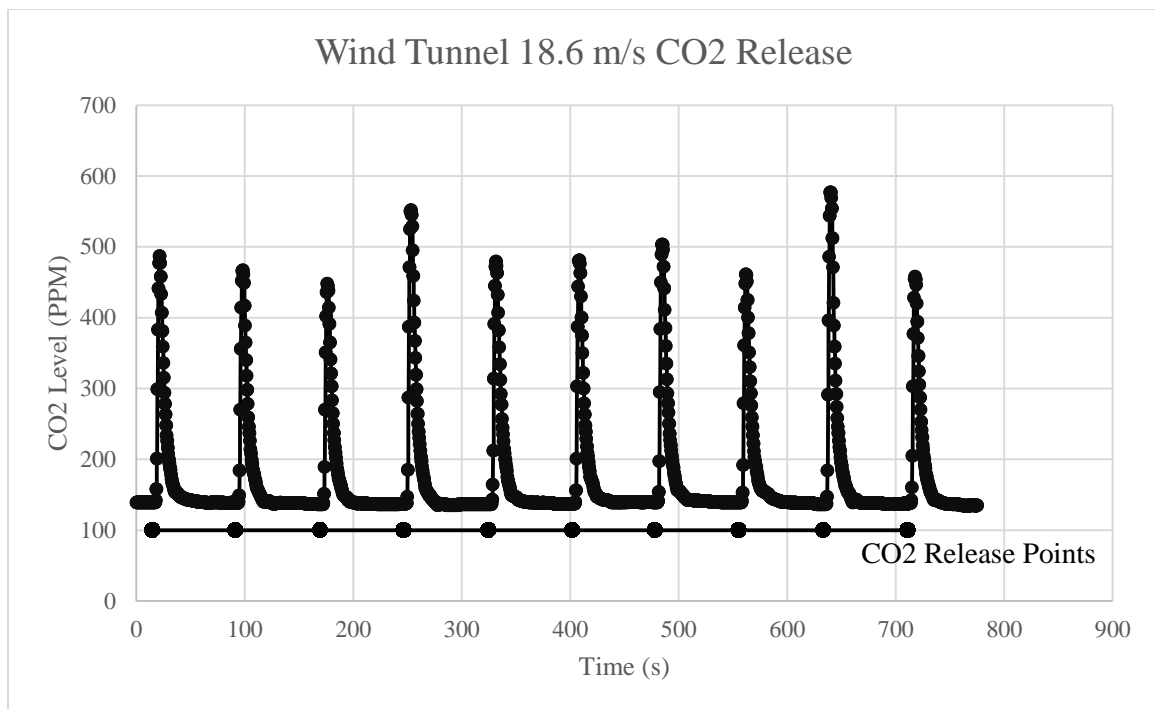
**Figure 89 - Pixhawk strain relief enclosure with wiring**

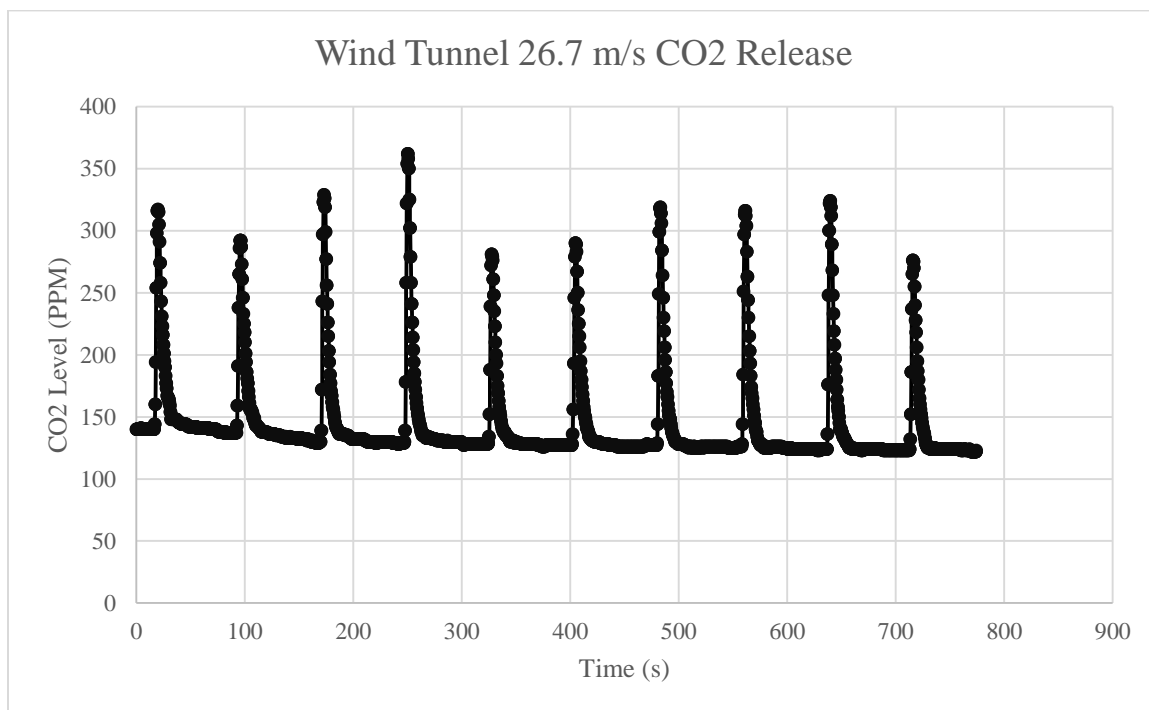
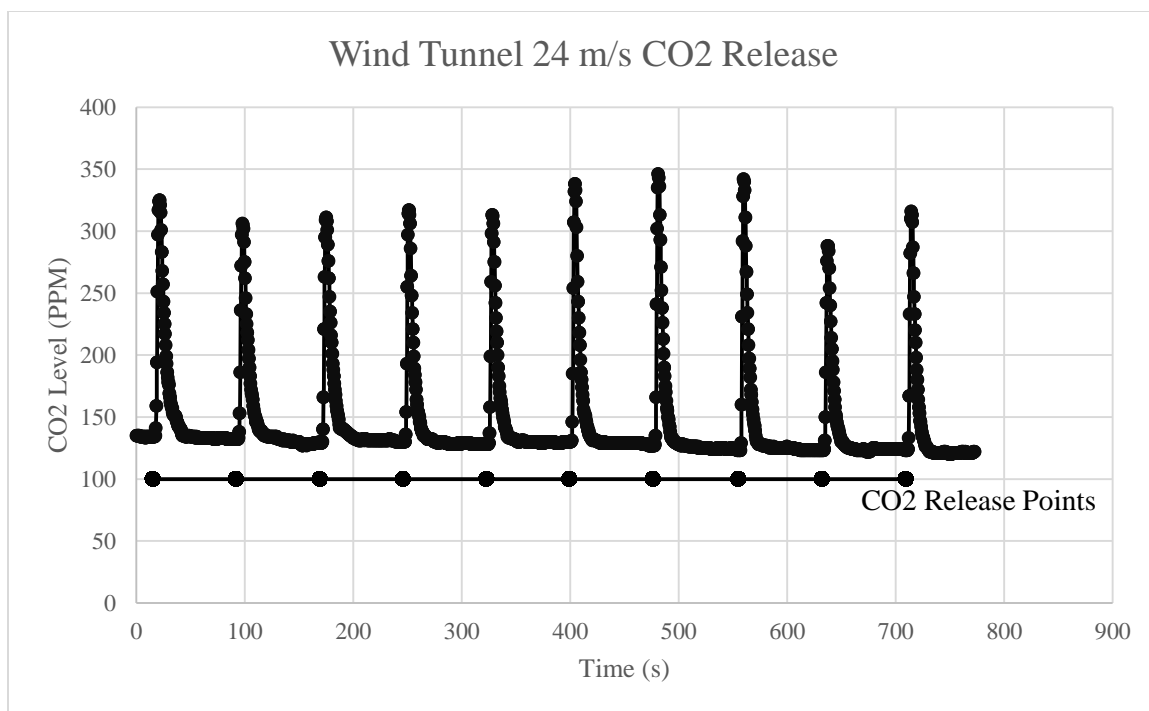


## APPENDIX B – Additional Figures

### I. WIND TUNNEL CO<sub>2</sub> RESPONSE TEST CHARTS







## VITA

Taylor Austin Mitchell

Candidate for the Degree of

Master of Science

Thesis: DEVELOPMENT OF A LOW COST UNMANNED AIRCRAFT SYSTEM  
FOR ATMOSPHERIC CARBON DIOXIDE LEAK DETECTION

Major Field: Mechanical and Aerospace Engineering with Unmanned Aerial Systems  
Option

Biographical:

Education:

Completed the requirements for the Master of Sciences in Mechanical and  
Aerospace Engineering at Oklahoma State University, Stillwater, Oklahoma in  
May, 2015.

Completed the requirements for the Bachelor of Science in Aerospace  
Engineering and Mechanical Engineering at Oklahoma State University,  
Stillwater, Oklahoma in 2012.

Experience:

Research Assistant – Oklahoma State University, Stillwater, OK

Launch Intern – Space Exploration Technologies Corporation (SpaceX), Cape  
Canaveral, FL

Chief Engineer – Capstone senior design project, Orange Team, Oklahoma  
State University

Wentz Research Scholar – Oklahoma State University, Stillwater, OK

Professional Memberships:

AUVSI, AIAA, ASME, Tau Beta Pi, Phi Kappa Phi